Crosstalk between innate and adaptive immune cells within lymph node microenvironments shapes immunity to vaccines

Joseph M. Leal IV

A dissertation submitted in partial fulfillment of the requirements for the degree of Doctor of Philosophy

University of Washington

2021

Reading Committee:

Michael Y. Gerner, Chair

Jessica Hamerman

Kevin Urdahl

Program Authorized to Offer Degree:

Immunology

University of Washington

Abstract

Crosstalk between innate and adaptive immune cells within lymph node microenvironments shapes immunity to vaccines

Joseph M. Leal IV

Chair of the Supervisor Committee

Michael Gerner, Ph.D.

Department of Immunology

Vaccines are critical to public health and have prevented the deaths of millions of people worldwide (*1*, *2*). However, the mechanisms that govern immune responses to vaccines are not well defined. If we can better understand how the vaccine immune response initializes, we can rationally design vaccines to elicit a desired immune response. Advances in our understanding of vaccines has been highlighted by the global COVID-19 pandemic caused by the SARS-CoV-2 virus, wherein rationally designed vaccines have played a critical role in combating the pandemic (*3*).

The initiation of immune responses is a complex and incompletely understood process that involves activation and careful crosstalk between the innate and adaptive arms of the immune system (*4*). This intricate initiation of immunity takes place in specialized immune organs called lymph nodes (LNs) that are highly spatially organized at steady state conditions. How this innate/adaptive crosstalk and spatial organization of immune interactions is restructured during inflammation and whether this influences generation of responses is incompletely understood.

Thus, understanding the microanatomical organization of immune cells in lymphoid tissues and the cell-cell interactions that take place during the early stages of the immune responses to vaccines is a matter of great public health importance.

Here, we utilized advanced imaging and cellular analysis techniques to dissect the spatial organization and the functional roles of various cells of the innate immune system in the generation of T cell immunity. In Chapter 3 we show that during Type 1, but not Type 2 inflammation during subunit vaccination, LN resident conventional dendritic cells (Res cDCs) capture antigen in the periphery of the LN and relocalize to the deep T cell zone (TZ). Concurrently, inflammatory monocytes (MOs) were recruited in large numbers to draining LNs. We found that Res cDC relocalization to the deep TZ required the chemotactic receptor CCR7, and that MO entered the LN from the blood through high endothelial venules (HEVs). Failure of Res cDCs to relocalize to the deep TZ greatly disrupted T cell priming and clonal expansion, while blocking MO entry or their ability to make a key inflammatory cytokine, interleukin-12 (IL-12), hindered T cell differentiation. Thus, the spatial and temporal cooperation of these distinct myeloid populations was critical for determining the magnitude and quality of the overall T cell response. Furthermore, asymmetric MO localization within LNs created distinct myeloid cell microenvironments, contributing to the heterogeneous differentiation of the T cell compartment.

In Chapter 4, we demonstrate that Res cDC maturation and relocalization was mediated by distinct direct and indirect inflammatory signals. Adjuvant-sensing was not intrinsic to Res cDCs, indicating substantial redundancy in how this myeloid cell population is able to respond to inflammation. We also found Res cDC2 cellularity was selectively increased during inflammation, and that direct sensing of draining adjuvant was required for this skewing in a cell

intrinsic fashion. We traced this increase in Res cDC2s to the enhanced recruitment of pre cDC2s during inflammation, and not to *in situ* proliferation of existing cells, albeit more work is required to further elucidate these changes in Res cDC2 cellularity during inflammation. Together, this Chapter describes the signaling requirements for Res cDC maturation and localization during inflammation, as well as the associated increases in Res cDC2 cellularity and the potential underlying mechanisms.

In Chapter 5, we describe a previously unappreciated role for sensing of draining TLR ligands in the activation of polyclonal naïve B cells. This activation was dependent on the adaptor of TLR signaling, MyD88, and regulated both the phenotypic maturation and intranodal localization of B cells. Importantly, we found that this large-scale B cell activation was also critical for the rapid generation of pre- T follicular helper (pre-Tfh) cells and their ability to relocalize to the B cell follicles, with significantly fewer Tfh cells generated when B cells lacked the ability to signal through MyD88. This early relocalization of T cells into the B cell follicles was also spatially correlated with B cell activation, further suggesting a tight association between B cell activation and follicular entry by newly generated pre-Tfh cells. Together, this Chapter describes how bystander B cell activation through direct sensing of draining TLR ligands can drive pre-Tfh follicular infiltration and differentiation.

In sum, this work has shed light on how vaccine adjuvant induced inflammation can impact profound changes in myeloid and antigen presenting cell composition and organization within LNs. In turn, our data describes fundamental and previously undescribed features of lymphoid tissue microenvironments and how they can drive adaptive cellular immunity. Harnessing the formation of lymphoid tissue microenvironments will improve design of vaccines to enhance immunity.

Acknowledgements

There are so many people to thank for helping me get here, but I will start by thanking my many mentors along this journey. Thank you to my high school biology teacher Mel Wendell, your enthusiasm for science was inspiring and started me down the path to becoming a biologist. Thank you to Dr. Brent Ybarrondo, Ph.D., my first college biology teacher. You gave me the confidence that I could do this, that I was good at this stuff. Thank you to Dr. David Nachman, Ph.D., and Dr. Stan Kikkert, Ph.D., my community college Chemistry and Microbiology teachers, respectively. Your patience and love for science was infectious. At community college there was not a lot of hope that a Ph.D. was ever something I could aspire to, but you supported my dream and stoked that flame. Thank you to my first scientific mentor, Dr. Yung Chang, Ph.D. You took a chance on me right out of community college before I'd even started at ASU. I will always be grateful for the opportunity you gave me to break into science. Thank you to Dr. Xiaowei Liu, Ph.D., my personal mentor in lab and a great friend. You showed me how to be a scientist.

Thank you to my thesis advisor and mentor, Dr. Michael Gerner, Ph.D. I joined your lab at the beginning, and we weathered many tough times and our share of exciting moments. Thank you for taking me on to your burgeoning lab. It has been such a privilege watching the lab grow into a place where cool science is happening. I am so excited to see where the science takes you and the lab next. Thank you to the rest of the Gerner lab, past and present. Thank you, Karan, for your early mentorship and friendship. Thank you to Brandy for putting up with me from the very beginning. Special thanks to Jessica and Miranda. You two were the first grad students to join

the lab after me, and you were instrumental in keeping me sane throughout grad school. Miranda, thank you so much for being an amazing person and friend. Jessica, thank you for your (sometimes begrudging) friendship, and thank you for the incredible work you put into our first author paper. Quite simply, the paper could not have existed without you.

Thank you to my family for your endless support. To my parents Joe and Tamara, your constant and unwavering support gave me the courage to strike out on my own and pursue this career. I have been so incredibly privileged to grow up in such a loving home. To my brother Jordan, thank you so much for always being there for me. To my grandma, your pride in me and my work has motivated me whenever I have felt down or like my work does not matter. Finally, I would like to express my gratitude to the laboratory mice whose lives have enabled my work.

TABLE OF CONTENTS

List of figures....iii
List of tables....iv

Chapter 1: Introduction 1
Introduction....1
Dendritic cell and monocyte ontogeny....4
Architecture of lymph nodes....5
Antigen and adjuvant trafficking to draining LNs....5
Microbial pathogen transport to lymph nodes....6
PRR dependent activation of dendritic cells....7
Crosstalk between innate and adaptive immune cells....9
T follicular helper cell differentiation and the role of B cells....10
Lymph node microenvironments guide T cell differentiation....11
Objectives and significance 13

Chapter 2: Materials and Methods
Mice....15
Bone Marrow Chimeras and Adoptive Transfers....16
Immunizations and Infections....17
Antibodies and Staining Reagents....18
ELISA....19
Confocal and two-photon intravital microscopy....19
Histocytometry analysis....20
Cell isolation and flow cytometry....21
Statistics....22
Experimental design....22

Chapter 3: Innate cell microenvironments in lymph nodes shape the generation of T cell responses during Type-I inflammation 23
Introduction....24
Results....26
Discussion 64

Chapter 4: Direct and indirect inflammatory signals direct the activation and composition of the cDC compartment in lymph nodes 69
Introduction....70
Results....72
Discussion 85

Chapter 5: Toll-like receptor dependent bystander B cell activation regulates T follicular helper cell responses 89

Introduction.....90
Results.....93
Discussion.....110

Summary and imapct.....114

References.....115

LIST OF FIGURES

Chapter 3:

Figure 1.....29
Figure S1.....30
Figure S2.....31
Figure 2.....35
Figure S3.....37
Figure 3.....41
Figure S4.....42
Figure 4.....46
Figure S5.....48
Figure 5 51
Figure S6.....53
Figure 6.....57
Figure S7.....59
Figure 7.....62
Figure S8.....63
Figure S9.....68

Chapter 4:

Figure 1.....74
Figure S1.....75
Figure 2.....77
Figure 3.....81
Figure 4.....84

Chapter 5:

Figure 1.....95
Figure 2.....98
Figure 3.....101
Figure 4.....104
Figure 5.....107
Figure 6.....110
Figure S1.....111

LIST OF TABLES

Chapter 4:

Table 1.....72

Chapter 5:

Table 1.....93

Chapter 1. Introduction

Conventional DCs (cDCs) are the critical antigen-presenting cells that initiate adaptive immunity in response to external inflammatory stimuli (*4*–*6*). cDCs that reside in the lymph node (Res cDCs) can be subdivided into two subsets, cDC1s and cDC2s, based on divergent gene expression and their respective specialization in generating CD8 vs. CD4 T cell responses (*5*, *6*). We have previously described that cDC1 and cDC2 populations occupy distinct spatial compartments in LNs during the steady-state, and that this localization influences the ability of these cells to carry out several critical DC functions, from antigen capture and presentation to T cell priming (*7*–*9*). Specifically, Res cDC2s reside in regions that are proximal to the lymphatic sinuses that enable superior acquisition of draining antigens but are distal from the paracortex where they can optimally interact with naïve T cells. In contrast, Res cDC1s are widely distributed throughout the LN parenchyma and are particularly enriched in the T cell zone (*8*). Whether Res cDC2s need to transit to the deep T zone to optimally induce CD4+ T cell responses is unknown. Furthermore, while Res cDCs are known to be critically required for T cell immunity, it is less clear whether additional myeloid cell types are also required. In preliminary studies we have observed that immunization with some, but not all, vaccine adjuvants induce cDC2 repositioning from peripheral LN regions into the deep T cell zone and extensive MO recruitment. However, the molecular mechanisms that drive such cellular repositioning and recruitment during inflammation, and the downstream consequences of these processes on the generation of CD4+ T cell responses, is currently not known. The major goal of my thesis work was to understand the molecular regulation of cDC repositioning and MO influx after vaccination, as well as to elucidate the roles of this process in the generation of adaptive immunity.

Over the past century, vaccines have enabled the eradiation or substantial reduction of numerous devastating diseases, from smallpox and measles to polio (*2*, *10*). While many types of vaccines exist, we will largely be discussing subunit vaccines, which contains only a fragment (i.e subunit) of the pathogen that protection is aimed against (*2*). Subunit vaccines typically consist of a protein antigen and an immune stimulating component, called an adjuvant. The adjuvant functions to activate antigen presenting cells (APCs), allowing them to present antigen and produce inflammatory cytokines that drive the effector differentiation of T cells. While subunit vaccines require an adjuvant, other advanced vaccine technologies such as mRNA vaccines function as their own adjuvant through cell intrinsic detection of foreign nucleic acid (*2*). The immune response to vaccines is generally thought to begin at the site of injection, commonly the skin or muscle, wherein professional APCs called migratory conventional dendritic cells (Mig cDC) can take up said antigen and traffic to draining LNs to initiate the immune response in a process that can take from 12 to 48 hours (*5*–*7*). Additionally, our lab has shown that antigen and adjuvant can drain extremely rapidly to LNs and enter the LN parenchyma within minutes after injection, thus kickstarting the immune response long before antigen-bearing Mig cDCs have made their way to the LN (*7*). Once inside the LN, adjuvants can directly activate a diverse array of innate immune cell types, many of which then produce inflammatory cytokines, thus setting of a downstream cascade that alerts the immune system to respond to an incoming threat. One such subset of adjuvants are toll-like receptor agonists, which function as ligands for the pattern recognition receptors (PRRs) called toll-like receptors (TLRs). These receptors, expressed on APCs such as cDCs and B cells, initiate an activation program that can culminate in the expression of a diverse array of downstream transcription factors and production of

inflammatory cytokines (*11*). This sensing of TLR ligands and activation is well described in cDCs, in which it augments antigen presentation by increasing the expression of MHC-II molecules, as well as elicits the expression of co-stimulatory molecules such as CD80 and CD86 (*4–6*, *12*). Furthermore, direct TLR sensing can elicit the production of inflammatory cytokines such as IL-12 and IL-6, which can instruct T cells to engage specific effector programs tailored to the threat at hand. Utilizing this specialized ability to detect and present antigen, cDCs function as the critical information carriers that relay pathogen-specific information to the adaptive arm of the immune system (*13*). While both types of cDCs are important for sculpting the adaptive immune response, LN-res cDCs are critical for the very early priming of antigen-specific T cells in the lymph node before migratory DCs arrive (*14–17*). In particular, the Res cDC2 subpopulation is optimally positioned in the LN periphery for optimal antigen sampling (*7*, *8*). Many of these cells reside directly within the lymphatic sinuses (LS-DCs), which allows them to directly sample lymph for antigens and to elicit rapid induction of T cell responses following particulate antigen and bacterial immunization (*9*). Similarly, Res cDC2s can efficiently capture and present soluble antigens that permeate the floor of the subcapsular sinus (SCS) and elicit robust CD4 T cell priming (*7*). However, this superior antigen acquisition ability of cDC2s due to their peripheral localization also raises the question of how these cells promote efficient T cell activation, as these cells are located distally to the T cell zone, and this would limit cognate DC-T cell interactions during priming.

The aim of my thesis work was to understand the spatial organization of myeloid cells during inflammation and how it influences adaptive immunity. These studies examined fundamental questions relating to DC biology and the role that spatiotemporal organization of these cells plays in facilitating rapid immune responses, with important implications for vaccine design.

Together, this work provided important insights into the fundamental biology of innate and adaptive immune responses with the potential to impact public health through improved vaccine design.

Spatiotemporal organization of the immune response in lymph nodes

Dendritic cell and monocyte ontogeny. Most conventional dendritic cells (cDCs) and monocytes (MO) are short lived cells that are constantly replaced by bone marrow (BM) derived precursors (*5*, *6*). cDCs are derived from pre cDCs, a cDC restricted progenitor that travels to lymphoid and non-lymphoid tissues and can differentiate into both cDC1 and cDC2 subsets. Furthermore, there is heterogeneity within the pre cDC compartment, with dedicated precursors that can give rise to both cDC1 and cDC2 subsets (*18*). Although additional heterogeneity of cDC2s has been proposed based on expression of the transcription factors Tbet and RORγt, this population of cDCs is generally defined by their expression of the transcription factor IRF4 (*5*, *6*, *19*). In contrast the cDC1 lineage is driven by expression of the transcription factor IRF8 (*20*). MO, on the other hand, develop from a committed monocyte progenitor (MOP) in the BM, distinct from the cDC lineage (*21*). Newly generated MO in the BM initially express high levels of Ly6C, and can then retain high expression or downregulate it. Expression of Ly6C dictates distinct functions outside the bone marrow in the circulation. While Ly6C low MO, classically named "patrolling monocytes", survey blood vessels and contribute to tissue repair, Ly6C^{hi} MO, classically named 'inflammatory monocytes", can be rapidly recruited to sites of inflammation and differentiate into inflammatory DCs or macrophages (Macs) (*21*, *22*).

Architecture of lymph nodes. Lymph nodes are a critical meeting space for cells of the immune system. These immune cells exist on a scaffold of stromal cells, consisting primarily of follicular dendritic cells (FDCs) in B cell follicles (BZ) and fibroblastic reticular cells (FRCs) that form the framework of the T cell zone (TZ) (*4*). FRCs have considerable heterogeneity that imparts distinct functions and localizations within the LN (*23*). They also encapsulate the lymphatic conduit system, which is responsible for carrying lymph draining from the subcapsular sinus (SCS) and connects the lymphatics to HEVs, thus facilitating communication between the lymph and the blood (*24*). FRCs in the TZ are responsible for the production of the chemokine CCL21, the ligand for the chemotactic receptor CCR7, which is critical for the localization of immune cells to the deep TZ. In the B cell follicles, FDCs produce the chemokine CXL13, the ligand for the chemotactic receptor CXCR5. The spatial segregation of CXCL13 and CCL21, and thus CCR7 expressing T cell and CXCR5 expressing B cells, forms the basic structure of the lymph node at steady state (*4*). Beyond this basic structure, more fine-grained organization of various immune cell types exists, driven by differential immune cell expression of chemotactic receptors. For example, the chemokine receptor EBI2 fine tunes the positioning of CD4+ T cells to the periphery of the TZ near B cell follicles (*25*).

Antigen and adjuvant trafficking to draining LNs. Antigen and adjuvant can traffic to LNs via two distinct mechanisms, one that depends on free drainage via the lymphatic system, and one that requires cellular uptake and migration (*16*, *24*, *26*). Both small soluble molecules and particulate antigens can quickly enter the lymphatics and drain rapidly to LNs, where they can be sampled by Res cDCs. Particulate antigens that drain into the LN are first captured by SCS macrophages and lymphatic sinus (LS) DCs, which can extend their dendrites into the lymphatic

luminal space and directly capture draining particulate antigen (*8*, *27*). Once drained to LNs, soluble antigen and adjuvant can pass directly through fenestrations in the membrane of the SCS, thus allowing direct access to antigen presenting cells positioned near the SCS. However, the drainage of antigen and adjuvant is not uniform, instead following a concentration gradient wherein the most antigen is present near the SCS and dwindles towards the deep TZ. This concentration gradient of soluble antigen increases the ability of Res cDC2s in the periphery to capture and present that antigen compared to Res cDC1, thereby functionally modulating the ability of those cells to induce CD4+ and CD8+ T cell responses, respectively (*7*). Antigen and adjuvant can also be taken up by Mig cDCs, which are then activated and express CCR7, allowing them to follow gradients of CCL21 and enter the lymphatics to dLNs. Cellular uptake of antigen and adjuvant takes significantly longer than direct drainage and thus antigen-bearing Mig cDCs take 12 to 24 hours to traffic to dLNs, compared to lymph-borne molecules which can enter LNs within seconds-minutes after injection. Although Res cDCs can be rapidly activated by lymph-borne antigens, much remains to be learned regarding the competing roles of Mig versus Res cDC in the generation of adaptive immune responses (*12*).

Microbial pathogen transport to lymph nodes. Although microbial pathogens are vastly more complex than simple vaccines, similar rules regulate their trafficking to LNs. For example, although certain viruses are highly tropic and require cell-mediated trafficking to dLNs, others can drain directly to LNs, where they can rapidly elicit T cell responses. Indeed, when the bacteria pseudomonas aeruginosa was injected subcutaneously into the footpad, it drained rapidly to LNs, where it could be sampled by LS-DC directly from the lymph (*9*). Similarly, multiple groups have shown that viruses such as Zika and Influenza can passively drain to the

lymph node through the lymphatics. There, they can pass through conduits into the TZ or accumulate in the medulla and captured by Res cDCs to initiate rapid T cell responses (*14*, *17*, *28*). In contrast, viruses that are tropic to the skin and do not readily disseminate, such as herpes simplex viruses (HSV) depend on the active transport of viral antigen to lymph nodes by Mig cDC (*15*).

PRR dependent activation of dendritic cells and monocytes. DCs express a diverse array of Pattern Recognition Receptors (PRR) that can sense a wide range of invading pathogens, and expression of PRRs is divergent between the cDC1 and cDC2 lineages. A primary set of PRRs are the toll-like receptors (TLRs), membrane-bound proteins capable of sensing a diverse array of microbial derived molecules, ranging from bacteria to viruses (*11*). TLRs can be located on the outer cell membrane, such as TLR4 (which senses the bacterial cell wall component LPS), or in intracellular vesicles, such as the TLRs 7,8, and 9 (which sense bacterial and viral derived nucleic acids). Although many other PRRs exist for the innate detection of pathogens, TLRs remain among the most important classes of such molecules yet discovered (*29*, *30*). According to the ImmGen consortium and other published sources, Res cDC2s express TLRs 4, 7, and 9, while Res cDC1s express TLRs 3 and 9. This divergent expression patterns dictate the ability of these cells to respond to specific pathogens and TLR agonists, thus further segregating the functional abilities of Res cDC1s and Res cDC2s (*5*, *6*).

Once antigen and adjuvant drain to LNs, it is available to be sensed by Res cDCs. Sensing involves the binding of a given TLR to its agonist, initiating a cascade of signaling that begins with the recruitment of the adaptor protein MyD88, or in the case of TLR3, TRIF. MyD88 activation leads to downstream activation of the transcription factor NF-κB, which can drive the

expression of multiple activation-associated cell markers critical for migration, cytokine production, and antigen presentation (*29*). This process in DCs is termed maturation and is a critical step in the ability of DCs to translate and communicate pathogen information to T cells. TLRs communicate information specific to a particular pathogen, so the resulting DC activation state is tailored to the TLR stimulated. For example, stimulation of TLR3 leads to enhanced production of Type I interferons, important for viral resistance, while TLR4 induces production of the cytokines IL-12 and TNF, both of which are important in instructing a Th1 cell fate (*5*, *29*, *31*, *32*). While direct sensing of pathogen derived material via TLRs is a critical first step in initiating the immune response, the secondary inflammatory mediators made in response to direct sensing act to further alert nearby cells to imminent threats (*33–35*). These secondary inflammatory mediators, such as Type I interferons (IFN-I) and tumor necrosis factor (TNF), allow for the initial sensors of inflammation to propagate that information and amplify it to the rest of the immune system. Receptors for these secondary inflammatory mediators are expressed widely on both hematopoietic and non-hematopoietic cells, thus the initial direct sensing of pathogens can be amplified to activate those cells that did not, or could not, directly sense the pathogen (*34*, *35*). While DCs can be activated by a wide range of direct and indirect stimuli, much is still unknown regarding the differences between the activation states induced by direct versus indirect inflammatory signals, what signals are absolutely required for full activation, and how combinatorial sensing of multiple stimuli influences the DC activation state and the downstream T cell priming capability. Furthermore, the separation of innate sensors coupled with the physical segregation of Res cDC subsets within LNs suggests that sensing of pathogens is also spatially separated. How this spatial separation influences the generation of the immune

response is unknown. How the direct versus indirect sensing of inflammation affects the activation and composition of the Res cDCs compartment will be explored in Chapter 4.

Crosstalk between innate and adaptive immune cells. At the center of innate/adaptive crosstalk is the cDC, which function as a professional "translator" passing antigen information and the nature of the incoming inflammation to T cells. This reputation is born from both extensive expression of PRRs, but also the high expression of major histocompatibility complex (MHC) -II and MHC-I, molecules critical for antigen presentation (*4*). Captured foreign antigens are processed and presented on MHC-II as well as cross-presented on MHC-I, whereas foreign intracellular proteins, such as those derived from viral replication, are mainly processed and directly presented on MHC-I (*5*, *6*). This antigen presentation, coupled with activation-dependent expression of costimulatory molecules and production of inflammatory cytokines, comprises the three canonical signals required for T cell activation. Historically, these interactions are thought to occur between a single T cell and DC in a complex known as the immunological synapse (*5*). While signal 1 and 2 are required for the general activation of a given T cell, signal 3 is what provides the inflammatory context by which T cells differentiate into a subset capable of mounting a tailored cellular immune response. Whether multiple different innate cell types can substitute the various signals required for T cell priming is debated. In numerous models, the inflammatory monocyte is capable of presenting antigen and producing cytokines that can direct T cell differentiation (*21*, *36*, *37*). While MO are capable of antigen presentation and effector cytokine production, their precise roles in T cell priming are often model specific and debated. While many studies have suggested that MO that traffic to LNs are inefficient APCs, other studies have suggested that MO possess APC ability comparable to bona fide cDCs (*21*, *22*). If

signals 1 through 3 can be provided by different innate cell types, then a given T cells differentiation could be controlled by the innate microenvironment surrounding it. The divergent PRR expression and differential steady state localization of Res cDC subsets strongly hints at the possibility of spatial niches where specific lineages of T cells are induced to differentiate. As described above, TLR sensing initiates cellular programming that leads to inflammatory cytokine production. Of note, TLR sensing is associated with Type 1 inflammation and cytokine production that drives the terminal differentiation of CD8+ T cells and T helper 1 (Th1) CD4+ T cells for the clearance of bacterial and viral infections (*38*). In contrast, Type 2 inflammation is thought to mainly be associated with danger associated molecular patterns (DAMPs) released by the activity of parasites or proteases that can physically damage cells. In contrast to the PAMPs that drive canonical Type 1 inflammation, the Type 2 inflammation driven by DAMPs leads to a divergent T cell response associated with distinct cytokine and effector functions (*38*). The focus of this dissertation is primarily on Type 1 inflammation and how it reconstructs LN organization, while Type 2 inflammation will be mostly used for contrast in Chapter 3. Understanding the spatial orchestration of T cell priming and differentiation and how Res cDCs and MO can cooperate to instruct these responses will be explored in Chapter 3.

T follicular helper cell differentiation and the role of B cells. B cells and Tfh cells have a highly interdependent relationship. Tfh cells provide help to antigen specific B cells in the form of IL-21 and CD40L, interactions that are necessary for B cell survival and differentiation into both GC and plasma cell fates (*39*, *40*). The differentiation of Tfh cells begins with cognate interactions between a naïve CD4+ T cell and an APC, canonically the cDC, but can also include B cells themselves. In particular, lack of strong IL-2 signaling allows newly activated T cells to

upregulate the master transcription factor controlling the Tfh cell fate, BCL-6 (*39*, *41*, *42*). In the presence of strong IL-2 signaling, T cells upregulate the transcription factor BLIMP-1, a potent repressor of BCL-6 and the Tfh lineage. BCl-6 expression then allows for the upregulation of CXCR5, which is critical for Tfh relocalization to the B cell follicles. Generally, cDCs are required for the initial differentiation of Tfh, but B cells are necessary for the full maturation of Tfh that go on to participate in the GC reaction (*40*, *42*). Beyond antigen presentation, DCs can produce membrane-bound and soluble forms of the high affinity IL-2 receptor CD25. Mig cDCs located at the TB border expressing CD25 act as an IL-2 sink, allowing T cells at the TB border to avoid IL-2 driven BLIMP-1 expression and instead upregulate BCL-6 (*43*). Once activated, ICOS-ICOSL interactions and IL-6 signaling are important for Tfh generation (*39*, *44*, *45*). The cellular sources for ICOSL and IL-6 is model specific and can include both B cells and cDCs (*46*, *47*). While CXCR5 is sufficient to drive Tfh to the TB border, ICOS-ICOSL interactions are necessary for follicular infiltration (*46*). Interestingly, these interactions occur in a non-cognate fashion between antigen specific T cells and bystander B cells, which constitutively express ICOSL. Furthermore, interactions between constituvely expressed PDL-1 on bystander B cells and PD-1 on T cells limits Tfh entry into follicles (*48*). Thus, bystander B cells can both positively and negatively regulate Tfh entry into the B cell follicles, acting as de facto follicular gatekeepers. In sum, B cells play a vital role in the differentiation of Tfh cells, and those interactions can occur in cognate and non-cognate fashions.

Lymph node microenvironments guide T cell differentiation. The LN is a highly organized and spatially regulated environment with cellular position governed by expression of distinct chemotactic receptors (*49*, *50*). In the absence of specific chemotactic receptor signaling, the

organization of the LN can be compromised, leading to intermixing of cells that normally reside in different zones. A classic example of this disorganization occurs in LNs from CCR7.KO mice, wherein cells of the immune system are unable to properly localize into distinct zones (*51*). While chemotactic receptor expression controls immune cells positioning at steady state, expression of these receptors changes dramatically during inflammation and can relocalize immune cells to different microenvironments within the LN. The ability of T cells to relocate to these different inflammatory microenvironments can influence the cells they interact with and the resulting signals they receive, thus instructing their differentiation and function. Under Type 1 inflammatory conditions, CD4+ T cells rapidly upregulate the chemokine receptor CXCR3, which relocalizes newly activated T cells from the deep TZ to the medulla, B cell follicles, and interfollicular areas (*52*). CXCR3 draws cells toward the chemokines CXCL9 and CXCL10, which were found to be differentially expressed by DCs and stromal cells in those regions outside of the deep TZ. When CD4+ T cells could not express CXCR3, they were unable to relocalize, and in turn, were found to be less Th1 differentiated than their CXCR3 competent counterparts (*52*). Additionally, it was found that CXCR3 directed anti-viral CD8+ T cells to different microenvironments in the LN that differentially directed the adoption of stem-like memory or effector fates (*53*). While these reports emphasize the ability of T cells to intranodally migrate to distinct microenvironments, T cells themselves can reorganize myeloid cells around them to create their own differentiation niche. Activated antiviral CD8+ T cells were found to produce chemokines that recruited both plasmacytoid dendritic cells (pDCs) and cDC1s (*54*). In these new inflammatory microenvironments, pDCs provide IFN-I to cDC1s that optimized their function and ability to interact with their T cell recruiter. Thus, T cells can both intranodally

migrate and recruit other immune cells to their location, creating unique niches that drive their differentiation.

In addition to microenvironments supporting the differentiation of inflammatory Th1 cells and cytotoxic T cells, LN microenvironments that support Th2 differentiation have been purported to exist in LNs. During nematode infection, it was found that both newly activated CD4+ T cells and DCs both upregulated CXCR5 and migrated intranodally to the T-B border (*55*). When both DCs and T cells were prevented from relocalizing in a CXCR5 dependent fashion, Th2 differentiation and IL-4 production was blunted. In addition to CXCR3 and CXCR5, the chemokine receptor EBI2 plays a major role in regulating T cell intranodal localization at steady-state and during inflammation (*25*, *43*, *56*). In the absence of inflammation, CD4+ T cells accumulate at the periphery of the T cell zone proximal to Res cDC2s in an EBI2-dependent fashion. During inflammation, this strategic localization allows for rapid interactions with Res cDC2s, leading to timely and efficient activation (*25*). Together, these reports suggest that microenvironments exist in LNs that support the differentiation of distinct T cell effector populations. If additional such LN microenvironments exist under different inflammatory conditions is not clear.

Objectives and significance

While there is a significant body of knowledge describing the differentiation of T cells under diverse inflammatory conditions, much less is known about the specific microenvironments where those responses are generated. Understanding the microanatomical organization of immunity could allow for the targeting of vaccines to recruit particular cell types or stimulate the

formation of distinct niches that drive a desired immune response. Overall, the objective of this thesis work was to identify and describe cellular microenvironments that influence T cell differentiation. Historically, visualizing the crosstalk between cDCs and T cells *in situ* has been difficult, owing to the limited number of markers able to be effectively imaged and the lack of analysis tools capable of processing such information. Here, we utilized highly multiplexed imaging and quantitation techniques to study the crosstalk between myeloid cells, T cells, and B cells. Overall, our data suggests that the spatial organization of cells during inflammation is critical in shaping the resulting immune response. The work here could potentially lead to innovative strategies to manipulate innate and adaptive immune microenvironments during vaccination and therapy to combat infection and disease.

Chapter 2. Materials and Methods

Mice

C57BL/6J, B6.129(Cg)-Ccr2tm2.1Ifc/J (CCR2-RFP), B6.Cg-Tg(Itgax-Venus)1Mnz/J (CD11c-YFP), B6(Cg)-Tyrc-2J/J (B6 albino), B6.Cg-Zbtb46tm4.1(HBEGF)MnzTyrc-2J/J (Zbtb46-DTR), B6.129P2(C)-Ccr7tm1Rfor/J (CCR7.KO), B6.129S1-Il12btm1Jm/J (IL-12p40.KO), B6.129S4-Ccr2tm1Ifc/J (CCR2.KO), B6.129P2(SJL)-Myd88tm1.1Defr/J (MyD88.KO), and B6.129S2-Ighmtm1Cgn/J (uMT) mouse strains were obtained from The Jackson Laboratory. CD45.1+ B6.Cg-Tg(TcraTcrb)425Cbn/J (OT-II), CD45.1+ C57BL/6-Tg(TcraTcrb)1100Mjb/J (OT-I), and B6.SJL-PtprcaPepcb/BoyCrl (CD45.1+) were obtained either from donating investigators (Dr. Pamela J. Fink, University of Washington) or Charles River. CD11c-YFP animals were crossed with B6 albino mice to homozygosity, and next crossed to CCR2-RFP mice to generate a CD11c-YFP x CCR2-RFPHetrozygous dual reporter mice. CCR2-DTR mice were obtained from donating investigators (Dr. Steven F. Ziegler, Benaroya Research Institute) and with approval from the originating investigators (Drs. Tobias M. Hohl and Eric G. Pamer, Memorial Sloan-Kettering Cancer Center) (95). 6–10-week-old male and female mice were kept in specific pathogen–free conditions at an Association for Assessment and Accreditation of Laboratory Animal Care–accredited animal facility at the University of Washington, South Lake Union campus. All procedures were approved by the University of Washington Institutional Animal Care and Use Committee.

Bone Marrow Chimeras and Adoptive Transfers

For BMCs, C57BL/6 mice were exposed twice to 600 rads of gamma irradiation from a cesium source separated by a 3-hour rest period, and injected with 2x106 donor BM cells intravenously the same day. Mice were kept on neomycin for 3 weeks or Baytril for 2 weeks, and used experimentally at least 6 weeks after transplant.

For CCR7 BMCs, irradiated recipients were reconstituted with a 50:50 mix of CCR7.KO or C57BL/6 and Zbtb46-DTR BM. For IL-12p40.KOs, irradiated recipients were reconstituted with IL-12p40.KO BM. For IL-12p40.KO:CCR2-DTR mixed BMCs, a 50:50 mix of IL-12p40.KO or C57BL/6 and CCR2-DTR BM was used for reconstitution. For CCR2.KO:IL-12p40.KO mixed BMCs, a 50:50 mix of CCR2.KO or C57BL/6 and IL-12p40.KO BM was used for reconstitution. For CCR7.KO:WT mixed BMCs, irradiated recipients were reconstituted with a 50:50 mix of congenically marked CCR7.KO BM and C57BL/6 BM. For uMT BMCs, irradiated recipients were reconstituted with a 20:80 mix of CCR7.KO, C57BL/6, or MyD88.KO and uMT BM. For WT:MyD88.KO and WT:IFNAR.KO mixed BMCs, a 50:50 mix of either MyD88.KO or IFNAR.KO and C57BL/6 BM was used for reconstitution. In experiments using DTR BMCs, mice were administered with DT in phosphate-buffered saline (PBS) at 20 ng / g bodyweight intraperitoneally every 2d. For adoptive transfers, naïve CD45.1+ OT-II or CD45.1+ OT-I T cells were isolated from LNs and spleens using either the Naïve CD4+ or CD8+ T cell isolation kits (Miltenyi Biotec), respectively. Average purity of OT-II and OT-I cells was about 75% and 90%, respectively. The indicated number of cells were transferred into CD45.2+ C57BL/6 hosts intravenously.

Immunizations and Infections

The following adjuvants and amounts per immunization site were used: 20 µg CpG ODN 1668 (AdipoGen), 10 µg R848 (Invivogen), 10-20 µg poly(I:C) or 'p(I:C)' (Amersham), 10 µg Lipopolysaccharides (LPS) from Escherichia coli O111:B4 (Sigma-Aldrich), 20 µg flagellin (FliC) from Salmonella enterica Typhimurium (kind gift from Kelly D. Smith, University of Washington) (96), Alhydrogel or 'Alum' (Invivogen) diluted 1:2 with PBS, 50 µg papain (Sigma-Aldrich), and Addavax (Invivogen) diluted 1:2 with PBS. Except for Alum and Addavax, the indicated adjuvants were mixed with PBS (20 µl total volume). All adjuvants were injected in either the front or hind footpads, or intradermally in the ear pinnae (brachial, popliteal, or auricular dLNs, respectively) as indicated. In indicated studies, the immunized ear pinnae were surgically removed 1-2 hours post immunization.

In some studies, ~1.2x107 heat-killed Escherichia coli BioParticles (ThermoFisher) in 20 µl of PBS were injected into the ear. For West Nile Virus infections, 100 plaque forming units (pfu) of West Nile virus (Texas strain) in 20 µl of PBS were injected into the footpad. For Nippostrongylus brasiliensis infections, infectious third-stage larvae (L3) were raised and maintained as described (97). Mice were infected subcutaneously at the base of the tail (dLN, inguinal) with 500 Nippostrongylus brasiliensis L3.

For in vivo antibody blocking studies, 100 µg anti-CD62L (clone Mel-14, BioXCell) and/or 100 µg anti-PSGL-1 (clone 4RA10, BioXCell) were injected intraperitoneally at the time of immunization. In some experiments, 20 µg of MC-21 CCR2-blocking antibody (kind gift from Matthias Mack, University Hospital Regensburg) was injected intraperitoneally at the time of

immunization, and administered daily for up to 3 days after (98). Intravascular labeling was achieved by injecting 2.5 μg of CD45.2-PE antibody 10 min prior to animal euthanasia (99). OVA immunizations used endotoxin-free OVA (InvivoGen), either 1 or 10 μg, as indicated, along with 20 μg of CpG or p(I:C). In some studies, 1 ug recombinant LCMV pre-glycoprotein GP complex (GPC, 10-90aa) (MyBioSource) along with 20 μg of CpG was injected intradermally in the ear pinnae. For antigen presentation studies, 10 μg of LPS-free EαGFP (gift from Marc K. Jenkins, University of Minnesota) plus 20 μg of CpG were injected intradermally in the ear pinnae.

Antibodies and Staining Reagents

Antibodies used for staining sections for confocal imaging or isolated cells for flow cytometry include: CD64 (clone X54-57.1; BioLegend), B220 (clone RA3-6B2; eBioscience), CD3 (clone 17A2; BD), SIRPa (clone P84; BD), CD169 (clone 3D6-112; BioLegend), CD11c (clone N418; eBioscience), CD11b (clone M1/70; eBioscience), Collagen IV (rabbit polyclonal; Abcam), MHC-II (clone M5/114.15.2; BioLegend), IRF4 (clone IRF4.3E4; BioLegend), CD45.1 (clone A20; BioLegend), Ki67 (clone B56; BD Pharmingen), Y-Ae (clone eBioY-Ae; eBioscience), CD3 (clone 17A2; BioLegend), CD69 (clone H1.2F3; BioLegend), CD62L (clone Mel-14; BD Biosciences), CD8 (clone 53-6.7; BioLegend), Ly6C (clone HK1.4; BioLegend), IL-12p40 (clone C15.6; BioLegend), Tbet (clone 4B10; BioLegend), TCF1 (clone C63D9; Cell Signaling), CCR7 (clone 4B12, Biolegend), NK1.1 (clone PK136; BioLegend), CD19 (clone 6D5; BioLegend), CD44 (clone IM7; BioLegend), Ly-6G (clone 1A8; BD Biosciences), XCR1 (clone ZET; BioLegend), IFN□ (clone XMG1.2; eBioscience), GATA3 (clone L50-823; BD Biosciences), IL-2 (clone JES6-5H4; BioLegend), CXCR3 (clone CXCR3-173; BioLegend),

CXCR5 biotin (clone 2G8; Fisher Scientific), pS6 (clone 2F9; Cell Signaling), PD-1 (clone RMP1-30; BioLegend), CD45.2 (clone 104; eBioscience), CD25 (clone PC61; BioLegend), F4/80 (clone BM8; eBioscience), TNFα (MP6-XT22; BD Pharmingen), EpCAM (clone G8.8; eBioscience), CD103 (clone 2E7; BD Biosciences), CD301b (clone MGL2; BioLegend), CD115 (clone CSF-1R; BioLegend), CD26 (clone: H194-112; BioLegend), CD88 (clone 20/70; BioLegend), and Ly-6B.2 (clone 7/4; Novus Biologicals).

For 2-photon intravital microscopy studies, CD90.2 (clone 30-H12; BioLegend), CD31 (clone 390; BioLegend), and Dextran-FITC (70,000 MW; Molecular Probes) were used.

ELISA

For ELISA experiments, dLNs from each mouse were harvested into 1x PBS in Precellys Soft tissue homogenizing tubes (Bertin Corp), and then homogenized for 20 seconds at 5500 rpm in a Precellys 24 Tissue Homgenizer (Bertin Corp). Tubes were then spun at 15000 rpm for 10 minutes at 4°C, and supernatants were concentrated to 50ul using Microcon 30kDa columns (EMD Millipore). ELISA assay was then performed on concentrated supernatants using the Mouse IL-12 p70 Quantikine ELISA kit (R&D Systems), using the manufacturer's described protocol.

Confocal and two-photon intravital microscopy

For confocal imaging, isolated LNs were fixed using Cytofix (BD Biosciences) buffer diluted 1:3 with PBS for 12h at 4o C and then dehydrated with 30% sucrose for 12-24h at 4o C. Tissues were then embedded in O.C.T. compound (Tissue-Tek) and stored at -80o C. LNs were sectioned

on a Thermo Scientific Microm HM550 cryostat into 20um sections and were then prepared and imaged as previously described [10]. A Leica SP8 tiling confocal microscope equipped with a 20x 0.7NA or 40x 1.3NA oil objectives were used for confocal image acquisition.

For two-photon intravital microscopy, immunized or control mice were anesthetized using an isoflourane vaporizer and popliteal LNs were surgically exposed. Imaging was done as previously described (6) using a Leica SP8 tiling confocal microscope outfitted with a Chameleon laser and a 20x, 1.0 NA water immersion objective. In some experiments, mice were administered dextran-FITC i.v. 1h prior to imaging to visualize the vasculature. All acquired raw imaging data was processed and analyzed in Imaris (Bitplane).

Histocytometry analysis

Histocytometry analysis was performed as previously described (7, 10), with some modifications. Multiparameter confocal images were corrected for fluorophore spillover using the built-in Leica Channel Dye Separation module. For acquisition of single stained controls, UltraComp eBeads (Invitrogen) were incubated with fluorescently conjugated antibodies, mounted on slides, and imaged. All images were visualized and analyzed in Imaris. Myeloid cell isosurface objects were created separately on CD11c, MHC-II, and CD64 signal using the surface object creation wizard in Imaris, as previously reported (10). In some analyses, histocytometry gating was further used to discriminate cDC2 and cDC1 populations using SIRPa and Clec9a markers, respectively. For some experiments, a combined myeloid cell channel was first created by adding normalized signals for SIRPa, CD11c, MHC-II and CD64 using the Imaris XT channel arithmetic module, and this sum channel was then used for object creation. For histocytometry involving T cells, objects were created directly using the congenic CD45.1

signal. Alternatively, all proliferating cells within the LN were analyzed by creating objects using the Ki67 signal. Object statistics were then exported to FlowJo software for gating and phenotypic characterization. TZ borders were manually created using B220 (B cell follicles), CD3 (T cell zone), and CD64 super bright staining (medullary macrophages), and the Spot creation function in Imaris. In some analyses lacking explicit B220 and CD3 staining, TCF1 and MHC-II were used for demarcating the TZ borders. Positional data for the spot objects were exported to FlowJo to generate a spatial T zone gate. TZ localization was calculated as the frequency of a given cell population found within the T zone gate. Cell distances from the deep TZ center were calculated in CytoMAP (25). Spatial correlation analysis was also performed in CytoMAP. In brief, position of all myeloid cells in LNs were spatially segmented into 30 □m radius neighborhoods and the Pearson correlation coefficient was calculated between the number cells of the different cell types in these neighborhoods.

Cell isolation and flow cytometry

For myeloid cells, tissues were disrupted and treated with 400 U/ml collagenase D (Roche Applied Science) solution for 30 min at 37o C with periodic agitation. In some studies, enhanced digestion was used for increased cell yield, as described (97, 98). Flow cytometry studies conducted on T cells did not use enzymatic digestion. Cell staining was conducted at 4o C for 30 min, except for: LCMV GP 66-77 tetramer (NIH Tetramer Core) - room temperature (RT) for 1 hr, CXCR5 - RT for 45 min, CCR7 - 37o C for 30 min. For T cell cytokine production, cells were restimulated with 100 ng/ml of phorbol 12-myristate 13-acetate (PMA), 1 μg/ml ionomycin (Sigma-Aldrich), and 1 μg/ml GolgiStop (BD Biosciences) in cRPMI media for 4-5 h at 37°C. For myeloid cell cytokine production, cells were stained in media containing GolgiStop, without

restimulation. FoxP3 Fix/Perm kit (Invitrogen) was used. Data was acquired on an LSR-II flow cytometer (BD Biosciences) and analyzed using FlowJo software (TreeStar).

Statistics

Statistical analysis was performed using GraphPad Prism software. The statistical significance of differences in mean values between two groups was analyzed by a two-tailed unpaired Student's t test with Welch's correction. When analyzing data with multiple side-by-side groups, a one-way ANOVA with Tukey's multiple comparisons test. In multi-adjuvant comparison studies where variance between groups could not be assumed to be equal, the Brown-Forsythe and Welch ANOVA tests with Dunnett's multiple comparison tests were performed. Paired t test was performed only when comparing responses within the same experimental animal or tissue. In bar graphs for all figures, bars represent data mean. Error bars represent standard deviation. ****, $P \leq 0.0001$; ***, $P \leq 0.001$; **, $P \leq 0.01$; *, $P \leq 0.05$; NS, $P > 0.05$. In all figures, unless otherwise noted, data points represent independent LNs.

Experimental design

Experimental animals were randomly allocated into treatment groups. The investigators were not blinded to allocation during experiments and outcome assessment. No statistical method was used to predetermine sample size. All experiments were repeated at least two independent times. No outliers were removed.

Chapter 3. Innate cell microenvironments in lymph nodes shape the generation of T cell responses during Type-I inflammation

This chapter is adapted from the following publication:

J. M. Leal*, J. Y. Huang*, K. Kohli*, C. Stoltzfus, M. R. Lyons-Cohen, B. E. Olin, M. Gale Jr., M. Y. Gerner, Innate cell microenvironments in lymph nodes shape the generation of T cell responses during type I inflammation. Sci. Immunol. 6, eabb9435 (2021). Reprinted with permission from AAAS.

* The following individuals contributed equally to this work

Introduction

Spatiotemporal coordination and crosstalk between various innate and adaptive immune cells is critical for timely generation of protective immunity (*57*). During infection or vaccination, conventional dendritic cells (cDCs) migrate from peripheral tissues to draining LNs (dLNs) in a C-C chemokine receptor type 7 (CCR7) dependent manner to present captured antigens on major histocompatibility complexes (MHC) to induce T cell responses (*5*, *12*, *26*, *58*). In addition, much faster transport of microbes, vaccine components and soluble antigens into dLNs occurs via lymphatic transport (*7*, *9*, *59*, *60*). Within LNs, steady-state LN-resident cDCs (Res cDC), and in particular Res cDC2s, localize near lymphatic sinuses (*8*). This promotes robust sampling of draining antigens, and in combination with the enhanced capacity of cDC2s for MHC-II presentation, allows efficient induction of CD4 T cell responses (*7*, *9*, *59*). Res cDC1s, cells specialized in MHC-I cross-presentation, are more homogeneously distributed throughout the TZ (*8*, *54*, *61*). This reduces efficiency of antigen capture after subunit vaccination (*7*, *9*), and instead promotes the interception of infected migratory cDCs and dying cells, leading to enhanced CD8 T cell responses during viral infections or cancer (*62–64*).

In response to Toll-like receptor (TLR) stimulation, cDCs increase expression of costimulatory molecules and produce various inflammatory cytokines, such as interleukin 12 (IL-12), to elicit the differentiation of effector T cells (*5*). Current models propose that a single cDC delivers all three signals (peptide-MHC, costimulation and polarizing cytokines) to cognate T lymphocytes to induce their programming (*5*). However, T cells can also integrate signals from serial interactions with multiple cDCs or other innate cell populations (*62*, *63*, *65*). In particular, inflammatory monocytes (MOs) can migrate to dLNs after infection or vaccination to modulate T cell responses (*21*, *36*, *37*). Detailed mechanisms of whether MOs transport antigens from peripheral tissues or

directly traffic into LNs via high endothelial venules (HEVs), and if they present antigens or promote cytokine-driven T cell responses are less clear (*21*, *22*, *36*, *37*, *66–68*).

Even at steady state, myeloid cells generate intricate spatial patterns within LNs (*4*, *8*, *69*). During inflammation, they can undergo further reorganization and together with influx of new myeloid cells are likely to generate additional microenvironments (*14*, *54*, *70*). T cells activated within different microenvironments may thus receive distinct stimuli and undergo divergent programs of activation. This is supported by substantial heterogeneity in clonal expansion and effector differentiation observed for individual T cells bearing identical T cell receptors (TCRs) (*71–74*). However, studying how local tissue microenvironments influence T cell priming has been challenging, as this requires use of advanced in situ imaging approaches capable of simultaneously mapping multiple myeloid and lymphoid cell populations, as well as their activation, differentiation, and functional states.

Here, we utilized advanced analytical imaging to characterize the spatial organization of innate and adaptive responses in dLNs during Type-I or Type-II inflammation elicited with distinct vaccine adjuvants or infections (*38*, *75–77*). We found that Type-I inflammation was associated with a signature of myeloid cell organization in dLNs, with rapid repositioning of Res cDCs from the LN periphery into the deep TZ, as well as robust infiltration of the TZ by inflammatory MOs. These changes were not observed during Type-II inflammation, suggesting specificity in myeloid cell patterning based on inflammatory conditions. Within the TZ, spatially juxtaposed Res cDCs and MOs functionally cooperated with one another, providing complementary stimuli to T cells to promote optimization of cellular responses. Moreover, MO infiltration was nonuniform across the LNs, leading to the formation of MO-rich vs cDC-dominated microenvironments. Priming of T cells within these different microenvironments led to generation of distinct early effector

populations, allowing for formation of effector heterogeneity. Thus, our findings reveal a signature of myeloid cell organization during Type-I inflammation, as well as demonstrate that innate cell microenvironments influence the magnitude, quality, and heterogeneity of adaptive responses.

Results

DC relocalization and Monocyte influx in LNs during Type-I inflammation

We previously reported that preferential localization of Res cDC2s in lymphatics-proximal regions promoted robust T cell responses to subunit vaccination (*7*, *9*, *25*). However, naïve T cells primarily reside in the TZ, and how efficient T cell activation was achieved remained unclear. One possibility is that during inflammation, innate cells are spatially reorganized to promote physical interactions with T cells. To investigate how intranodal positioning of myeloid cells changes during inflammation, we injected mice with a broad array of vaccine adjuvants, including Type-I inflammatory TLR agonists: CpG (TLR9), R848 (TLR7/8), Flagellin (TLR5), LPS (TLR4), and pIC (TLR3); Type-II adjuvants: Alhydrogel (Alum) and Addavax (MF59 analog), as well as the protease allergen, papain. Adjuvants were initially used as they are clinically relevant and have well-defined drainage and inflammatory properties. One day post immunization (subcutaneous, footpad or intradermal), dLNs were isolated and the localization of myeloid cell subsets was visualized with multiparameter confocal imaging and analyzed with histocytometry. Multiplexed staining for CD11c, MHC-II, CD169, CD64, SIRPa, Clec9a and other myeloid markers allowed clear discrimination of migratory and Res cDC populations as well as other myeloid cell types (fig. S1A and table S1). We observed that all tested TLR agonists elicited marked repositioning of Res cDC2s from the peripheral LN regions into the deep TZ (Fig. 1A). This was quantified using a

positional TZ gate generated with CD3 and B220 staining delineating the B cell follicles and TZ, respectively (Fig. 1B and fig. S1B). Although Res cDC1s were less abundant in the lymphatics-proximal regions as compared to cDC2, these cells re-localized to the deep TZ after TLR agonist immunization (Fig. 1, A and B). cDC repositioning was similarly detected by calculating the distance of cells from the deep TZ (fig. S2A). As expected, after repositioning, Res cDC1s and cDC2s did not occupy the same regions within the TZ (Fig. 1A and fig. S2A), supporting previous observations of Ebi2-mediated compartmentalization (*56*, *78*). Notably, none of the tested Type-II stimuli elicited Res cDC repositioning, suggesting that this response is specific to Type-I inflammatory conditions (Fig. 1, A and B, and fig. S2, B and C). Kinetics studies revealed that Res cDC relocalization began by 9h post immunization (Fig. 1C and fig. S2D), indicating that this was a relatively rapid phenomenon likely associated with the drainage of soluble TLR agonists into the dLNs (*79*).

In addition, TLR agonist immunization elicited the appearance of large numbers of $CD64^{+}SIRPa^{+}CD169^{-}$ cells, markers associated with inflammatory MOs (*80*, *81*), within the deep TZ of dLNs (Fig. 1A and B, and fig. S2A). This was confirmed by flow cytometry, which demonstrated robust influx of $Ly6C^{+}CD64^{+}CD11b^{+}Ly6G^{-}CD3^{-}CD19^{-}NK1.1^{-}$ MOs into immunized dLNs (fig. S2E-G and table S1), beginning as early as 8h, and peaking at 12-16h post immunization (Fig. 1, C and D, and fig. S2D). Some differences in MO recruitment between the different TLR-agonists were noted, with LPS inducing comparably lower responses. Minor increases in MO number were also seen after papain administration, albeit these cells did not efficiently penetrate the deep TZ (Fig. 1, A and B). Both the centralization of Res cDCs and presence of MOs within the TZ were observed on day 2 post immunization (see below), suggesting that Type-I inflammation is associated with lasting changes in the composition and organization

of innate cells within the dLNs. Immunization also led to increased number of migratory cDCs, and as expected these cells were localized within the TZ (fig. S2, A and H).

We next investigated whether these phenomena also applied to the Type-I inflammatory settings seen during infection. Indeed, robust Res cDC relocalization and MO recruitment were seen after administration of heat-killed *Escherichia coli* (fig. S2I) and after West Nile virus infection (Fig. 1, E and F). In contrast, infection with *Nippostrongylus brasiliensis*, which is associated with Type-II inflammation, did not elicit these effects in skin-draining LNs (fig. S2J). Together, these data demonstrated that Type-I inflammation induced by TLR-agonist administration, bacterial inoculation, and West Nile virus infection induced the redistribution of Res cDCs into the deep TZ and robust recruitment of MOs into the dLN.

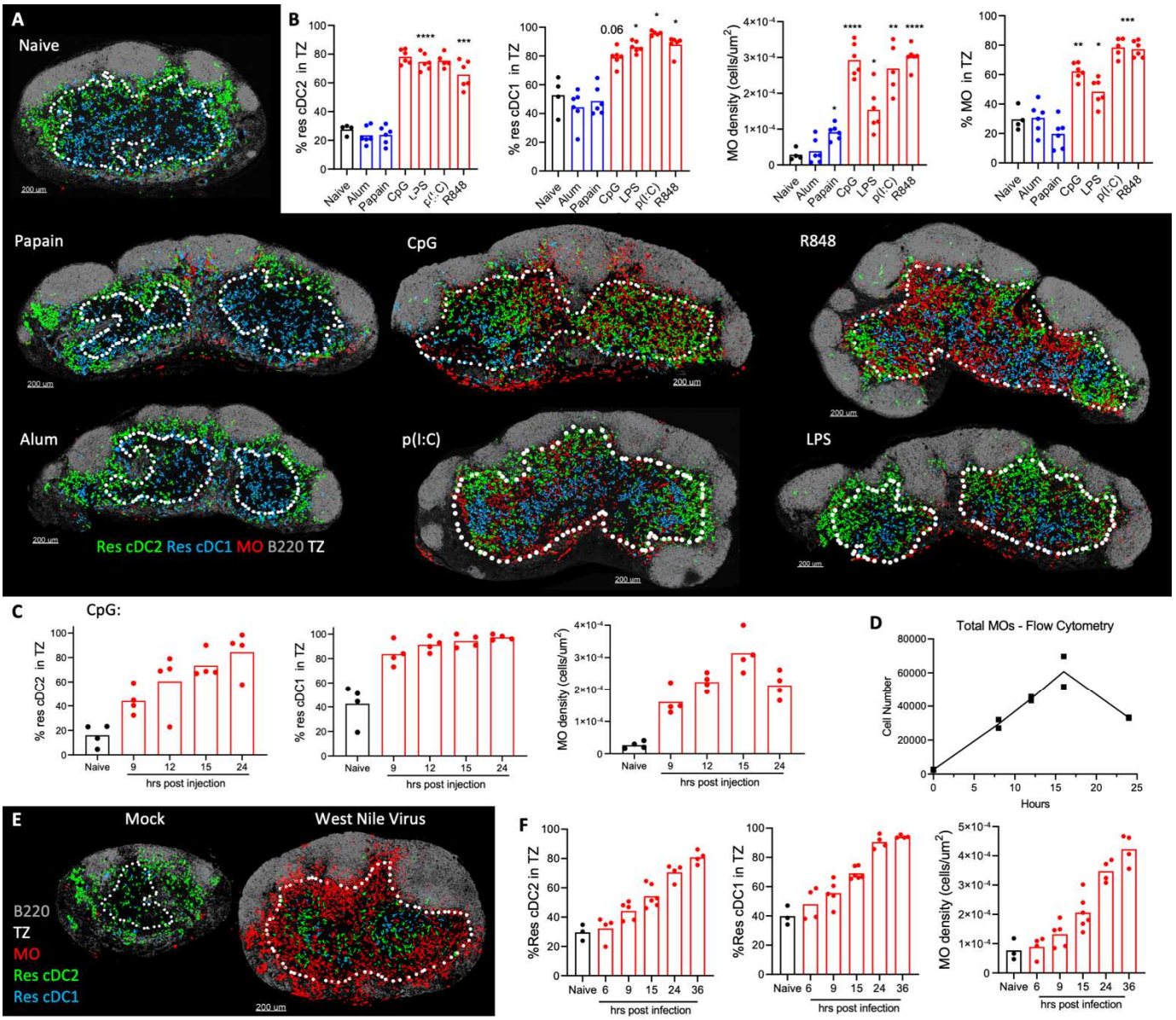

Fig. 1. MO influx and Res cDC TZ relocalization during type 1 inflammation. (**A** and **B**) B6 mice were injected in the ears with the indicated adjuvants, and dLNs were analyzed 24 hours later by histocytometry. (A) Representative images depicting Imaris 3D surfaces for indicated cell types, overlayed with B220 staining. White circles denote the TZ boundary (see fig. S1A for gating). (B) Frequency of Res cDCs and MOs within the TZ, as well as MO density. Data analyzed using Brown-Forsythe and Welch ANOVA tests with Dunnett's multiple comparison. (**C** and **D**) B6 mice were immunized with CpG in both ears, and dLNs were analyzed at indicated time points. (C) Histo- cytometry for Res cDC localization and MO density. (D) MOs in dLNs enumerated by flow cytometry. Data representative of five independent experiments. (**E** and **F**) B6 mice were infected in the footpad with 100 PFU of West Nile virus TX, and dLNs were analyzed by histocytometry. (E) Representative images from mock infected and 36 hours after

infection. (F) Localization of Res cDCs and MO density at the indicated time points. Scale bars, 200 μm. Data represent at least two independent experiments.

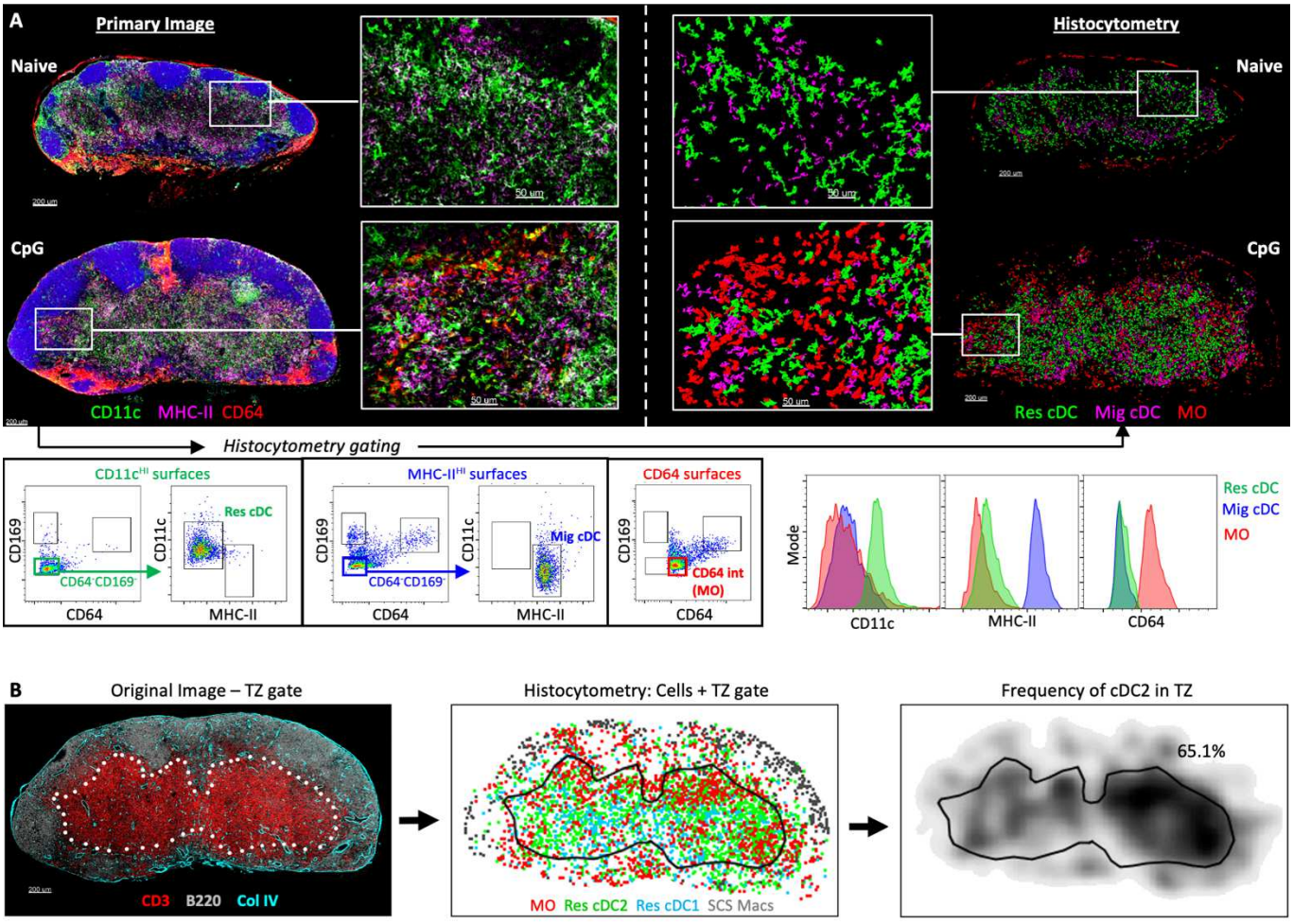

Fig. S1. Histocytometry analysis of myeloid cell positioning.
(A) B6 mice were injected in the ears with CpG and dLNs were harvested 24 hours later for imaging. Representative staining for the indicated cell markers is shown (top left). Surface objects were next created using CD11c, MHC-II, and CD64 channels and exported for histocytometry analysis. Histocytometry gating scheme demonstrates identification of Res cDCs, migratory cDCs (Mig cDC), and MOs (bottom dot plots), as well as analysis of indicated marker expression (bottom histograms). These populations were next positionally mapped to visualize cell distribution (top right). Zoom-in panels demonstrate congruency between the original image (top left) and histocytometry data (top right). **(B)** Representative TZ gating scheme. Both CD3 and B220 markers were used to identify the border of the TZ within the primary image, and the positional data of this TZ boundary was exported to FlowJo for spatial gating of the myeloid cell populations via histocytometry. SCS Macs, subcapsular sinus macrophages.

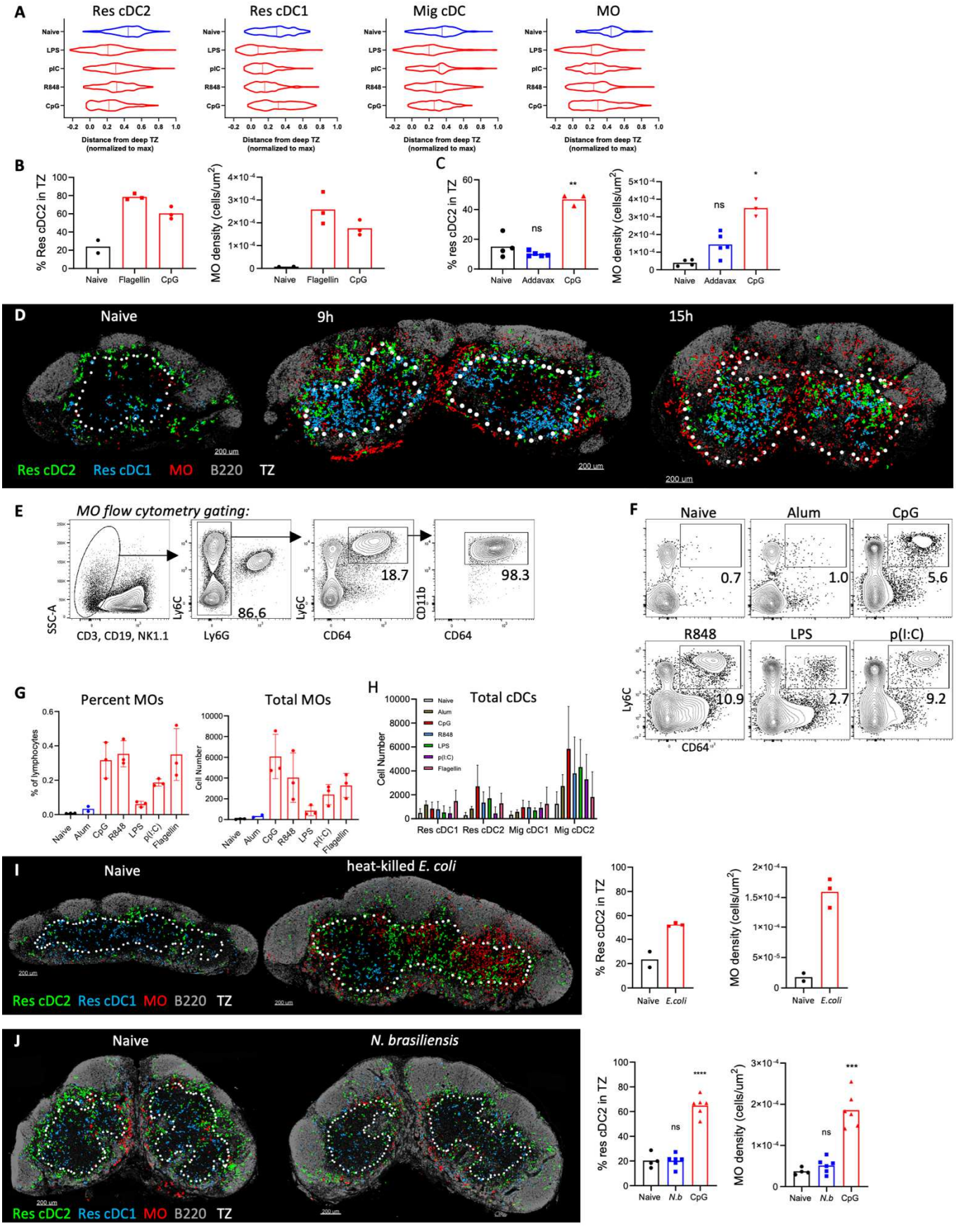
A
Res cDC2
Res cDC1
Mig cDC
MO
Naive
LPS
pIC
R848
CpG
Distance from deep TZ (normalized to max)
B
% Res cDC2 in TZ
MO density (cells/um2)
Naive
Flagellin
CpG
C
% res cDC2 in TZ
MO density (cells/um2)
ns
**
*
Naive
Addavax
CpG
D
Naive
9h
15h
200 um
Res cDC2
Res cDC1
MO
B220
TZ
E
MO flow cytometry gating:
SSC-A
CD3, CD19, NK1.1
Ly6C
Ly6G
86.6
CD64
18.7
CD11b
98.3
F
Naive
Alum
CpG
R848
LPS
p(I:C)
0.7
1.0
5.6
10.9
2.7
9.2
Ly6C
CD64
G
Percent MOs
% of lymphocytes
Total MOs
Cell Number
Naive
Alum
CpG
R848
LPS
p(I:C)
Flagellin
H
Total cDCs
Cell Number
Naive
Alum
CpG
R848
LPS
p(I:C)
Flagellin
Res cDC1
Res cDC2
Mig cDC1
Mig cDC2
I
Naive
heat-killed E. coli
200 um
Res cDC2
Res cDC1
MO
B220
TZ
% Res cDC2 in TZ
MO density (cells/um2)
Naïve
E.coli
J
Naive
N. brasiliensis
200 um
Res cDC2
Res cDC1
MO
B220
TZ
% res cDC2 in TZ
MO density (cells/um2)
ns
****
***
Naive
N.b
CpG

Fig. S2. Analysis of myeloid cell recruitment and localization within LNs in response to various stimuli.
(A) Positional data for histocytometry-gated cell populations were imported into CytoMAP and cell distances from the deep TZ center were calculated. Violin plots demonstrate the distribution of different cell types in representative LNs (images shown in Fig. 1A) after injection with the indicated adjuvants. For comparison of LNs of varying sizes, cell distances were normalized to the maximum possible distance for each tissue. Positive values represent cells outside of the deep TZ boundary; negative values represent cells within the deep TZ boundary. **(B)** B6 mice were administered flagellin or CpG in the ears. Frequency of Res cDC2s within the TZ and MO density in dLNs was quantified by histocytometry 1 day later. **(C)** B6 mice were immunized with Addavax or CpG in the ears and footpads. Percentage of Res cDC2s in the TZ and MO density in dLNs was assessed by histocytometry 1.75 days later. ns, not significant. **(D)** Additional imaging data for the experiment presented in Fig. 1C, showing representative dLNs after CpG immunization at the indicated time points. **(E)** Representative flow cytometry gating scheme for MOs 1 day after CpG injection. **(F** to **H)** B6 mice were immunized with the indicated adjuvants in the ears and footpads and dLNs were harvested for flow cytometry 1 day later. (F) Representative flow cytometry plots of MOs, as well as (G) quantification of the frequency and total number of MOs per dLN. Cells in flow plots were first pre-gated on $CD3^{-}CD19^{-}NK1.1^{-}$ $Ly6G^{-}CD11b^{+}$ populations. (H) Total number of Res and Mig cDC subsets in dLNs. For each group, n = 3 to 4. **(I)** B6 mice were injected in the ears with heat-killed *Escherichia coli* (*E. coli*). Res cDC localization and MO density in dLNs was quantified by histocytometry 1 day later. **(J)** B6 mice were infected with 500 *Nippostrongylus brasiliensis* (*N.b.*) worms, or injected with 40 μg of CpG, subcutaneously in the tail base. Inguinal dLNs were assessed by histocytometry 36 hours later for Res cDC localization and MO density. In (C) and (J), data analyzed by Brown-Forsythe and Welch ANOVA tests with Dunnett's multiple comparison. In (D), (I), and (J), Imaris-generated 3D surfaces are shown depicting the indicated cell types. Each point represents an independent LN. All data represent at least two independent experiments.

CCR7-mediated Res cDC intranodal repositioning during inflammation

We hypothesized that intranodal Res cDC repositioning was driven by chemotaxis (*82*). Peripheral tissue cDCs up-regulate CCR7 expression for migration into the dLNs (*13*, *51*). Splenic cDCs also utilize CCR7 to relocalize into the white pulp during systemic inflammation (*31*, *56*, *78*, *83*, *84*). We thus examined CCR7 expression on Res cDCs after immunization. We found that after Type-I, but not Type-II, adjuvant administration CCR7 expression was markedly increased on both Res cDC subsets (Fig. 2, A and B, and fig. S3A). This was also associated with higher surface expression of MHC-II, indicative of Res cDC maturation (Fig. 2A and fig. S3A). Both CCR7 and

MHC-II expression increased as early as 4h post immunization, and rapidly approached levels found on migratory cDCs (Fig. 2A). In contrast, expression of Ebi2, which can also influence cDC localization, was not substantially changed with immunization (fig. S3B).

To test the role of CCR7 in intranodal relocalization of Res cDCs, we generated mixed bone marrow chimeras (BMCs) consisting of a 50:50 mix of CCR7.KO, or control WT, and *Zbtb46*-DTR BM (fig. S3C). This allowed specific depletion of *Zbtb46*-DTR donor cDCs using diphtheria toxin (DT), while leaving the CCR7.KO (DC-CCR7.KO) or control WT (DC-WT) cDCs intact (*43*, *85*). This setup maintains normal LN architecture (fig. S3D), which is otherwise disrupted in CCR7 deficient animals (*51*). No notable changes in the total number of Res cDCs or the size of the LNs were detected between DC-CCR7.KO and DC-WT BMCs after DT administration, though as expected, migratory cDCs were absent in the DC-CCR7.KO LNs (fig. S3D). The DC-CCR7.KO and DC-WT mice were treated with DT and one day later immunized with CpG (fig. S3C). Disruption of CCR7 upregulation after immunization in DC-CCR7.KO was verified by flow cytometry (fig. S3E). As expected, Res cDCs in the control DC-WT BMCs efficiently relocalized into the deep TZ. In contrast, Res cDCs in DC-CCR7.KO BMCs were largely excluded from the TZ, and instead were frequently observed proximal to B cell follicles and medullary sinuses (Fig. 2, C and D, and fig. S3F). In contrast to cDCs, MOs still efficiently infiltrated the TZ in DC-CCR7.KO dLNs (fig. S3G), indicating that MO trafficking to and localization within dLNs was not interdependent with Res cDC repositioning. Mixed BMCs, consisting of a 50:50 mix of CCR7.KO and WT BM, also showed that CCR7.KO MOs did not display major defects in TZ infiltration (fig. S3H), confirming previous reports that MOs do not require CCR7 for migration into LNs (*37*, *66*). Collectively, these data demonstrated that during Type-I inflammation,

upregulation of CCR7 expression by Res cDCs leads to intranodal relocalization from the LN periphery into the deep TZ.

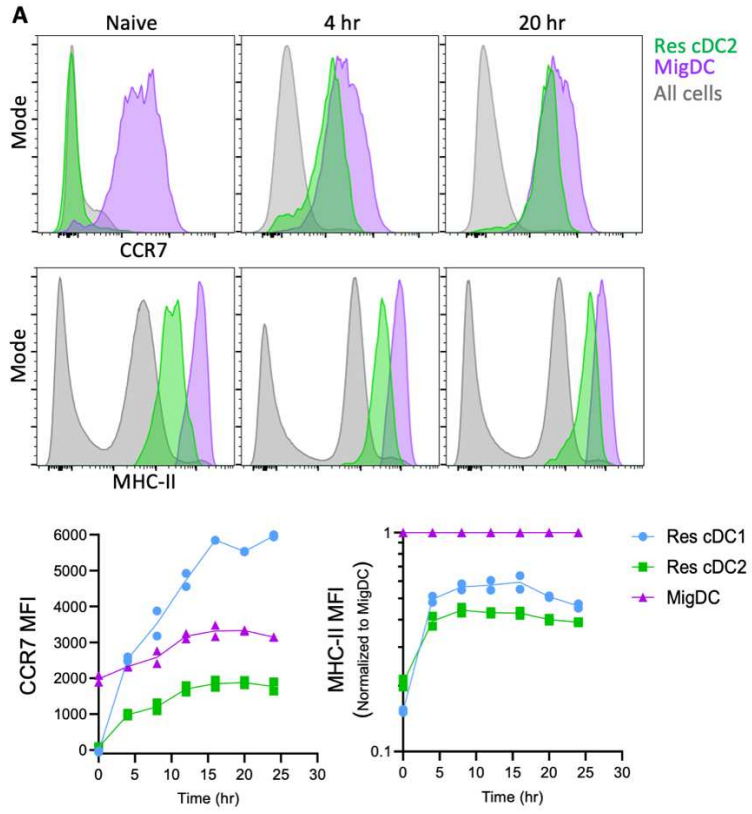
A
Naive
4 hr
20 hr
Res cDC2
MigDC
All cells
Mode
CCR7
Mode
MHC-II
CCR7 MFI
Time (hr)
MHC-II MFI
(Normalized to MigDC)
Time (hr)
Res cDC1
Res cDC2
MigDC

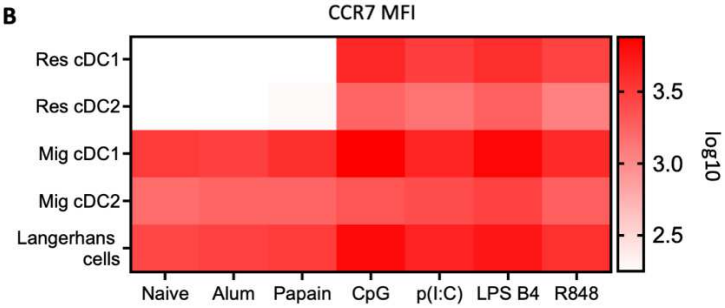
B
CCR7 MFI
Res cDC1
Res cDC2
Mig cDC1
Mig cDC2
Langerhans cells
Naive
Alum
Papain
CpG
p(I:C)
LPS B4
R848
log10

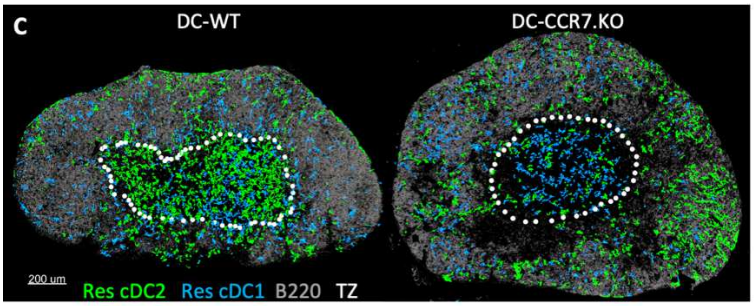
C
DC-WT
DC-CCR7.KO
200 um
Res cDC2
Res cDC1
B220
TZ

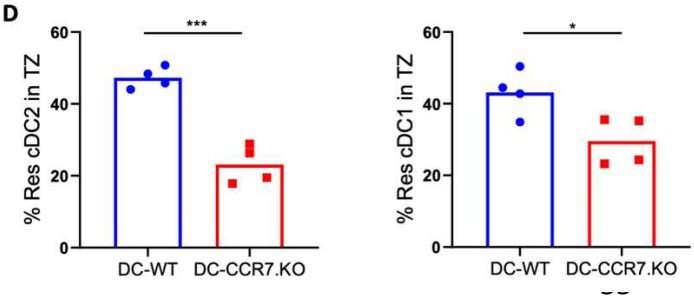
D
% Res cDC2 in TZ
DC-WT
DC-CCR7.KO
% Res cDC1 in TZ
DC-WT
DC-CCR7.KO

Fig. 2. CCR7-mediated Res cDC intranodal relocalization after immunization. (**A**) B6 mice were injected in the ears with CpG, and dLNs were analyzed for cDC expression of MHC-II and CCR7 by flow cytometry (see fig. S3A for gating scheme). MHC-II geometric mean fluorescence intensity (MFI) was normalized to MHC-II on migratory cDCs (Mig cDC). (**B**) Heatmap depicting CCR7 geometric MFI on cDCs 24 hours after immunization with indicated adjuvants. Each square represents mean of $n = 4$. (**C** and **D**) DC-CCR7.KO and DC-WT mixed BMCs were administered DT and injected with CpG 1 day later in the footpad. Histocytometry of popliteal dLNs 1.5 days later. Data analyzed by unpaired *t* test with Welch's correction. Data represent at least two independent experiments.

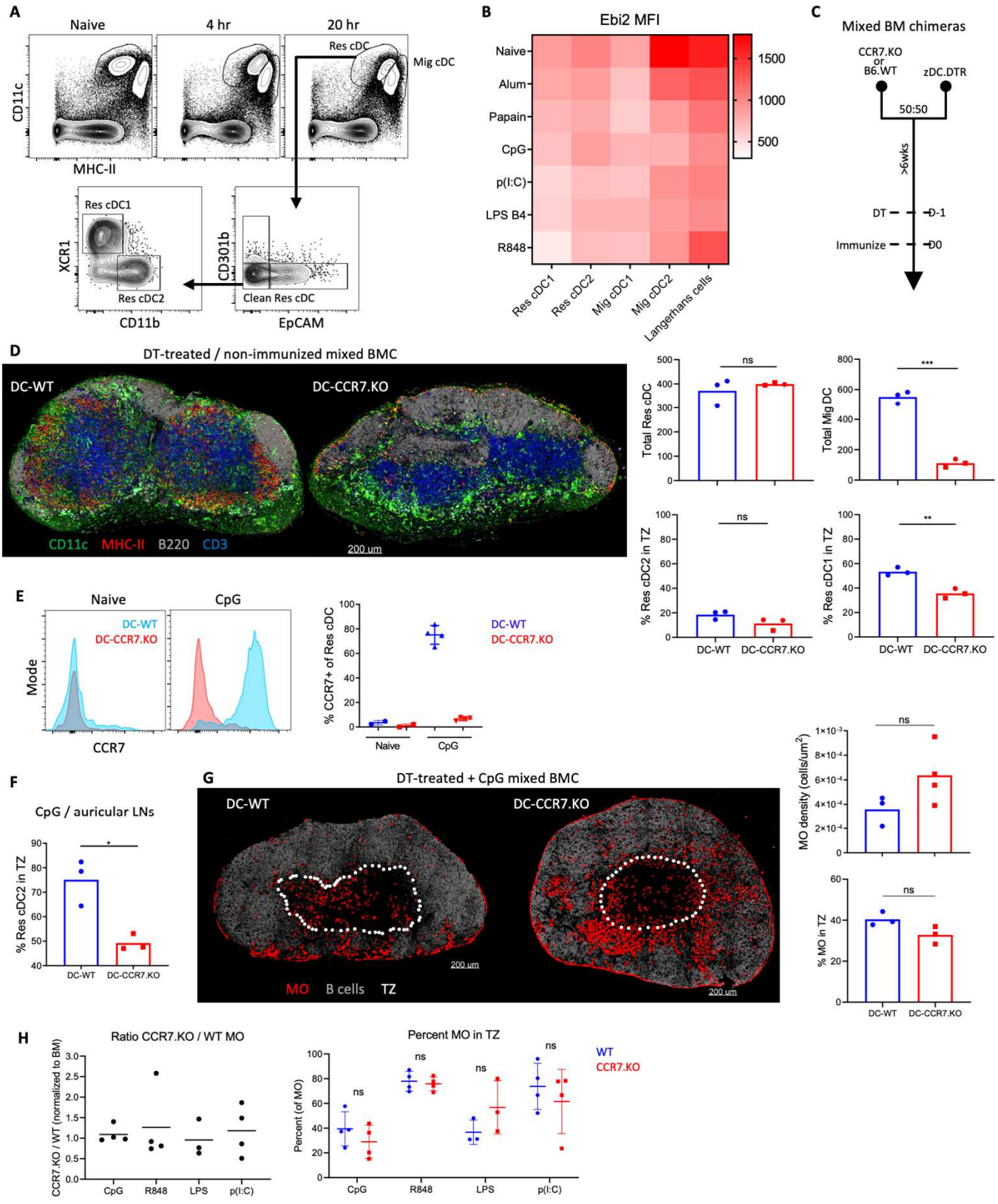
A
Naive
4 hr
20 hr
Res cDC
Mig cDC
CD11c
MHC-II
Res cDC1
Res cDC2
XCR1
CD11b
CD301b
Clean Res cDC
EpCAM
B
Ebi2 MFI
Naive
Alum
Papain
CpG
p(I:C)
LPS B4
R848
1500
1000
500
Res cDC1
Res cDC2
Mig cDC1
Mig cDC2
Langerhans cells
C
Mixed BM chimeras
CCR7.KO or B6.WT
zDC.DTR
50:50
>6wks
DT
-1
Immunize
0
D
DT-treated / non-immunized mixed BMC
DC-WT
DC-CCR7.KO
CD11c MHC-II B220 CD3
200 um
Total Res cDC
ns
Total Mig DC
***
% Res cDC2 in TZ
ns
% Res cDC1 in TZ
**
DC-WT
DC-CCR7.KO
E
Naive
CpG
DC-WT
DC-CCR7.KO
Mode
CCR7
% CCR7+ of Res cDC
Naive
CpG
F
CpG / auricular LNs
% Res cDC2 in TZ
*
DC-WT
DC-CCR7.KO
G
DT-treated + CpG mixed BMC
DC-WT
DC-CCR7.KO
200 um
MO
B cells
TZ
MO density (cells/um2)
ns
% MO in TZ
ns
H
Ratio CCR7.KO / WT MO
CCR7.KO / WT (normalized to BM)
CpG
R848
LPS
p(I:C)
Percent MO in TZ
Percent (of MO)
WT
CCR7.KO
ns

Fig. S3. Chemokine receptors expressed by cDCs and validation of DC-CCR7.KO BMC system.
(A) Flow cytometry gating scheme used to identify cDC populations in LNs from the experiment described in Fig. 2A. To improve subset discrimination, cells staining positive for migratory cDC markers, EpCAM and CD301b, were excluded from Res cDC gating. **(B)** B6 mice were injected in the ears with the indicated adjuvants and cDC populations within dLNs were analyzed for the expression of Ebi2 by geometric mean fluorescence intensity (MFI) 24 hours later. Each square represents mean of n = 4. **(C)** Experimental schematic for the creation of DC-CCR7.KO and DC-WT mixed BMCs and subsequent immunization. **(D)** Representative primary images of auricular LNs from non-immunized DC-WT and DC-CCR7.KO mixed BMCs (left), as well as histocytometry analysis of cDC cellularity and frequency within the TZ (right). **(E** and **F)** DC-CCR7.KO and DC-WT mixed BMCs were treated with DT and then injected in the ears with CpG 1 day later. dLNs were harvested 1.5 days later. (E) Flow cytometry analysis verifying lack of CCR7 expression on Res cDCs in DC-CCR7.KO mice after CpG immunization. (F) Histocytometry analysis of the percent of Res cDC2 found within the TZ of auricular dLNs. **(G)** Supplementary material for Fig. 2, C and D. DT-treated DC-CCR7.KO and DC-WT mixed BMCs were injected with CpG in the footpads. MO cellularity and localization was analyzed 1.5 days later. **(H)** B6 mice were irradiated and reconstituted with a 50:50 ratio of congenically marked CCR7.KO BM and B6 (WT) BM. Six weeks after BM transplant, mice were immunized in the footpads with the indicated adjuvants. dLNs were analyzed by histocytometry 1 day later. The ratio of total CCR7.KO MO to WT MO as normalized to MO reconstitution ratio in the BM (left), and the percentage of MOs in the TZ (right) was quantified. (D and F to H) Data analyzed by unpaired *t* test with Welch's correction. Each point represents an independent LN. In (H), data is representative of one independent flow cytometry experiment and one independent histocytometry experiment. All other data represent at least two independent experiments.

HEV-mediated recruitment of MOs into the dLNs

We next studied the mechanisms of MO recruitment during Type-I inflammation. MOs enter the circulation from the BM in a CCR2-dependent manner (*22*). Indeed, blockade of CCR2 using an anti-CCR2 antibody significantly reduced MO recruitment into dLNs after immunization (Fig. 3A), without affecting the total numbers and localization of Res cDCs (fig. S4A). Further trafficking of MOs into dLNs could have occurred via two distinct routes: 1) initial MO recruitment into inflamed peripheral sites of immunization, followed by continued migration into dLNs via the afferent lymphatics, or 2) direct MO entry into dLNs from blood via HEVs (*22*). To investigate the former possibility, mice were administered CpG in the ear, and the site of

immunization was surgically removed 1-2h later. This allows for drainage of administered TLR agonists to dLNs during the initial hour after immunization, while the site removal precludes the subsequent migration of cells from the immunization site. This is especially true for MOs, which require additional time to traffic to the inflamed skin (*86*, *87*). We observed similar numbers of MOs in both site-intact and site-removed dLNs 24h post immunization, suggesting that peripheral tissue trafficking was not the primary mechanism of early MO recruitment (Fig. 3B). Nevertheless, surgical trauma associated with site removal could independently promote MO mobilization and confound the results. We thus injected mice with a blocking antibody against P-selectin glycoprotein ligand-1 (PSGL-1), an adhesion molecule predominantly involved in trafficking to inflamed peripheral tissues (*88*), and again immunized the animals in the ear, as well as performed site removal in some of the mice (Fig. 3B). PSGL-1 blockade, with or without site removal, led to a modest, but non-significant decrease in MO numbers in the dLNs, corroborating that early MO trafficking into dLNs was not predominantly occurring via the peripheral tissues. To test the possibility of direct migration of MOs via the HEVs, mice were treated with an anti-CD62L blocking antibody at the time of immunization, as CD62L is essential for HEV-mediated trafficking (*89*). CD62L blockade led to a dramatic loss in MO cellularity (Fig. 3B). Combined anti-PSGL-1 and anti-CD62L blockade caused more minor additional decreases (Fig. 3B). This indicated that although minor trafficking of MOs via the afferent lymphatics may occur (*66*), HEV-mediated entry was the dominant pathway of early MO recruitment into the dLNs during Type-I inflammation.

To directly visualize the dynamics of MO trafficking, we performed 2-photon intravital microscopy of dual-reporter CCR2-RFP x CD11c-YFP mice, which allowed concurrent visualization of both MOs and cDCs, respectively. LN vasculature was also intravenously labeled

with fluorescently-labeled anti-CD31 antibody or dextran, which do not alter cellular trafficking (*90*). As anticipated, unimmunized mice exhibited very few MOs (RFP^+YFP^-) in the vasculature, and the few detected cells rapidly moved through the vessels (movie S1). In contrast, markedly increased numbers of RFP^+ MOs were observed in the dLN blood vessels starting 6h post immunization, and many cells exhibited slow rolling-type behavior and frequently extravasated into the parenchyma (Fig. 3, C and D, and movie S1). CCR2 can also be expressed by cDCs or effector T cells (*91*). However, the rolling and extravasating RFP^+ cells were CD11c-YFP-negative. Additional intravenous labeling for CD90, a T cell specific molecule, also did not label most RFP^+ cells (fig. S4B). Moreover, the timing of MO detection within the HEVs with intravital microscopy correlated with the kinetics data obtained by confocal imaging and flow cytometry (Fig. 1, C and D, and fig. S2D), collectively suggesting that Type-I inflammation elicits rapid MO recruitment into the dLNs via HEVs.

We next analyzed MO morphology and expression of CD11c and MHC-II, markers associated with MO differentiation. At early time points after immunization, MOs within the LN parenchyma exhibited a round morphology (fig. S4C), similar to cells within the HEV lumen (Fig. 3, C and D, and fig. S4B). Moreover, these recently arrived MOs were CD11c and MHC-II negative and were mainly localized in the TZ periphery (fig. S4C). Over time, MOs progressively displayed reduced sphericity and acquired a dendritic-like appearance, expressed CD11c, and migrated into the deeper LN paracortex (fig. S4, C and D). Flow cytometry confirmed that the early infiltrating MOs phenocopied intravenously-labeled blood MOs, displaying minimal surface levels of CD11c and MHC-II (fig. S4E), and that with time they gradually increased expression of both markers (fig. S4, F-H). Together, these data indicated that MOs were recruited into dLNs via local vasculature and underwent differentiation over time.

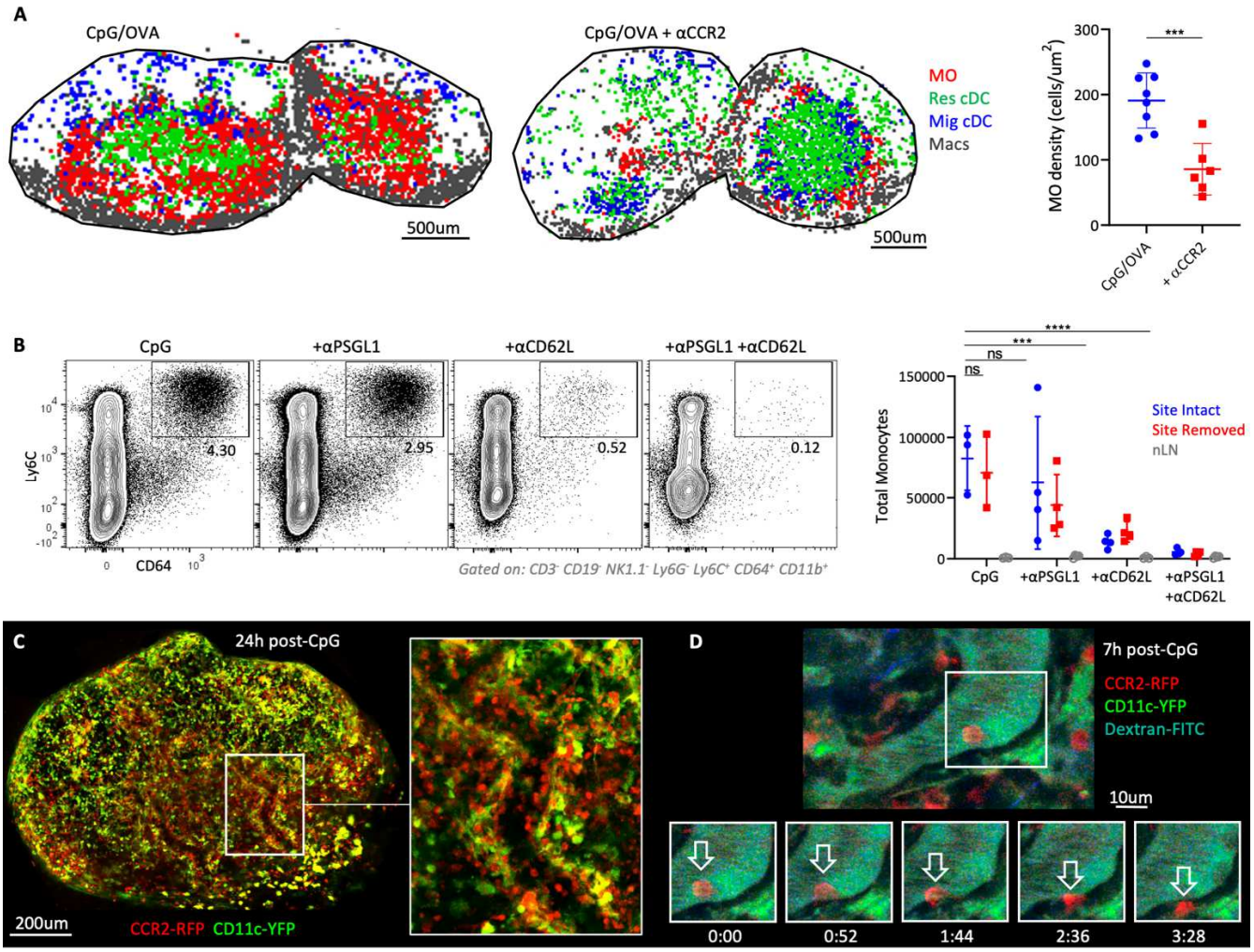

Fig. 3. HEV-mediated recruitment of MOs into the dLNs. (**A**) OT-II–transferred B6 mice were immunized with CpG plus OVA in ears and footpads. Some animals were treated with αCCR2. Myeloid cell localization (left) and MO density (right) in dLNs were assessed by histocytometry 1.75 days later. Data analyzed by unpaired *t* test with Welch's correction. Macs, macrophages. (**B**) B6 mice were immunized with CpG in the ears. Some mice had the immunization site surgically removed 1 to 2 hours later and/or were treated with αPSGL-1 and/or αCD62L. Total MOs in dLNs and nondraining LNs (nLN) were quantified 1 day later by flow cytometry. Data analyzed via one-way ANOVA with Dunnett's multiple comparisons test. ns, not significant. (**C** and **D**) CCR2-RFP × CD11c-YFP mice were administered CpG in the footpad, and popliteal LNs were imaged by two-photon intravital microscopy (C) 24 hours or (D) 7 hours after immunization. Representative time-lapse images demonstrate MO extravasation. Data represent at least two independent experiments.

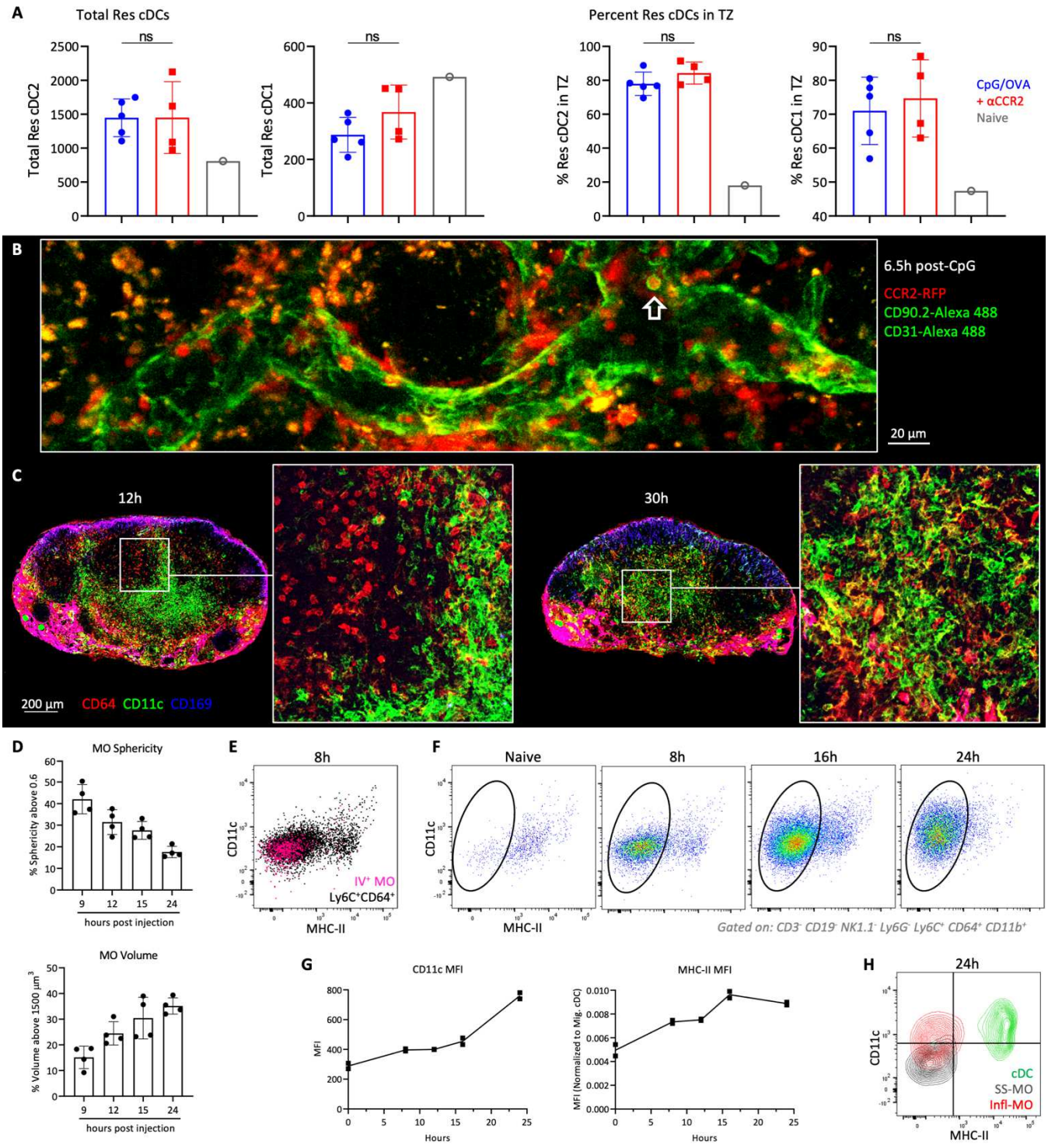

Fig. S4. HEV-mediated recruitment of MOs in the dLNs.
(A) Extended analysis for Fig. 3A, showing total Res cDCs (left) and percent of Res cDCs in the TZ (right) after CpG plus OVA immunization, with or without αCCR2 treatment. Data analyzed by unpaired *t* test with Welch's correction. **(B)** CCR2-RFP x CD11c-YFP mice were injected

with CpG in the footpad and popliteal dLNs were imaged by two-photon intravital microscopy 6.5 hours later. 1.5 hours prior to imaging, mice were also intravenously administered both anti-CD31-Alexa 488 and anti-CD90.2-Alexa 488 to visualize the vasculature and to label T cells, respectively. Arrow shows a single RFP^+ cell labeled with the anti-CD90.2 antibody within the vasculature. Remaining $CCR2^+$ cells within the vasculature in this representative image are negative for CD90.2 staining. **(C** and **D)** B6 mice were injected with CpG in the ears and dLNs were examined by imaging and histocytometry at the indicated time points. (C) Representative images demonstrating a change in morphology of $CD64^+CD169^-$ MOs, and their change in expression of CD11c at 12 versus 30 hours. (D) Histocytometry quantification of the percent MOs with spherical morphology (sphericity above 0.6) or with enlarged cell volume (volume above 1500 μm^3) at the indicated time points. **(E** to **H)** B6 mice were injected with CpG in the ears and dLNs were assessed at the indicated time points by flow cytometry. 10 minutes prior to harvest, mice were administered anti-CD45.2-PE intravenously (IV) to label cells within the vasculature. (E) Representative flow plot comparing CD11c and MHC-II expression on IV^+ MOs (pink) overlaid on top of all $Ly6C^+CD64^+$ ($CD3^-CD19^-NK1.1^-Ly6G^-CD11b^+$) cells in the dLN (black), 8 hours after CpG injection. (F) Representative flow plots demonstrating CD11c and MHC-II expression on MOs at the indicated time points. Gated cells ($CD3^-CD19^-NK1.1^-Ly6G^-Ly6C^+CD64^+CD11b^+MHC\text{-}II^{-/INT}$) indicate proposed inflammatory MOs recruited into dLNs. (G) CD11c and MHC-II geometric MFI on inflammatory MOs at the indicated time points. MHC-II geometric MFI was normalized to migratory cDCs. Line connects means at each time point. Data is representative of five independent experiments. (H) Representative flow plot comparing CD11c and MHC-II expression on MOs from steady-state LNs (SS-MO, gray) to that on inflammatory MOs (Infl-MO, red) and cDCs (green) in dLNs 24 hours after CpG administration. Each point represents an independent LN. All data represent at least two independent experiments.

Antigen presentation and initiation of T cell priming by repositioned Res cDCs

We next studied the functional roles of Res cDCs and MOs in the generation of adaptive immunity. Considering that Res cDC2s specialize in MHC-II presentation, while MOs have delayed kinetics of MHC-II expression (fig. S4, F-H), we hypothesized that early antigen presentation was not equivalent between these populations. To test this, mice were immunized with CpG plus E□GFP, a model protein which allows detection of antigen uptake via GFP fluorescence and MHC-II presentation using a YAe antibody, specific for the E□ □peptide-MHC-II complex (*86*). One day post immunization, Res cDC2s and migratory cDC2s were the dominant cell types that captured and presented antigen (Fig. 4A). While some MOs had detectable GFP fluorescence, they did not

stain positive with the YAe antibody, indicating minimal MHC-II antigen processing (Fig. 4A). Similar results were seen 2 days post immunization (fig. S5A). Notably, a minor fraction of $CD64^+$ GFP^+YAe^+ cells were observed (fig. S5A), albeit these cells were phenotypically distinct from inflammatory MOs, expressing lower levels of Ly6C and higher levels of MHC-II (fig. S5A). A similar population was found in steady state LNs, and their numbers demonstrated a much more modest increase following vaccination as compared to the $Ly6C^{HIGH}$ MOs (fig. S5B), indicating that they are distinct from inflammatory MOs and may represent tissue-derived cells or inflammatory cDCs (*22*, *66*, *92*, *93*). These results indicated that cDCs, but not the early-recruited inflammatory MOs, were the dominant antigen presenting cells in dLNs after Type-I agonist immunization.

To test how the repositioning of antigen-presenting Res cDCs influences T cell activation, we adoptively transferred $1x10^6$ naïve, OVA-specific CD4 OT-II T cells into DC-WT or DC-CCR7.KO mixed BMCs and immunized these mice with OVA plus CpG. dLNs were analyzed 1.5-2 days after, just prior to extensive T cell proliferation. Although migratory cDCs presented antigens on MHC (Fig. 4A and fig. S5A), removal of the immunization site 1-2h after vaccination recapitulated previous findings that migratory cDCs were largely dispensable for CD4 T cell responses (Fig. 4B). Nevertheless, we performed site removal in all animals, as this restricted effects of CCR7 deficiency to intranodal Res cDC repositioning and minimized additional changes in migratory cDC trafficking. As expected, OT-II T cells in DC-WT animals were robustly activated, as demonstrated by T cell clustering, enlarged cell volume, as well as interferon regulatory factor 4 (IRF4) and Ki67 expression, indicating TCR engagement and proliferation, respectively (Fig. 4, C-E) (*94*, *95*). In contrast, early OT-II T cell activation was drastically impaired in the DC-CCR7.KO mice (Fig. 4, C-E). DC-CCR7.KO mice also elicited substantially

reduced clonal expansion of OT-II T cells 4 days after immunization, when using a more physiological (10^5) cell transfer number (Fig. 4F). While the numbers of expanded T cells were markedly different between DC-WT and DC-CCR7.KO mice, there were no major differences in their expression of T-box transcription factor (Tbet) or B-cell lymphoma 6 (BCL6), or in their ability to produce interferon gamma (IFN□) post restimulation (Fig. 4G and fig. S5C). This indicated that the few CD4 T cells that were activated in the DC-CCR7.KO settings underwent relatively normal effector differentiation, albeit additional differences cannot be ruled out. We also examined polyclonal CD4 T cell responses by immunizing mice with lymphocytic choriomeningitis virus (LCMV) -derived recombinant glycoprotein complex (GPC) and CpG. Seven days post immunization and site removal, large numbers of GPC MHC-II tetramer positive $CD44^+$ CD4 T cells were detected in DC-WT but not DC-CCR7.KO mice (Fig. 4H). T cells in both expressed equivalent levels of Tbet and Gata binding protein 3 (Gata3) proteins (Fig. 4I).

Given that the Res cDC1 also upregulated CCR7 to move into the deep TZ (Fig. 1 and 2), and these cells specialize in cross-presentation, we also examined CD8 T cell priming using OVA-specific CD8 OT-I T cells. Site removal again did not impact CD8 T cell expansion, indicating minimal contribution of migratory cDCs (fig. S5D). Similar to CD4 T cells, we observed a drastic reduction in OT-I T cell clustering and expression of activation markers in DC-CCR7.KO animals 1.5d after immunization (fig. S5, E and F). A significant reduction in OT-I T cell expansion in DC-CCR7.KOs was also observed 4d after immunization (fig. S5G). The few responding OT-I T cells in DC-CCR7.KO mice again displayed no major differences in expression of Tbet and TCF1, nor in their ability to produce IFN□ post restimulation (fig. S5H). Together, these data demonstrated that CCR7-mediated relocalization of both Res cDC2s and cDC1s into the TZ during Type-I inflammation controls the activation and clonal expansion of both CD4 and CD8 T cells.

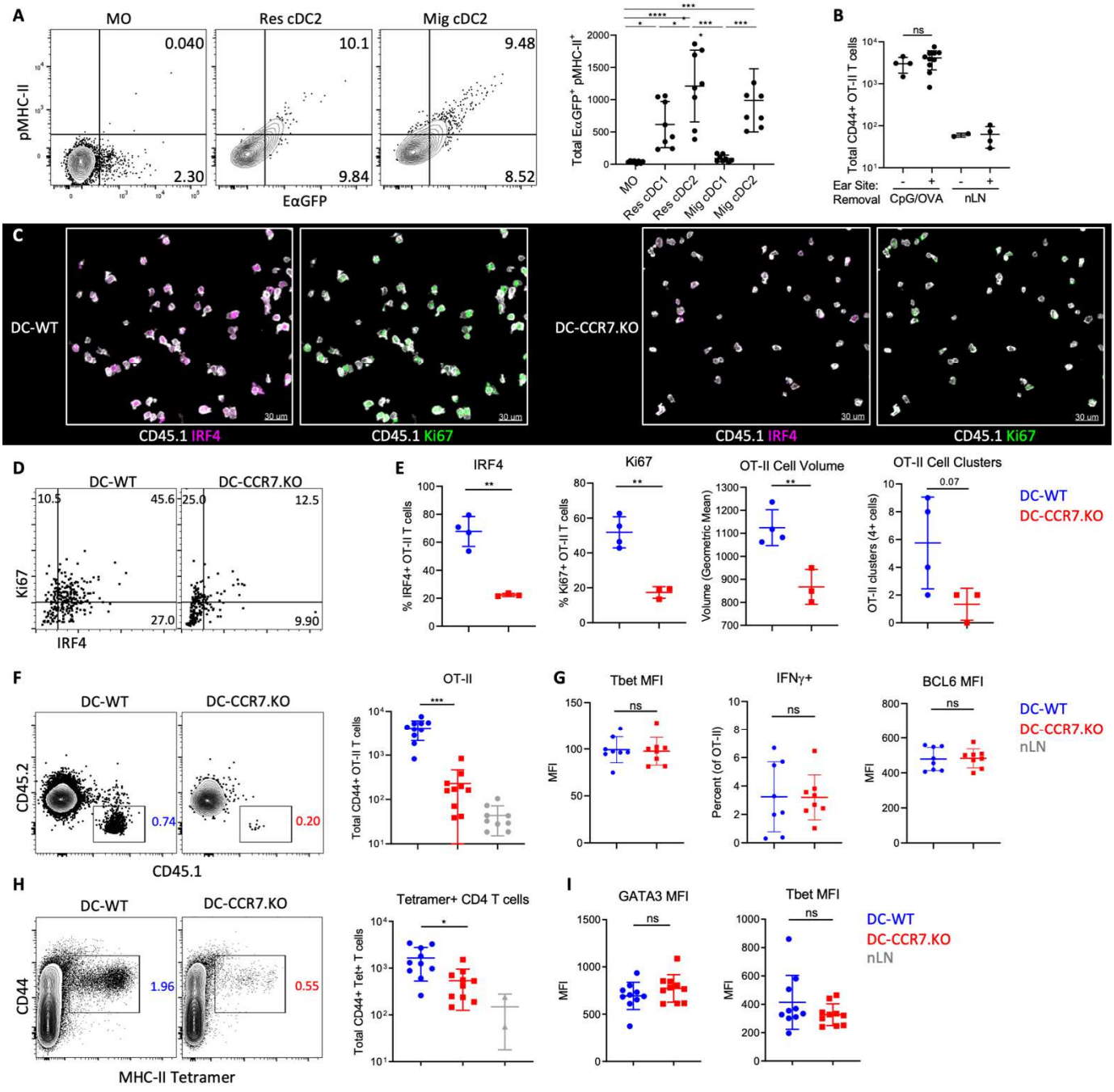

Fig. 4. Induction of T cell priming and clonal expansion via Res cDC repositioning. (**A**) B6 mice were immunized with CpG plus EαGFP in both ears and analyzed by flow cytometry for GFP fluorescence and peptide–MHC-II staining (YAe) 1 day later. Data analyzed by one-way ANOVA with Tukey's multiple comparison test. (**B**) DC-WT mixed BMCs were transferred with 10^5 OT-II T cells, and 1 day later, ears were immunized with OVA plus CpG. Some mice also had site removal 1 to 2 hours later. Four days after immunization, LNs were analyzed by flow cytometry for T cell cellularity. (**C** to **G**) DC-WT and DC-CCR7.KO mixed BMCs were

transferred with (C to E) 10^6 or (F and G) 10^5 OT-II T cells, treated with DT, immunized with OVA plus CpG in both ears, and had site removal. dLNs were assessed (C to E) 1.5 days later by histocytometry or (F and G) 4 days later by flow cytometry. (C) Representative areas in the TZ, with the presented IRF4 and Ki67 signal masked outside of CD45.1$^+$ OT-II T cells for visual clarity. (D) Represent- ative gating and (E) quantification of OT-II T cell expression of IRF4 and Ki67, as well as average T cell volume and number of OT-II clusters (>4 cells in direct contact) per section. (F) Total CD44$^+$ OT-II T cells and (G) Tbet and Bcl6 geometric MFI and percentage of IFNγ^+ after restimulation. (**H** and **I**) DT-treated DC-CCR7.KO and DC-WT mixed BMCs were immunized with GPC plus CpG in the ear, followed by site removal 2 hours later. (H) Cellularity and (I) differentiation of CD44$^+$ GPC-tetramer binding T cells were quantified in dLNs 7 days after immunization. (B and E to I) Data analyzed by unpaired *t* test with Welch's correction. Data represent at least two independent experiments.

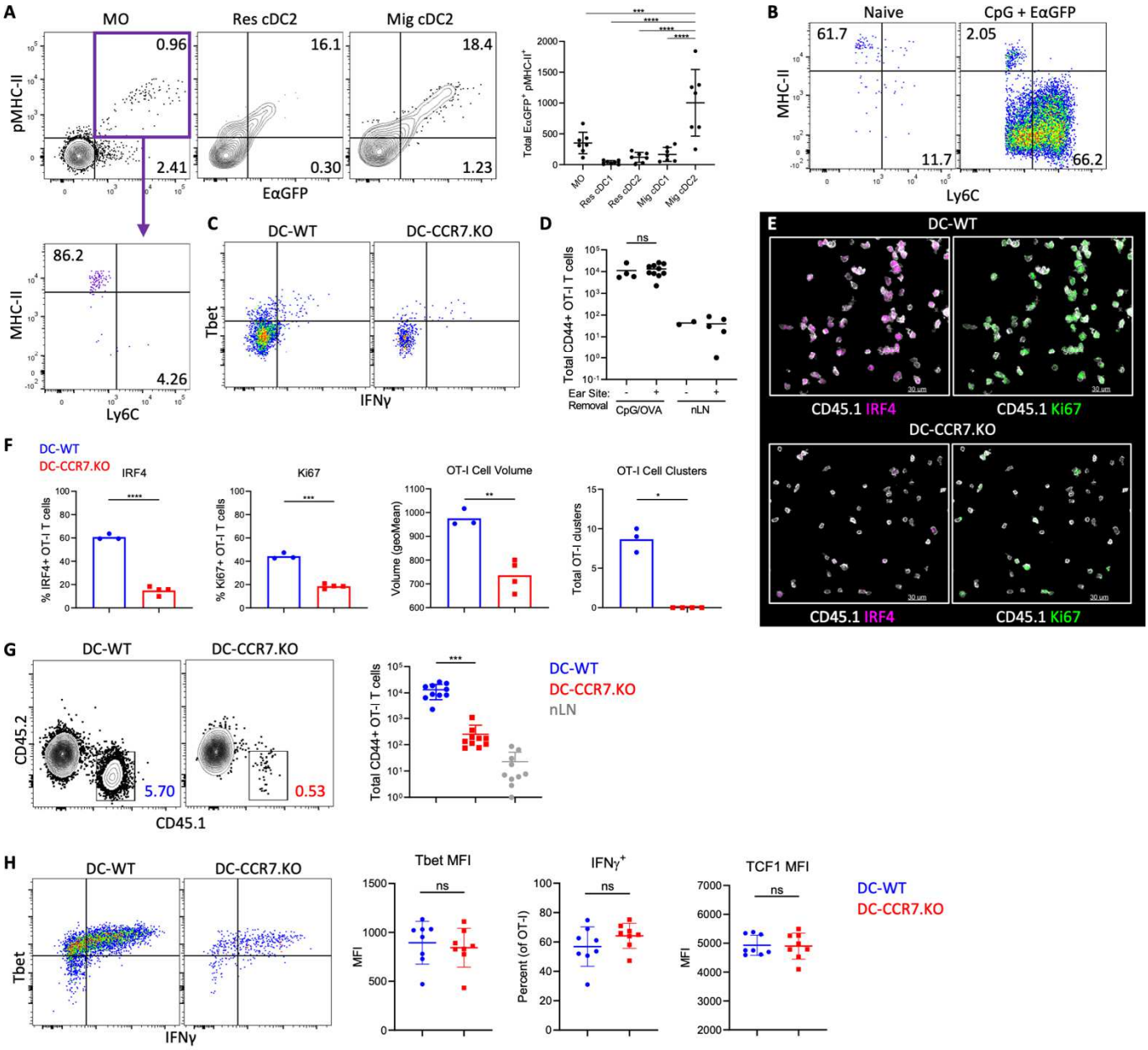

Fig. S5. Res cDC relocalization and antigen presentation in the regulation of CD8 T cell responses.

(A and **B)** B6 mice were immunized with CpG plus EαGFP in the ears. GFP fluorescence and surface peptide–MHC-II staining (YAe) were analyzed by flow cytometry 2 days later. (A) Representative flow cytometry plots (left) and quantification of total EαGFP$^+$ peptide-MHC-II$^+$ myeloid cells in dLNs (right). Data analyzed by one-way ANOVA with Tukey's multiple comparison test. (B) Representative flow plots demonstrating presence of Ly6C^{LO}MHC-II^{HI} CD64$^+$CD11b$^+$ cells in naïve versus CpG-immunized LNs. MOs were gated on CD3$^-$CD19$^-$ NK1.1$^-$Ly6G$^-$Ly6C$^+$CD64$^+$CD11b$^+$ cells. **(C)** Supplementary material for Fig. 4G. Representative flow plots demonstrating staining for Tbet and IFNγ on restimulated OT-II CD4

T cells, 4 days after OVA plus CpG immunization. **(D)** DC-WT mixed BMCs were transferred with 5 x 10^4 OT- I CD8 T cells and immunized with OVA plus CpG in the ears 1 day later. Some mice also had site removal 1 to 2 hours later. Four days after immunization, dLNs and non-draining LNs (nLN) were analyzed by flow cytometry for T cell cellularity. **(E** to **H)** DC-CCR7.KO and DC-WT mixed BMCs were transferred with (E and F) 10^6 or (G and H) 5 x 10^4 OT-I CD8 T cells, treated with DT, immunized with OVA plus CpG, and had site removal. dLNs were assessed (E and F) 1.5 days later by histocytometry or (G and H) 4 days later by flow cytometry. (E) Representative areas in the TZ are shown, with the presented IRF4 and Ki67 signal first masked outside of CD45.1$^+$ OT-I T cells for visual clarity. (F) Histocytometry quantification of OT-I T cell expression of IRF4 and Ki67, as well as the average T cell volume and the number of detected OT-I clusters (defined as >4 cells in direct contact) per imaged section. (G) Flow cytometry analysis of total CD44$^+$ OT- I T cells, as well as (H) Tbet geometric MFI, percent IFNγ^+, and TCF1 geometric MFI after restimulation. (D and F to H) Data was analyzed by unpaired *t* test with Welch's correction. Each point represents an independent LN. All data represent at least two independent experiments.

Production of IL-12 by TZ-localized monocytes during Type-I inflammation

Activated MOs can express inflammatory cytokines, such as IL-12, although where in LNs MOs generate this cytokine and whether this coincides with early T cell differentiation is not known (*36*, *37*, *96*). To this end, we first looked for expression of IL-12p40 by various myeloid cell subsets using flow cytometry, as verified using IL-12.KO BMC mice (Fig. S6, A and B). We found that 1 day post CpG immunization, some of the MOs produced copious quantities of IL-12p40 and this became more apparent on day 2 (Fig. 5, A and B, and fig. S6, A-C). As previously described, migratory and Res cDC1 cells also produced large amounts of IL-12p40 (*97–99*). While the frequency of IL-12-positive MOs was relatively modest compared to cDCs, due to substantial increases in cellularity, MOs represented the most numerically dominant IL-12-producing cell type within the dLNs.

We next used histocytometry to visualize where IL-12 producing cells were located. IL-12p40 staining, as verified using IL-12.KO BMC mice, was detectable in small quantities in steady state

LNs, primarily associated with migratory cDC1 and some Res cDC1 (fig. S6, D and E), as described (*100*, *101*). A substantial increase in MO-associated IL-12p40 signal was observed in dLNs 1.75 days after CpG immunization and was localized within the TZ (Fig. 5C and D, and fig. S6E). Of note, the frequency of IL-12p40 positive cells appeared higher by imaging vs. flow cytometry. This may represent difficulties in cellular extraction, potential cell death, or degranulation during enzymatic tissue digestion for flow cytometry (*8*, *102*, *103*). Quantification of the imaging data revealed that MOs were a dominant IL-12p40-producing cell population in the TZ after immunization with multiple TLR agonists and following West Nile virus infection (Fig. 5. E-G). Blockade of MO trafficking with anti-CCR2 resulted in substantial loss of MO-derived, but not cDC-derived, IL-12p40 in the TZ (Fig. 5H). In contrast, little MO-associated IL-12p40 signal was seen within the TZ during Type-II inflammation (fig. S6F). Since IL-12p40 does not necessarily reflect the immunologically relevant IL-12p70 (IL-12p40 and IL-12p35 heterodimer), we examined IL-12p70 levels within dLNs in the presence or absence of MOs with ELISA. IL-12p70 was markedly increased 2 days after CpG immunization, reflective of adjuvant induced inflammation (fig. S6G). Blockade of MO trafficking led to a partial and highly significant decrease in IL-12p70 signal (Fig. 5I and fig. S6G). Collectively, these data indicated that in addition to the conventional contributions by cDCs, MOs provide a substantial source of IL-12p70 in the TZ of dLNs during Type-I inflammation.

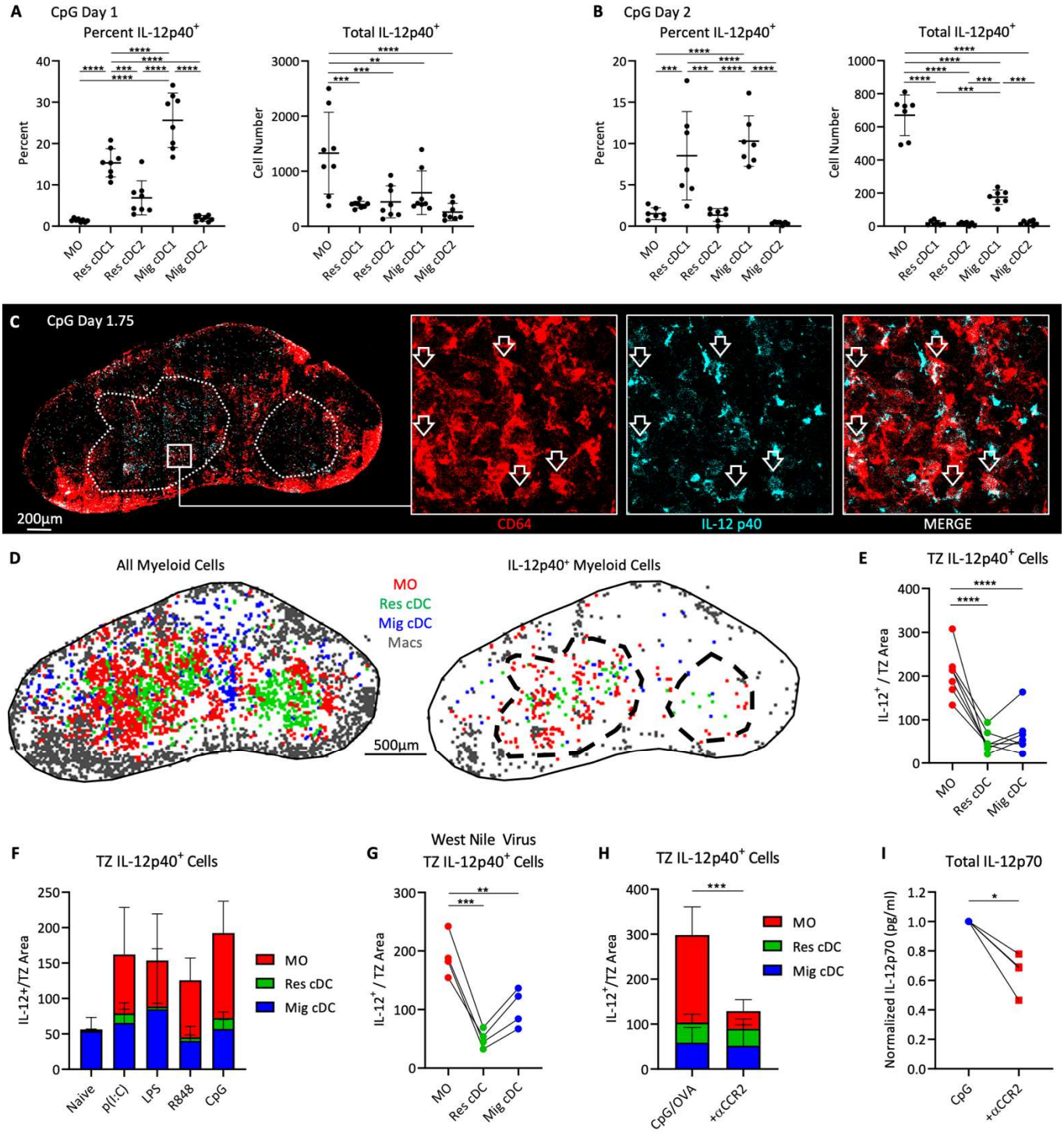

Fig. 5. IL-12 production by TZ-localized inflammatory MOs. (**A** and **B**) B6 mice were given CpG plus EαGFP in both ears, and dLNs were analyzed (A) 1 day or (B) 2 days later by flow cytometry. Percent IL-12p40$^+$ (left) and total IL-12p40$^+$ cells (right) is shown. (**C** to **E**) OT-I–transferred B6 mice were immunized with CpG plus OVA in ears and footpads. dLNs were

analyzed by histocytometry 1.75 days later. (C) Representative images demonstrating IL-12p40–expressing $CD64^+$ MOs (arrows) and (D) positional analysis of all myeloid cells (left) and IL-$12p40^+$ myeloid cells (right). Dashed line demarcates the TZ. (E) Quantification of total IL-$12p40^+$ cells within the TZ for the indicated subsets. (**F**) OT-I–transferred B6 mice were immunized with indicated adjuvants plus OVA. dLNs were analyzed 1.5 days later by histocytometry for total IL- $12p40^+$ myeloid cells within the TZ. For each group, $n = 3$ to 6. (**G**) B6 mice were infected in the footpad with 100 PFU of West Nile virus TX. dLNs were analyzed by histo- cytometry 24 hours later for total IL-$12p40^+$ cells within the TZ. (**H**) OT-I–transferred B6 mice were immunized with CpG plus OVA in ears and footpads. Some mice were also treated with αCCR2. Histocytometry analysis of total IL-$12p40^+$ cells within the TZ of dLNs 1.75 days after immunization. (**I**) B6 mice were immunized with CpG in ears and footpads, and dLNs were harvested 2 days later. Some mice were treated with αCCR2. ELISA quantification of total IL-12p70 signal in dLNs. Data analyzed via paired *t* test with Welch's correction. Individual points represent means from four independent experiments. Lines connect experimental means, with the αCCR2 group normal- ized to the CpG group. Data in (A), (B), (E), and (G) analyzed by one-way ANOVA and Tukey's multiple comparisons test. Linked points in (E) and (G) indicate data from the same LNs. All data represent at least two independent experiments.

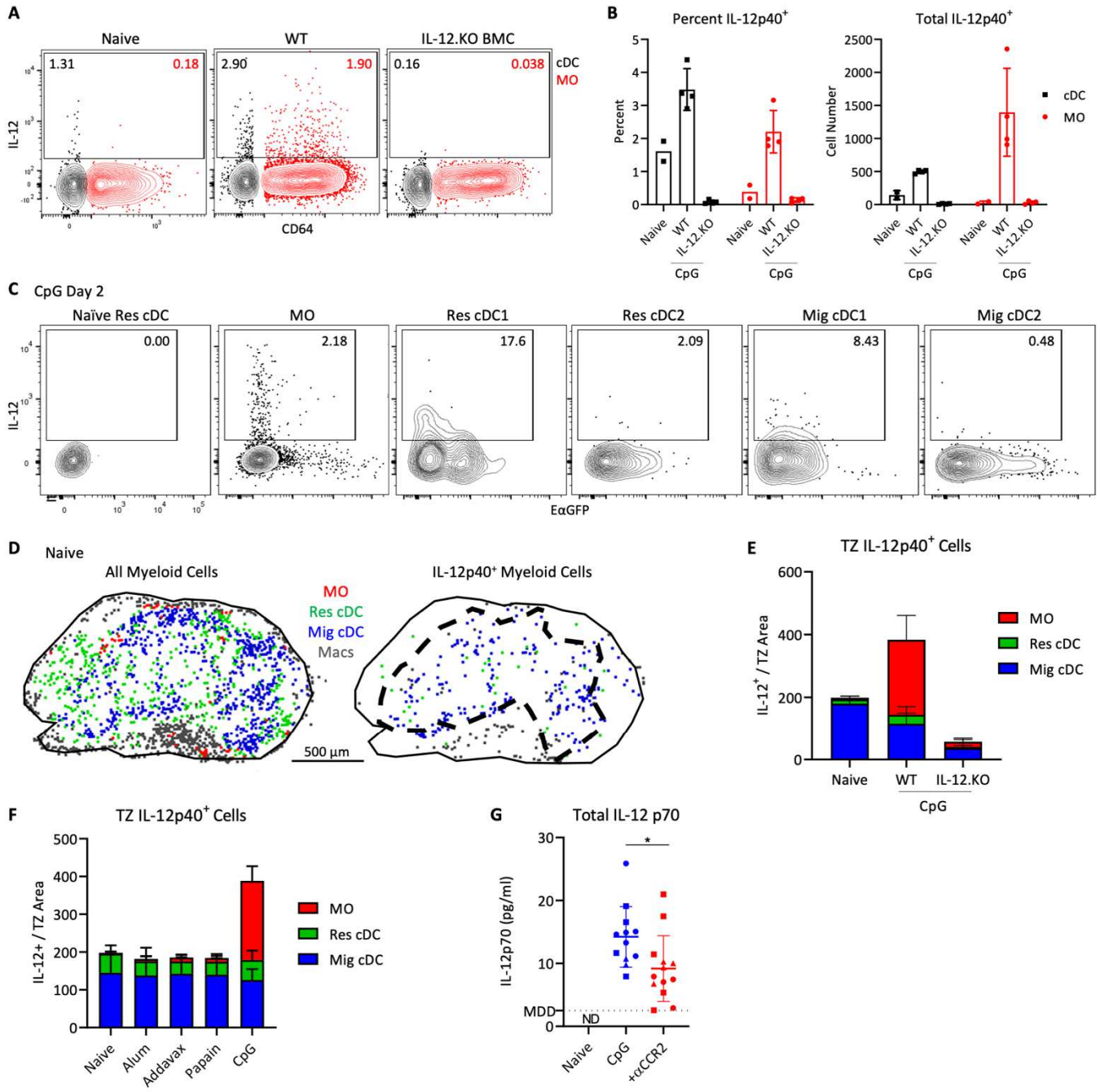

Fig. S6: IL-12 production by TZ-localized inflammatory MOs after immunization.
(A and **B)** B6 mice and IL-12p40.KO BMCs were administered CpG in the footpads and 2 days later, dLNs were analyzed by flow cytometry. (A) Representative flow plots and (B) quantification of IL-12p40 expression by MOs and cDCs is shown. **(C)** Representative flow plots for experiment described in Fig. 5B, showing IL-12p40 expression by the indicated myeloid cell subsets 2 days after CpG plus EαGFP immunization. **(D)** Representative histocytometry positional analysis of all myeloid cells (left) and IL-12p40^{+} myeloid cells (right) within a naïve

LN. Macs, macrophages. **(E)** B6 mice and IL-12p40.KO BMCs were injected with CpG in the ears and 2 days later dLNs were analyzed for total IL-12p40$^+$ myeloid cells within the TZ by histocytometry. For each group, n = 4. **(F)** B6 mice were injected with the indicated adjuvants in the ears and footpads. Total IL- 12p40$^+$ myeloid cells within the TZ was assessed by histocytometry 1.75 days later. For each group, n = 5 to 7. **(G)** B6 mice were administered CpG in the ears and footpads. Some mice were also treated with αCCR2. Two days later, total IL-12p70 signal in dLNs was measured by ELISA. ELISA data from multiple independent experimental repeats were pooled together, as indicated with different symbols. Data analyzed by unpaired *t* test with Welch's correction. All data represent at least two independent experiments.

Association of early effector T cells with MO-rich LN microenvironments

IL-12 plays a critical role in T cell differentiation (*104*, *105*). Given the spatiotemporal coalescence of antigen-presenting Res cDCs and IL-12 expressing MOs in the TZ of dLNs, we hypothesized that both cell types may functionally cooperate to modulate effector T cell responses. Supporting this notion, 1.5-1.75d after OVA plus CpG immunization, we observed large numbers of activated OT-I and OT-II T cells embedded within a dense, interwoven network of both Res cDCs and CD11c-expressing CD64$^+$ MOs (fig. S7, A and B). To quantify these observations, we calculated the spatial correlation of different immune cells with respect to one another using CytoMAP (*69*). Use of 30 μm radius spatial neighborhoods for this also accommodated for potential effects of cellular motility or cytokine diffusion which may occur at these time points (*106*). This analysis confirmed that the spatial distribution of activated OT-I and OT-II T cells was positively correlated with the location of both Res cDC and MOs, but not migratory cDCs or macrophages (fig. S7, C and D), indicating preferential cell-cell interactions. The positive spatial correlation of activated T cells with Res cDC was reduced in DC-CCR7.KO mixed BMCs as compared to the DC-WT counterparts, reflective of poor Res cDC repositioning in these settings (Fig. S7E). In contrast, OT-I T cells still maintained a positive correlation with MOs in DC-CCR7.KOs (Fig. S7E),

corroborating the findings that MOs still efficiently entered the T zone irrespective of Res cDC relocalization (fig. S3G).

A closer examination of dLNs across multiple experiments also revealed a nonuniform, polarized distribution of MOs across the tissues, being particularly noticeable at later time points and in larger, bilobular auricular and brachial dLNs (Fig. 1A, 5C, 5D, and 6A, and fig. S2I and S7A). In contrast to MOs, both lobes in these polarized dLNs displayed a more homogeneous centralization of Res cDCs. The polarization of MOs likely corresponds to non-uniform TLR agonist biodistribution and inflammation across the dLNs after afferent drainage (*7*). We hypothesized that this myeloid heterogeneity could impact the local signals that T cells encounter during priming. To investigate this, we analyzed the expression of various markers associated with effector differentiation in responding OT-I T cells in relation to the different myeloid populations (Fig. 6A). Considerable heterogeneity in expression of Tbet, TCF1, and CD25 by the activated ($Ki67^+$) OT-I T cells was observed, suggesting early bifurcation of responses (Fig. 6, A and B). Importantly, we observed distinct spatial distribution patterns for the early effector subpopulations, with the more differentiated $Tbet^+TCF1^-CD25^+$ OT-I T cells preferentially localizing in regions heavily infiltrated by MOs, and with the less differentiated $Tbet^-TCF1^+$ OT-I T cells predominantly distributed in areas with more Res cDCs and fewer MOs (Fig. 6C). Correlation analysis of multiple tissues confirmed these observations, demonstrating that the more differentiated effector OT-I T cells ($Tbet^+TCF1^-$) were spatially correlated with (i.e. more proximal to) MOs, while the less differentiated T cells ($Tbet^+TCF1^-$) were correlated with both MOs and Res cDCs (fig. S7F). We examined the relative myeloid cell composition within regions that were dominantly populated by either the $Tbet^+TCF1^-$ or $Tbet^-TCF1^+$ OT-I T cells (fig. S7G). Examination of larger regions also further accommodated for effects of T cell motility across the tissues. While MOs and Res cDCs,

and in particular cDC1s, were found in relatively equal proportions in $Tbet^{-}TCF1^{+}$ OT-I regions, MOs greatly outnumbered other myeloid cells in regions populated by $Tbet^{+}TCF1^{-}$ early effector T cells (Fig. 6D and fig. S7H). Notably, there was no difference between the regions in the frequency of OT-I T cells expressing IRF4 and phosphorylation of the S6 ribosomal protein (pS6), suggesting that early TCR engagement was more homogenous across the compartments (Fig. 6E, fig. S7I). Polarized distribution of $Tbet^{+}TCF1^{-}$ and $Tbet^{-}TCF1^{+}$ OT-I T cells was also observed at later time points, when T cells begin to undergo extensive proliferation and start to leave the tissues (fig. S7J). In addition, we found a similar spatial heterogeneity of OT-I effector cells after administration of OVA plus p(I:C), with marked segregation of $Tbet^{HI}$ and $Tbet^{LO}$ T cells across the polarized dLNs (Fig. 6F). $Tbet^{HI}$ regions were again dominantly populated by MOs, while the $Tbet^{LO}$ regions were more equally populated by cDCs and MOs (Fig. 6, G and H). Collectively, these data indicate that distinct myeloid microenvironments in dLNs, as determined by the local

density of MOs, are associated with distinct patterns of CD8 T cell effector differentiation.

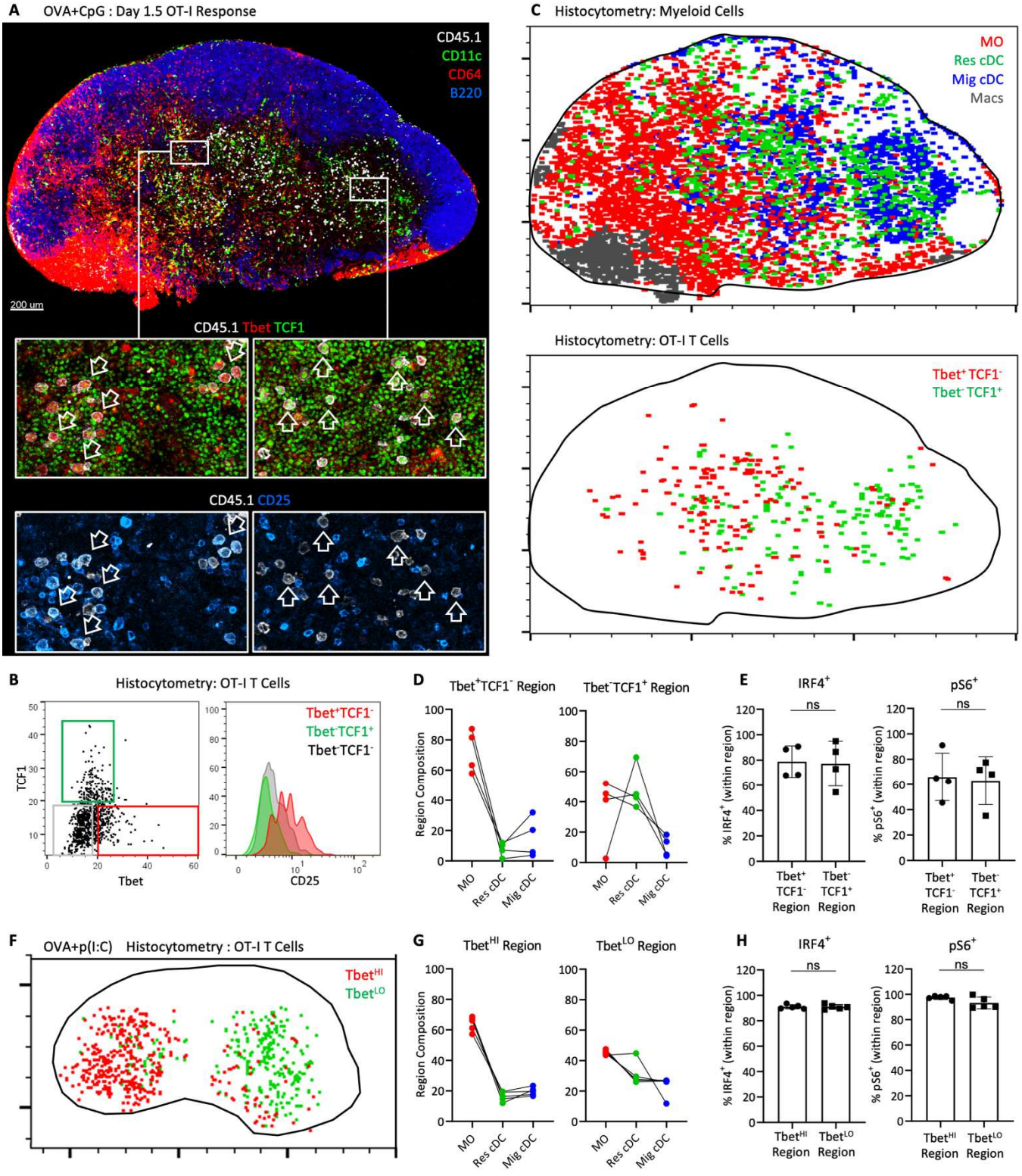

Fig. 6. Regulation of T cell response heterogeneity by myeloid cell microenvironments. (**A** to **H**) B6 mice were transferred with 10^6 OT-I T cells and immunized with (A to E) OVA plus CpG in ears and footpads or (F to H) OVA plus p(I:C) in ears. Auricular and brachial dLNs were analyzed 1.5 to 1.75 days later by histocytometry. (A) Representative dLN image demonstrating staining for various myeloid cells (top) and markers of T cell differentiation (bottom). Left versus right zoom-in panels demonstrate differential staining of CD45.1$^+$ OT-I cells for Tbet, TCF1, and CD25. (B) Representative histocytometry gating of OT-I cells based on Tbet and TCF1 expression and the corresponding CD25 expression. (C) Histocytometry analysis of the image from (A), showing the distribution of myeloid cell populations (top) or OT-I cell subsets (bot- tom). (D and E) dLNs were subdivided into regions dominantly associated with either Tbet$^+$TCF1$^-$ or Tbet$^-$TCF1$^+$ Ki67$^+$ OT-I T cells (representative spatial gating is shown in fig. S7G). (D) Composition of myeloid cells and (E) percent of IRF4$^+$ and pS6$^+$ OT-I cells within each region. (F) Representative positional analysis of Tbet^{HI} and Tbet^{LO} Ki67$^+$ OT-I cells in dLN after OVA plus p(I:C) immunization. (G and H) dLNs were subdivided into Tbet^{HI} or Tbet^{LO} regions. (G) Composition of myeloid cells and (H) percent of IRF4$^+$ and pS6$^+$ OT-I cells within each region. Data in (E) and (H) analyzed by unpaired *t* test with Welch's correction. In (D) and (G), linked points indicate data from the same LNs. All data represent at least two independent experiments.

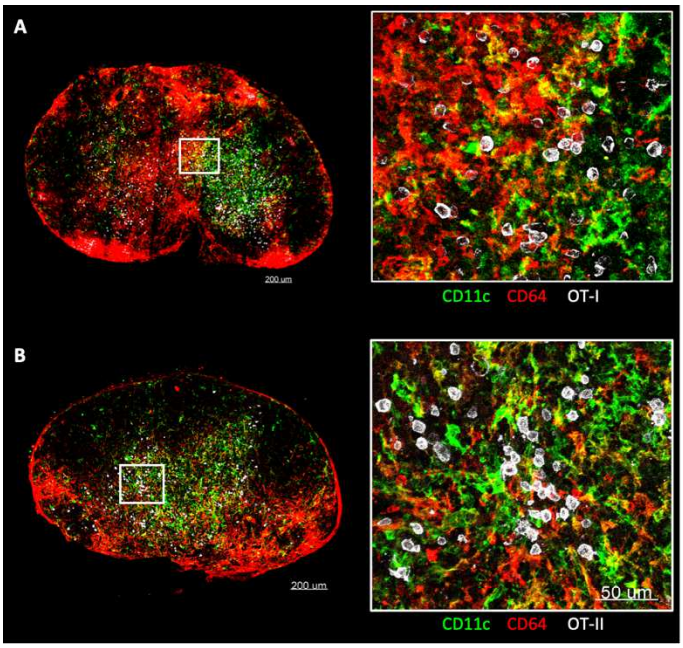
A
200 um
CD11c CD64 OT-I
B
200 um
50 um
CD11c CD64 OT-II

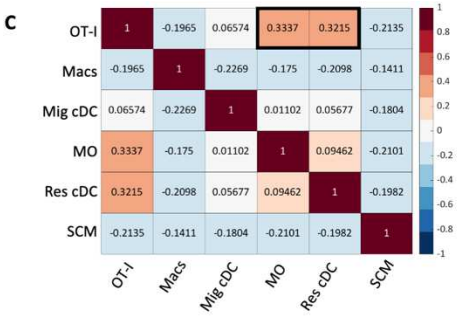
C
OT-I
Macs
Mig cDC
MO
Res cDC
SCM
1 -0.1965 0.06574 0.3337 0.3215 -0.2135
-0.1965 1 -0.2269 -0.175 -0.2098 -0.1411
0.06574 -0.2269 1 0.01102 0.05677 -0.1804
0.3337 -0.175 0.01102 1 0.09462 -0.2101
0.3215 -0.2098 0.05677 0.09462 1 -0.1982
-0.2135 -0.1411 -0.1804 -0.2101 -0.1982 1

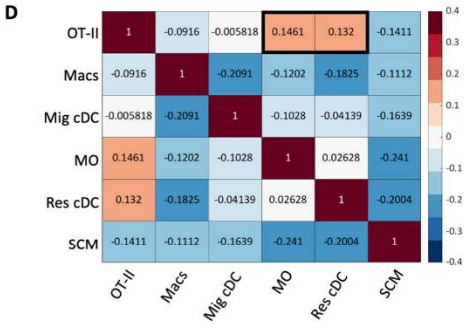
D
OT-II
Macs
Mig cDC
MO
Res cDC
SCM
1 -0.0916 -0.005818 0.1461 0.132 -0.1411
-0.0916 1 -0.2091 -0.1202 -0.1825 -0.1112
-0.005818 -0.2091 1 -0.1028 -0.04139 -0.1639
0.1461 -0.1202 -0.1028 1 0.02628 -0.241
0.132 -0.1825 -0.04139 0.02628 1 -0.2004
-0.1411 -0.1112 -0.1639 -0.241 -0.2004 1

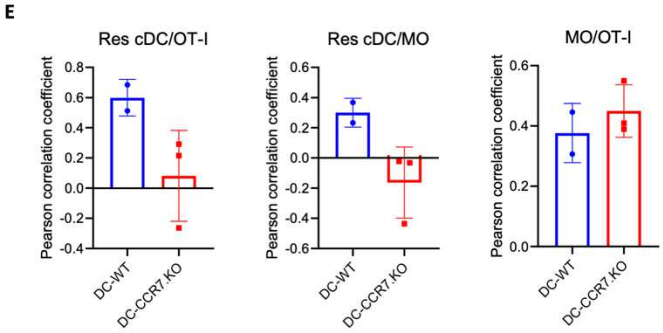
E
Res cDC/OT-I
Res cDC/MO
MO/OT-I
Pearson correlation coefficient
DC-WT
DC-CCR7.KO

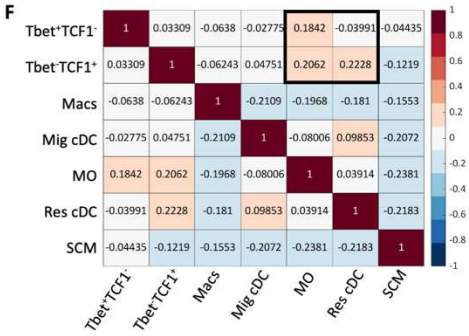
F
Tbet+TCF1-
Tbet-TCF1+
Macs
Mig cDC
MO
Res cDC
SCM
1 0.03309 -0.0638 -0.02775 0.1842 -0.03991 -0.04435
0.03309 1 -0.06243 0.04751 0.2062 0.2228 -0.1219
-0.0638 -0.06243 1 -0.2109 -0.1968 -0.181 -0.1553
-0.02775 0.04751 -0.2109 1 -0.08006 0.09853 -0.2072
0.1842 0.2062 -0.1968 -0.08006 1 0.03914 -0.2381
-0.03991 0.2228 -0.181 0.09853 0.03914 1 -0.2183
-0.04435 -0.1219 -0.1553 -0.2072 -0.2381 -0.2183 1

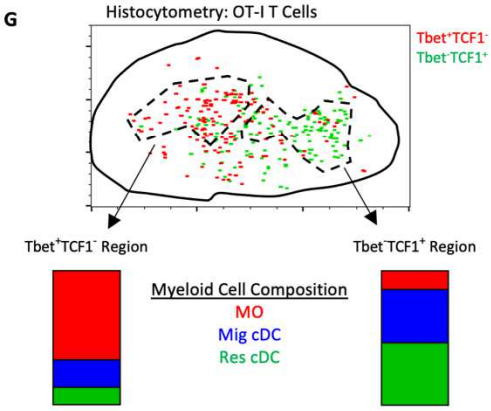
G
Histocytometry: OT-I T Cells
Tbet+TCF1-
Tbet-TCF1+
Tbet+TCF1- Region
Tbet-TCF1+ Region
Myeloid Cell Composition
MO
Mig cDC
Res cDC

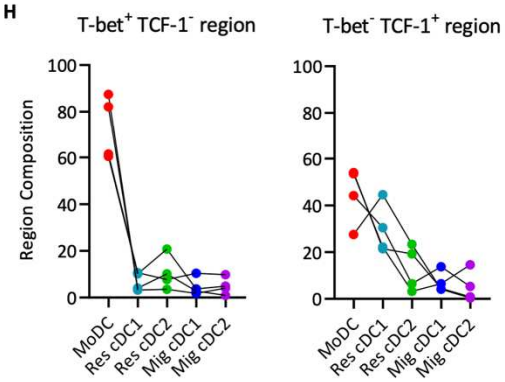
H
T-bet+ TCF-1- region
T-bet- TCF-1+ region
Region Composition
MoDC
Res cDC1
Res cDC2
Mig cDC1
Mig cDC2

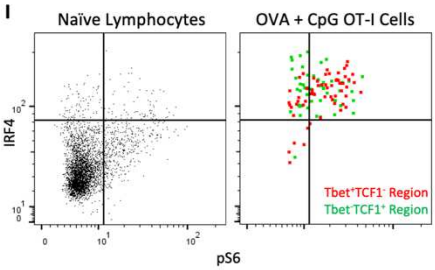
I
Naïve Lymphocytes
OVA + CpG OT-I Cells
IRF4
pS6
Tbet+TCF1- Region
Tbet-TCF1+ Region

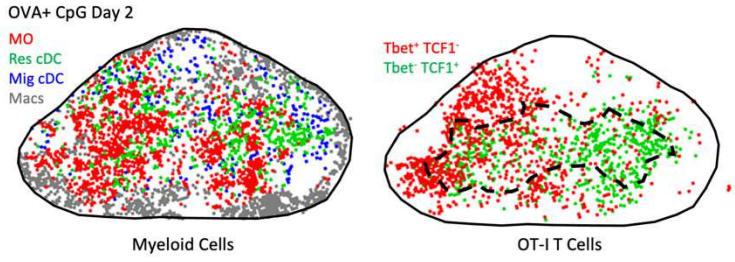
J
OVA+ CpG Day 2
MO
Res cDC
Mig cDC
Macs
Myeloid Cells
Tbet+ TCF1-
Tbet- TCF1+
OT-I T Cells

Fig. S7: Myeloid cell microenvironments in the generation of T cell responses.
(A to **D)** B6 mice were transferred with (A and C) 10^6 OT-I CD8 T cells or (B and D) 10^6 OT-II CD4 T cells and immunized with OVA plus CpG in ears and footpads 1 day later. Auricular and brachial dLNs were assessed 1.75 days later by imaging and histocytometry. (A and B) Representative image demonstrating the distribution of CD11c and CD64 expressing cells and their proximity to (A) OT-I cells and (B) OT-II cells. (C and D) Heatmaps of the spatial correlations of the indicated myeloid cell populations with respect to (C) OT-I and (D) OT-II T cell positioning. Macs, medullary macrophages; SCM, subcapsular sinus macrophages. For (C), n = 7 and for (D), n = 8. Positive values indicate spatial colocalization, negative values indicate spatial avoidance. **(E)** Same experimental setup as in fig. S5, E and F. DC-WT and DC-CCR7.KO mixed BMCs were transferred with 10^6 OT-I CD8 T cells, treated with DT, immunized with OVA plus CpG, and had site removal. 1.5 days after immunization, dLNs were analyzed by histocytometry and CytoMAP. Spatial correlations of the indicated cell populations in DC-WT versus DC-CCR7.KO dLNs. Each point represents an independent dLN. **(F)** Same dataset as (C), but with extended analysis of the spatial correlation of $Tbet^+TCF1^-$ versus $Tbet^-TCF1^+$ OT-I T cells with respect to the indicated myeloid cell subsets. **(G)** Representative spatial gating for Fig. 6, demonstrating $Tbet^+TCF1^-$ and $Tbet^-TCF1^+$ OT-I T cell regions for analysis of myeloid cell composition within those respective regions. **(H)** Extended analysis for Fig. 6D, showing the composition of the indicated myeloid cell subsets within the $Tbet^+TCF1^-$ regions and $Tbet^-TCF1^+$ regions. Linked points represent data from the same dLN. **(I)** Supplementary material for Fig 6E, showing representative histocytometry gating of $IRF4^+$ and $pS6^+$ $Ki67^+$ OT-I T cells in $Tbet^+TCF1^-$ and $Tbet^-TCF1^+$ regions. **(J)** B6 mice were transferred with 10^6 OT-I CD8 T cells and immunized with OVA plus CpG in ears and footpads 1 day later. dLNs were analyzed by histocytometry 2 days later. Representative dLN showing the positioning of indicated myeloid cell populations (left) and OT-I subsets (right). All data represent at least two independent experiments.

MO-dependent differentiation of effector T cells

To test the contribution of MOs to CD4 and CD8 T cell responses, we transferred OT-I and OT-II T cells, immunized the mice with OVA plus CpG, and in some of the animals also blocked MO recruitment with anti-CCR2. In these experiments, we also injected a higher dose of OVA (10ug) to provide MOs with maximal opportunity for antigen presentation. Nevertheless, minimal impact of MO blockade was seen on T cell expansion and expression of Ki67, IRF4 or pS6, indicating that MOs play a negligible role in MHC-I and MHC-II antigen presentation (fig. S8, A and B). In contrast, we observed a drastic reduction in the spatial polarization and generation of

$Tbet^{HI}TCF1^{LO}$ OT-I cells in dLNs of mice that received CCR2-blocking antibody (Fig. 7A), suggesting a major role for MOs in driving localized effector differentiation of CD8 T cells. Similar decreases in the generation of $Tbet^{+}$ effector OT-II CD4 T cells were seen following CCR2 blockade (fig. S8B). Reduced CD8 and CD4 T cell differentiation, but not clonal expansion, was also observed on day 4 (Fig. 7, B and C). Similarly, blockade of MO trafficking resulted in marked attenuation in Tbet and CXCR3 expression, as well as IFNg production upon restimulation by polyclonal GPC-specific CD4 T cells after GPC plus CpG immunization (fig. S8C).

Finally, we tested the direct contribution of IL-12 production by MOs using two distinct mixed BMC models. In the former, we reconstituted irradiated B6 recipients with a 50:50 mix of CCR2-DTR BM and either WT or IL-12.KO BM (fig. S8, D and E). Ablation of MOs using DT administration allowed examination of T cell responses in the presence of MOs derived only from either the WT or the IL-12.KO donors. In the latter model, B6 recipients were reconstituted with IL-12.KO BM together with either WT or CCR2.KO BM, which allowed testing the role of MO-derived IL-12 in the absence of DT-mediated cell toxicity or possible off-target effects (Fig. 7, D and E). In both models, no major changes in T cell expansion were observed 4 days after immunization (Fig. 7, D and E, and fig. S8, D and E). In contrast, we observed significantly reduced OT-I and OT-II T cell effector differentiation and IFN□ □production upon restimulation, indicating that MO-derived IL-12 directly contributes to effector T cell programming. Similar results were seen for polyclonal T cell responses (fig. S8F), as well as after p(I:C) plus OVA immunization (fig. S8G). Collectively, these findings demonstrated that MOs provided a localized source of IL-12 to T cells to drive optimized effector differentiation during Type-I inflammation.

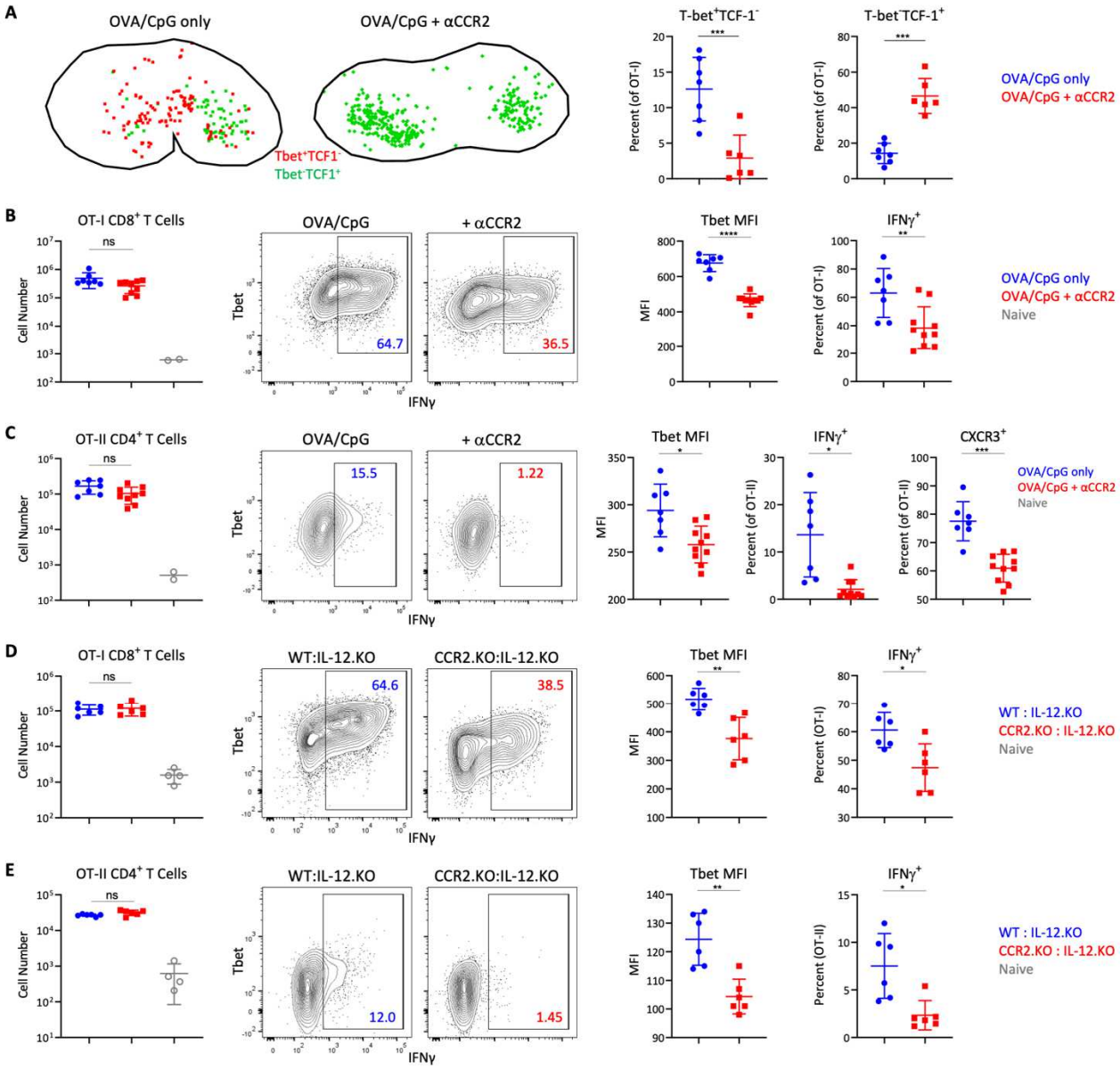

Fig. 7. Optimization of CD4 and CD8 T cell effector differentiation by MOs. (**A**) B6 mice were transferred with 10^6 OT-I T cells and immunized with OVA plus CpG in ears and footpads. Some animals were treated with αCCR2. dLNs were analyzed 1.75 days later by histocytometry for location (left) and frequency (right) of $Tbet^+TCF1^-$ and $Tbet^-TCF1^+$ OT-I cells. (**B** and **C**) B6 mice were cotransferred with 10^5 OT-I and OT-II T cells and immunized with OVA plus CpG in the ears. Some mice were treated with αCCR2. dLNs were analyzed 4 days later by flow cytometry. Total $CD44^+$ cells, Tbet geometric MFI, percentage of $IFN\gamma^+$ T cells after restimulation, and percent $CXCR3^+$ for (B) OT-I and (C) OT-II cells. (**D** and **E**) WT:IL-12p40.KO and CCR2.KO:IL-12p40.KO mixed BMCs were cotransferred with 10^5 OT-I and

OT-II T cells and immunized with OVA plus CpG 1 day later. (D) OT-I and (E) OT-II cellularity and differentiation in dLNs was assessed by flow cytometry 4 days later. Data analyzed by unpaired *t* test with Welch's correction. Data represent at least two independent experiments.

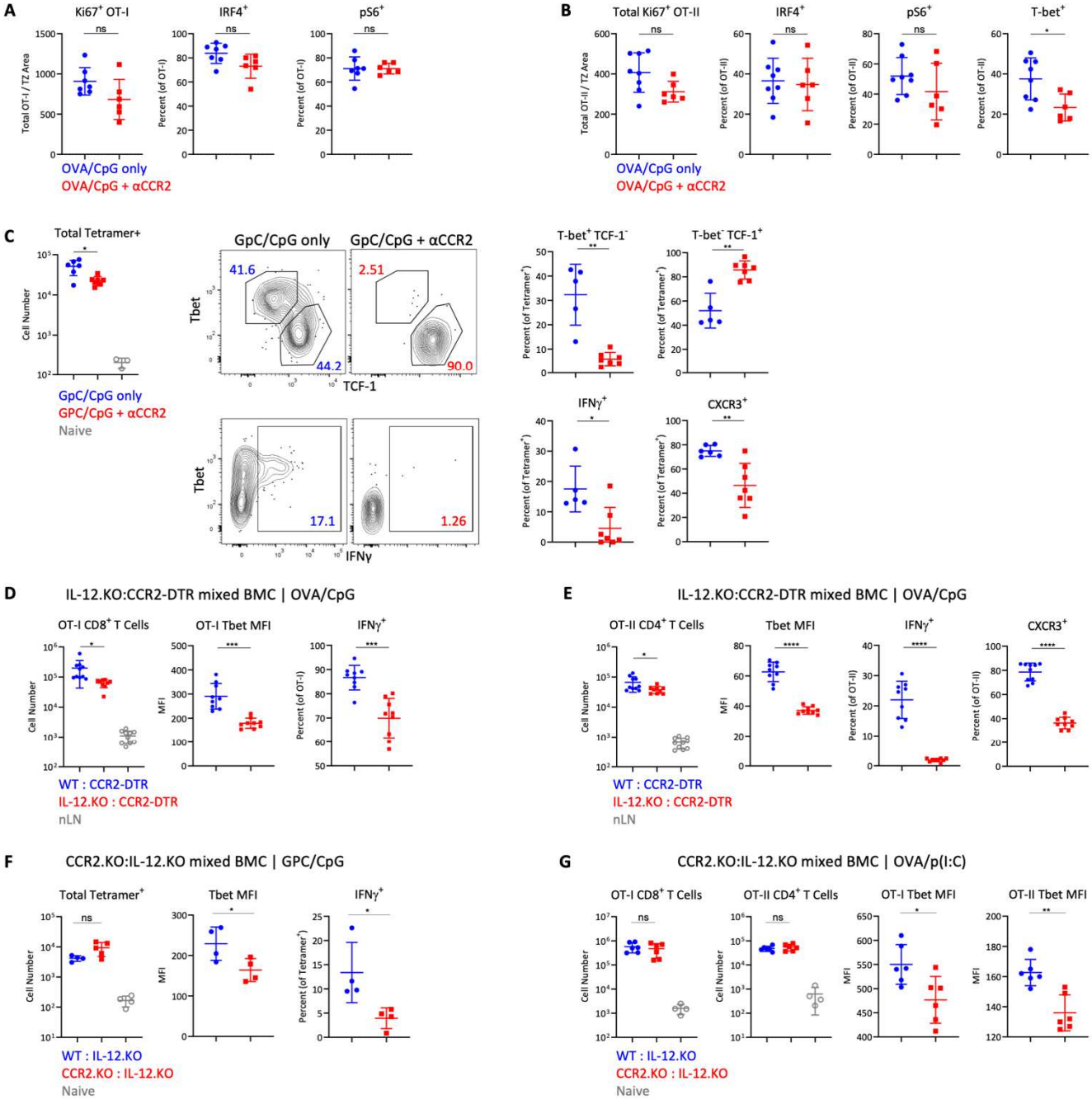

Fig. S8: Regulation of T cell differentiation by inflammatory MOs.
(A and **B)** B6 mice were transferred with (A) 10^6 OT-I CD8 T cells or (B) 10^6 OT-II CD4 T cells and immunized with OVA plus CpG in ears and footpads 1 day later. Some mice were also treated with αCCR2. dLNs were analyzed by histocytometry 1.75 days later. Total $Ki67^+$ OT-I or OT-II cells per TZ area, and percent OT-I or OT-II cells expressing the indicated markers is shown. **(C)** B6 mice were immunized with GPC plus OVA in the ear. Some mice were additionally treated with αCCR2. dLNs were assessed by flow cytometry 7 days later. Total number of $CD44^+$ GPC- $tetramer^+$ CD4 T cells was quantified (left). Tbet and TCF1 expression (top), IFNγ production after restimulation (bottom), and percent $CXCR3^+$ (bottom) were also measured. **(D** and **E)** WT:CCR2- DTR and IL-12p40.KO:CCR2-DTR mixed BMCs were cotransferred with 10^5 OT-I CD8 and OT- II CD4 T cells, treated with DT 1 day later, and then immunized with OVA plus CpG the day after. Cellularity and differentiation of CD44+ (D) OT-I and (E) OT-II T cells were analyzed by flow cytometry 4 days later. (F) WT:IL-12p40.KO and CCR2.KO:IL-12p40.KO mixed BMCs were immunized with GPC plus CpG in the ear. Cellularity and differentiation of CD44+ GPC-tetramer+ CD4 T cells was assessed by flow cytometry 7 days later. (G) WT:IL-12p40.KO and CCR2.KO:IL-12p40.KO mixed BMCs were cotransferred with 105 OT-I CD8 and OT-II CD4 T cells and immunized with OVA plus p(I:C) in the ears. Four days later, dLNs were analyzed by flow cytometry for total number of CD44+Ki67+ OT-I and OT-II cells, as well as Tbet geometric MFI. All data analyzed by unpaired t test with Welch's correction. Each point represents an independent LN. Data represent at least two independent experiments.

Discussion

Here, we defined several critical features of myeloid cell organization that shape T cell responses during Type-I but not Type-II inflammation (fig. S9). We found rapid repositioning of Res cDCs from the LN periphery and concomitant influx of blood-derived inflammatory MOs into the deep TZ of dLNs. The repositioning of Res cDCs allowed for efficient MHC presentation of draining antigens in the appropriate anatomical compartment to elicit early T cell activation and differentiation. MO influx on the other hand provided an additional source of signal-3 cytokines to responding T cells, promoting generation of fully differentiated effector responses. Together, these distinct innate cell types functionally cooperated with one another to promote the generation of optimized adaptive immunity. We found extensive heterogeneity in MO infiltration across the TZ, which generates distinct microenvironments with varied MO and cDC abundance. Priming of

T cells within these microenvironments influenced the exposure of T cells to different activating stimuli, such as MO-produced IL-12, and promoted localized generation of different effector subsets. Thus, inflammatory innate microenvironments within dLNs regulated the overall quality and heterogeneity of the resulting T cell responses.

The finding that LN Res cDCs respond to inflammatory stimuli and use CCR7 to reposition within the dLNs is consistent with the migration programs of peripheral tissue and splenic cDC subsets (*12*, *56*, *78*, *83*). Our data connect these observations, demonstrating that cDCs across multiple different tissues utilize the CCR7 axis during inflammation for migration into the most proximal T cell compartments. These observations also highlight caveats in studies using CCR7.KO animals to dissect the role of migratory cDCs, as we showed that the same pathway was utilized by LN Res cDCs for intra-nodal repositioning. Similar considerations likely apply to other models in which the migratory capacity of multiple cDC populations may be affected (*83*, *107–109*). Our findings do not argue against the role of migratory cDCs in T cell immunity, as these cells are critical during highly tropic infections (*15*, *110*), and for promoting Th2 and TfH responses (*108*, *111*, *112*). Migratory cDCs and pDCs can also cargo antigens to Res cDCs (*16*, *26*, *58*, *63*, *113*, *114*). Indeed, we did not find efficient Res cDC repositioning or MO recruitment in Type-II inflammatory conditions, supporting the importance of migratory cDCs in these settings. Instead, our observations indicated that in conditions of ample antigen drainage after vaccination or during certain microbial infections, Res cDCs are exceptionally potent at inducing T cell activation (*7*, *9*, *14*, *86*, *115*). A better understanding of the distinct contributions of peripheral vs. Res cDC populations in different immunologic settings will aid in vaccine design (*116*). Of note, the responses seen for LN-res cDC1s, cDC2s and MOs occurred in response to multiple Type-I

agonists regardless of TLR expression on these populations (*117–119*). This suggests that secondary inflammatory mediators, such as IFN-I or TNFα, may be involved (*33*, *87*, *120*, *121*).

In addition, we provided substantial insight into the organization and role of MOs during Type-I inflammation. As early as 6h after immunization, MOs entered the dLNs, primarily via the local HEVs instead of the afferent lymphatics, and rapidly occupied various LN regions, including the medulla, B cell follicles and parts of the TZ. CCR2 appears critical for this process and it is likely that CCR2 ligands in both the BM and inflamed dLNs are involved (*37*, *68*, *87*). In contrast, CCR7 was not essential for MO trafficking to the dLNs during inflammation, and if anything, previous studies have reported increased numbers in CCR7.KO mice (*37*, *66*). There was substantial heterogeneity in MO infiltration across the TZ, likely driven by localized afferent drainage and polarized dispersal of inflammatory stimuli (*7*). This heterogeneity generated distinct microenvironments in dLNs which were directly associated with different effector CD8 T cell subtypes, with more differentiated effector T cells primarily observed within MO-rich regions, and less differentiated cells found in cDC1-dominated regions with lower MO abundance. Divergent T cell programming appeared to be at least in part MO-derived IL-12 mediated, as blockade of MO trafficking or IL-12 production resulted in loss of effector T cell spatial polarity and reduced differentiation. Thus, MOs generated highly inflammatory microenvironments in LNs to promote the generation of fully differentiated effector T cells in a localized fashion. Our findings do not contradict previous observations that cDC1s can produce IL-12 and promote effector T cell differentiation (*97*, *98*, *100*, *101*, *122*, *123*). Indeed, we observed potent IL-12 production by Res and migratory cDC1s, and MO blockade suppressed but did not abolish effector T cell responses. Instead, our data suggested that cDCs provide an early source of IL-12 and this is further amplified

by the IL-12 derived from MOs in a localized fashion. Therefore, the collaborative action of both cDCs and MOs was important for optimized generation of adaptive immunity.

It is important to note that our spatial analysis was largely limited to use of tissue sections from individual timepoints, and that generation of effector T cells in MO-rich regions could be in part influenced by cellular repositioning after initial priming. This may particularly be true for CD4 T cell responses, which have distinct kinetics of effector programming and additional chemotactic properties as compared to CD8 T cells (*25*, *39*, *43*, *52*). Statistical region analysis, as performed here, minimized this issue, but the development of next generation technologies capable of comprehensive spatiotemporal tracking of T cell fates across entire organs and over time is necessary. In addition, our study did not thoroughly investigate all possible immunologic settings. Whether similar processes occur in other conditions, such as autoimmunity or cancer, and how distinct myeloid cell microenvironments influence T cell priming remain to be investigated. Our findings do highlight the concept that rational vaccine strategies to simultaneously target multiple innate cell populations, including MOs, should be explored (*1*, *124*). MOs are a highly plastic innate cell population capable of a wide spectrum of functions (*125*). Given their abundance and ability to infiltrate most tissues, strategies to modulate MO trafficking and function may prove of value in a variety of settings. In conclusion, our findings revealed fundamental features of innate-adaptive cell crosstalk during Type-I inflammation, demonstrating that the spatial coordination and functional cooperation of innate cells within dLNs was critical for the generation and shaping of adaptive responses to vaccines and infections.

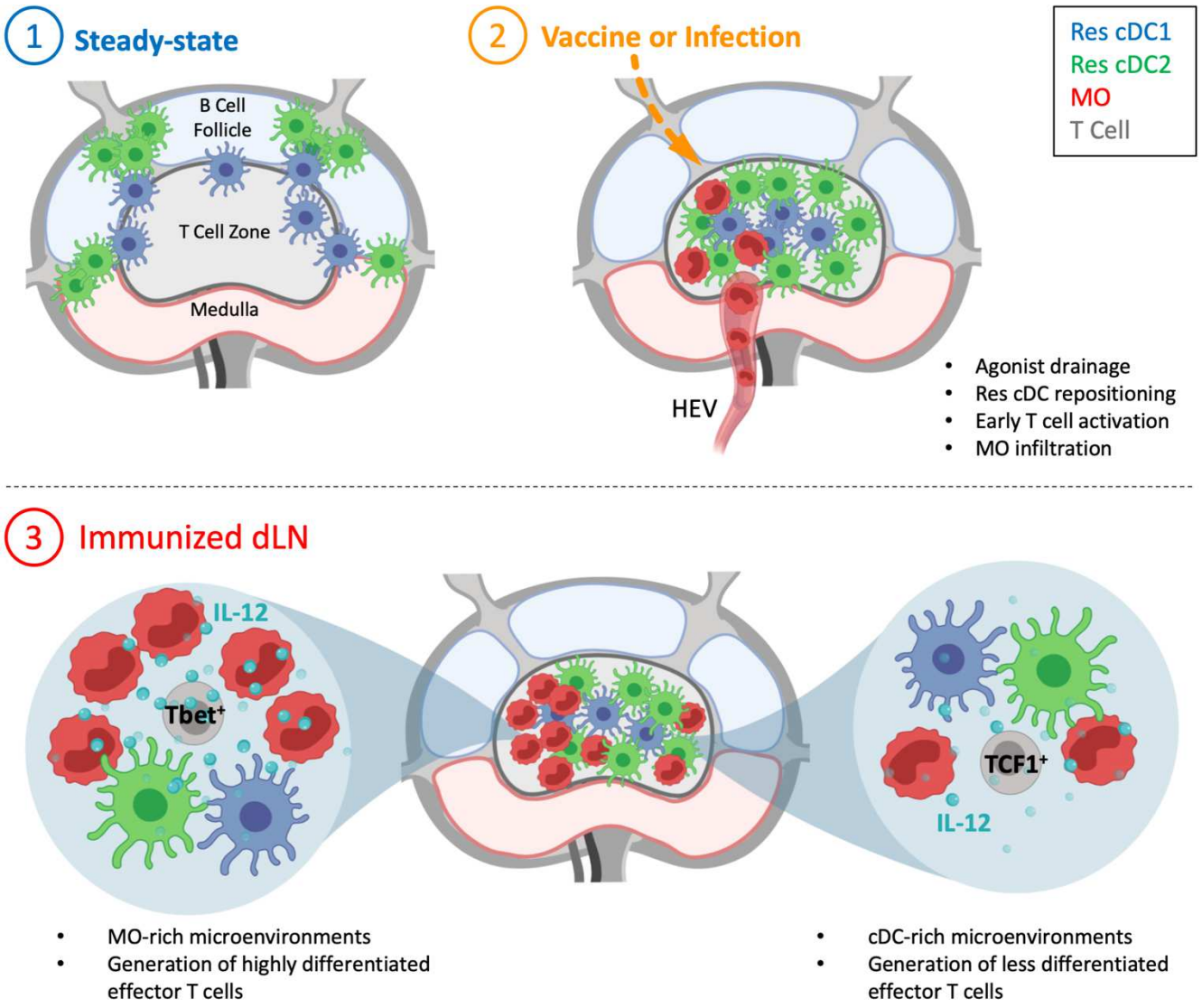

Fig. S9: Model of innate and adaptive immune cell cross-talk during type I inflammation. **(1)** Within steady-state LNs, Res cDC are localized in the interfollicular and medullary peripheral regions, promoting robust sampling of draining antigens. **(2)** During type I inflammation, Res cDCs rapidly relocalize from the LN periphery into the deep TZ in a CCR7-mediated fashion to induce early T cell activation. Concurrently, MOs begin to infiltrate the dLNs in large numbers via HEVs and migrate into the TZ, bringing in an additional and substantial source of IL-12 cytokine for effector T cell differentiation. **(3)** MO infiltration is nonuniform across the TZ, leading to heterogeneity in the local abundance of MOs and cDCs, and the generation of MO-rich vs cDC- rich LN microenvironments. These distinct LN microenvironments support divergent T cell programming across the tissue, with the highly differentiated effector T cells primarily being found in the MO-rich regions, and less differentiated T cells predominantly found in areas rich with cDCs and with lower MO abundance.

Chapter 4. Direct and indirect inflammatory signals direct the activation and composition of the cDC compartment in lymph nodes

Introduction

Myeloid cell sensing of pathogens is a hallmark of innate immunity, as the ability of myeloid cells to become alerted to foreign invaders is a first and critical step in ramping up the immune response to instruct the adaptive immune system and protect the body from harm (*126*). Myeloid cell sensing of pathogen derived material relies on their expression of pattern recognition receptors, or PRR, that bind to pathogen associated molecular patterns (PAMPs). Signaling through PRRs leads to a cascade of important cellular changes that creates an activation state conducive to shutting down bacterial or viral replication and priming T cells (*29*, *126*). Namely, PRR activated myeloid cells are licensed to traffic to draining LNs and secrete potent inflammatory cytokines, which can then alert the rest of the immune system to the growing threat.

Although it has been previously shown that both direct sensing of PAMPs and secondary inflammatory mediators by Res cDCs leads to similar activation profiles, it was unclear what signals were required to fully license Res cDCs to initiate the immune response (*121*). Previous studies have suggested that DCs activated via secondary inflammatory mediators like IFN-I or TNFα were incapable of fully priming effector T cells, instead generating T cell that clonally expanded but were less differentiated (*121*). This inability to generate fully differentiated T cells was linked to deficient IL-12 production in the absence of direct pathogen sensing. However, this view has been challenged by other reports, namely ones suggesting that the adjuvant activity of p(I:C) is dependent entirely on its ability to elicit the generation of copious amounts of Type I interferon (*32*, *33*). Direct sensing by stromal cells, not cDCs, drove IFN-I production and subsequent cDC activation, representing a paradigm shift in the field and showing that direct sensing of pathogen derived material by cDCs is not always necessary. Given the conflicting

roles in the literature of direct versus indirect signaling in the maturation and priming ability of cDCs, we sought to clarify the signals required for Res cDC maturation and inflammatory cytokine production after immunization with distinct vaccine adjuvants.

The observation that Res cDC relocalization and monocyte influx was consistent across the Type 1 agonists we tested (Chapter 3), despite heterogeneous expression of TLRs, was intriguing. While TLR expression differs significantly between Res cDC1 and Res cDC2 (Table 1), these DCs can still express the Type I interferon alpha/beta receptor (IFNAR) and the TNFα receptor (*5*). This suggested that many Res cDCs were upregulating CCR7 and relocalizing to the deep T zone in response to secondary inflammatory mediators and not in response to direct sensing of draining adjuvant via TLRs.

Here, we surprisingly found that direct TLR agonist sensing was not needed for efficient maturation and relocalization of Res cDCs in a cell intrinsic manner after CpG, while IFN-I was mainly required for expression of so-stimulatory molecules by Res cDC after p(I:C). Whether Res cDC were unable to directly sense TLR agonists or IFN-I, they were unrestricted in their ability to upregulate CCR7 or in the ability to produce IL-12, suggesting a high degree of redundancy in the ability of DCs to become activated by different inflammatory cytokines generated during vaccination. Furthermore, we found that vaccination with MyD88-dependent TLR ligands increased the frequency and cellularity of Res cDC2s in dLNs. This increase was dependent on cDC intrinsic MyD88 signaling, and was accompanied by enhanced recruitment of pre cDC2s, but not pre cDC1s, to the dLN, suggesting that TLR signaling can potentially modulate the recruitment and differentiation of DC precursors to augment the ongoing immune response.

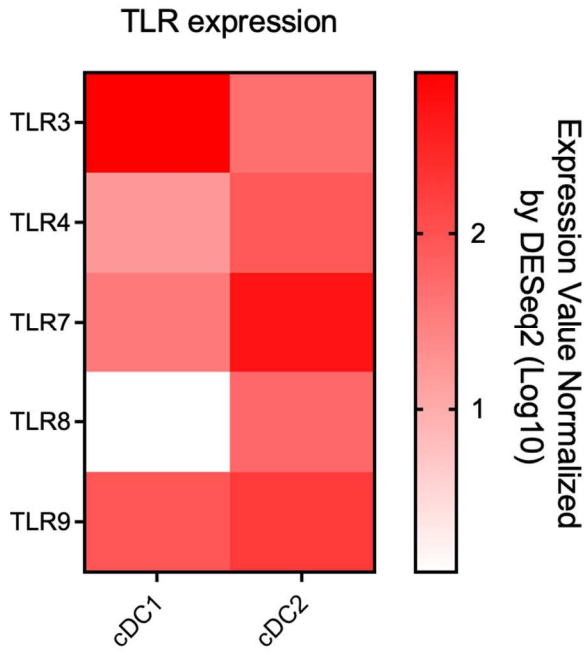

Table 1. Relative expression of toll-like receptors by splenic cDCs at steady state
Source: ImmGen

Results

Immunization with TLR ligands activates Res cDCs and leads to a selective increase in Res cDC2 cellularity

We first investigated Res cDC maturation and cellularity in dLNs after vaccination with TLR agonists with distinct mechanisms of action, CpG and p(I:C). As in Chapter 3, we immunized mice s.c in the ear and then examined Res cDC maturation and localization 1 day later via flow and histocytometry. We found that as previously described, both CpG and p(I:C) induced maturation of Res cDC1s and cDC2s, as indicated by upregulation of CCR7 and the costimulatory molecule CD80 (Figure 1A). Of note, we observed increased CD80 expression on

Res cDC after immunization with p(I:C) compared to CpG, likely reflective of the larger Type I interferon response associated with p(I:C). We found that Res cDCs sensed IFN-I by 6hrs in LNs after p(I:C), as indicated by phosphorylation of STAT1 (Figure S1A), whereafter they relocalized to the deep TZ and expressed the interferon stimulated gene 15 (ISG15) (Figure S1, B and C). Interestingly, when we examined Res cDC cellularity we found a significant increase in the numbers of Res cDC2s, but not cDC1s, after vaccination with CpG (Chapter 3, Supplementary Figure 1H). This increase in Res cDC2 cellularity was observed with CpG, R848, and LPS adjuvants, all of which signal through MyD88, but not but not with p(I:C), which signals through the adaptor TRIF. The observed increase in cellularity was accompanied by a marked skewing of the cDC ratio towards Res cDC2s and away from Res cDC1s (Figure 1B). We next aimed to uncover when this shift in the Res cDC ratio was occurring by immunizing mice with CpG and then harvesting dLNs at multiple time points up to 24 hours for analysis by flow cytometry. We found that although small fluctuations occurred in the ratio of Res cDC2s to Res cDC1s at early timepoints, the increase was not readily apparent until 24 hrs post immunization (Figure 1C). This timing indicates that unlike other observed Res cDC phenotypic changes that occur within several hours post vaccination, there is a temporal delay in the skewing of the Res cDC compartment towards cDC2s. Together, these data indicated that Res cDC maturation in LNs is accompanied by a significant shift in the frequency and number of Res cDC2s.

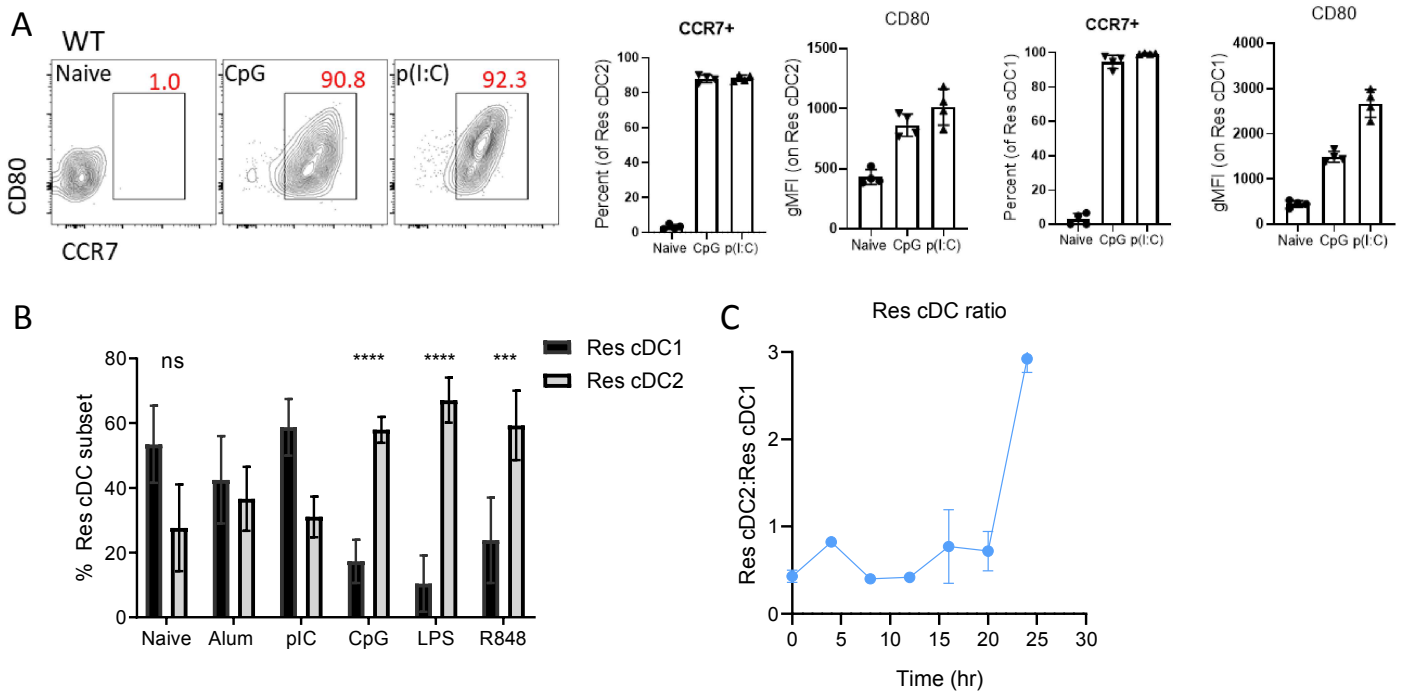

Figure 1. Immunization with TLR ligands activates Res cDCs and leads to a selective increase in Res cDC2 cellularity. (A) WT B6 mice were injected i.d in the ear with p(I:C) or CpG and draining auLNs were harvested 24 hrs later for flow cytometry analysis of Res cDC maturation. (B) The frequency of each indicated Res cDC subset of total Res cDCs in auLNs 1 day post immunization with the indicated adjuvant i.d in the ear. (C) WT B6 mice were injected with CpG and auLNs were harvested at the indicated time points for flow cytometry analysis of the Res cDC ratio, calculated as the frequency of Res cDC2s divided by the frequency of Res cDC1s.

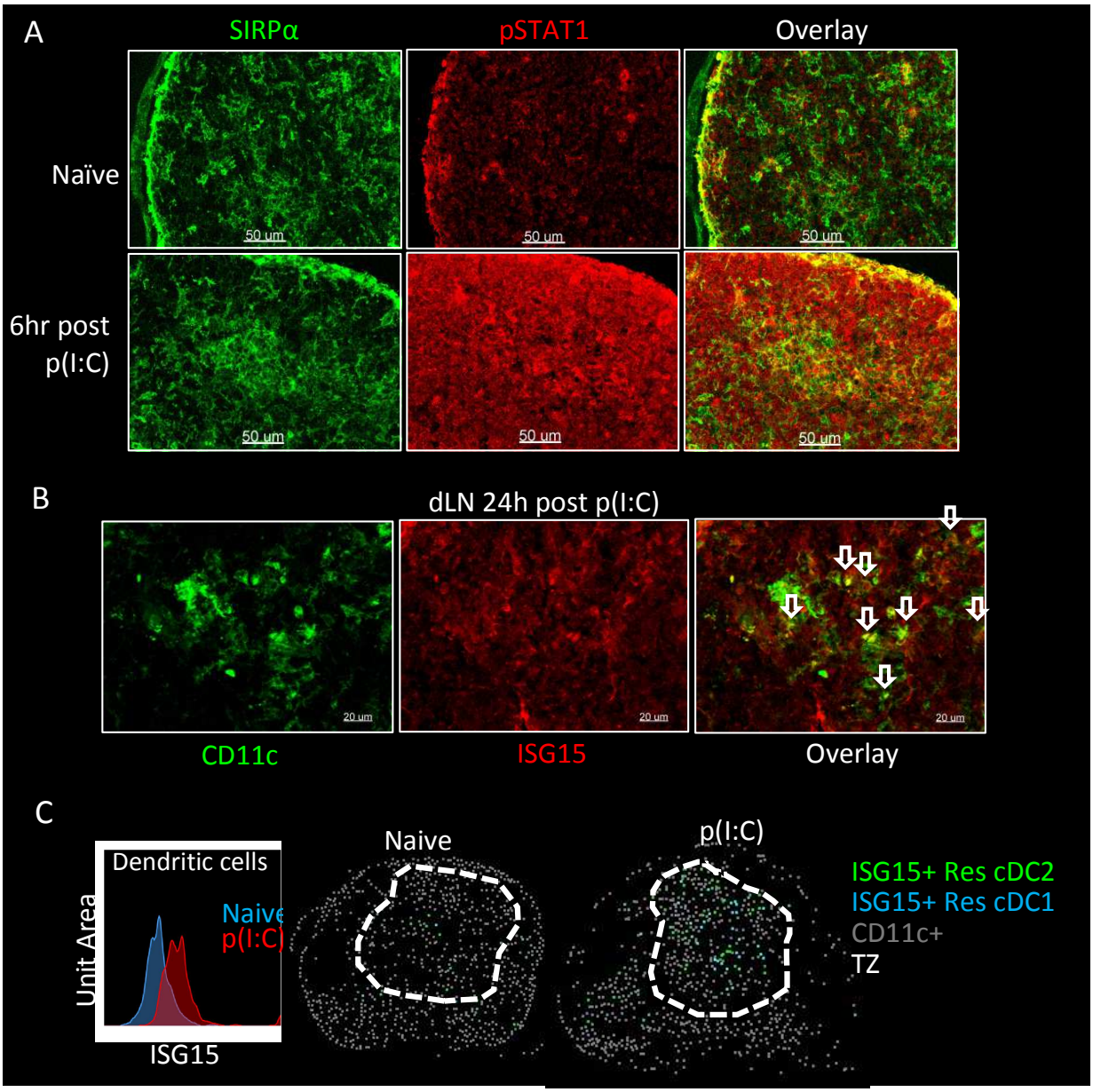

Supplemental Figure 1. Res cDCs rapidly sense Type I interferon and relocalize to the TZ. (A) WT B6 mice were injected with p(I:C) and auLNs were harvested 6 hrs later for confocal imaging analysis of pSTAT1 staining, indicating signaling downstream of IFNAR activation. (B) WT B6 mice were injected with p(I:C) and auLNs were harvested 24 hrs later for confocal imaging analysis of ISG15 staining, an interferon stimulated gene, and the corresponding histocytometry analysis (C).

The MyD88 and IFNAR signaling pathways are important for Res cDC maturation and relocalization

Next, we investigated the role of the MyD88 and IFNAR signaling axes in the maturation of Res cDCs by immunizing mice that were either sufficient or deficient in the ability to directly sense draining TLR agonist (MyD88.KO mice) or sense the secondary inflammatory mediator Type I IFN through IFNAR (IFNAR.KO mice) with CpG or p(I:C). We used p(I:C) and IFNAR.KO mice as a control for indirect activation since it has been described that stromal cell produced IFN-I is essential for cDC maturation in response to p(I:C) immunization (*32*, *33*). We found that Res cDC did not become activated after immunization with CpG in MyD88.KO mice (Figure 2A), as expected, since CpG signals through TLR9 and the adaptor of TLR signaling, MyD88. Also as expected, Res cDC maturation was intact after immunization with p(I:C) in MyD88.KO mice (Figure 2A), as p(I:C) signals primarily through TLR3 and the adaptor TRIF, not MyD88. When we immunized mice lacking IFNAR, we found a complete defect in the ability of Res cDCs to become mature after p(I:C), confirming previous reports (Figure 2B). We observed some minor defects in CCR7 expression and CD80 expression of Res cDCs after CpG immunization in IFNAR.KO mice, suggesting some dependence on this signaling access for reaching full maturation (Figure 2B). In contrast, the maturation of Res cDCs after p(I:C) was fully dependent on sensing IFN-I, as has been reported in the literature. We next investigated the localization of Res cDCs in IFNAR.KO mice after p(I:C) or CpG immunization. Given the defect in CCR7 upregulation by Res cDCs was largely limited to p(I:C) and not CpG, we expected only that group to display defects in relocalization. Indeed, when Res cDC relocalization was assessed by histocytometry, we found a significant defect in entry of Res cDCs into the TZ of IFNAR.KO mice compared to WT (Figure 2C). Together, these data

indicate that the MyD88 and IFNAR signaling axes can be required for Res cDC maturation and localization depending on the given inflammatory stimuli.

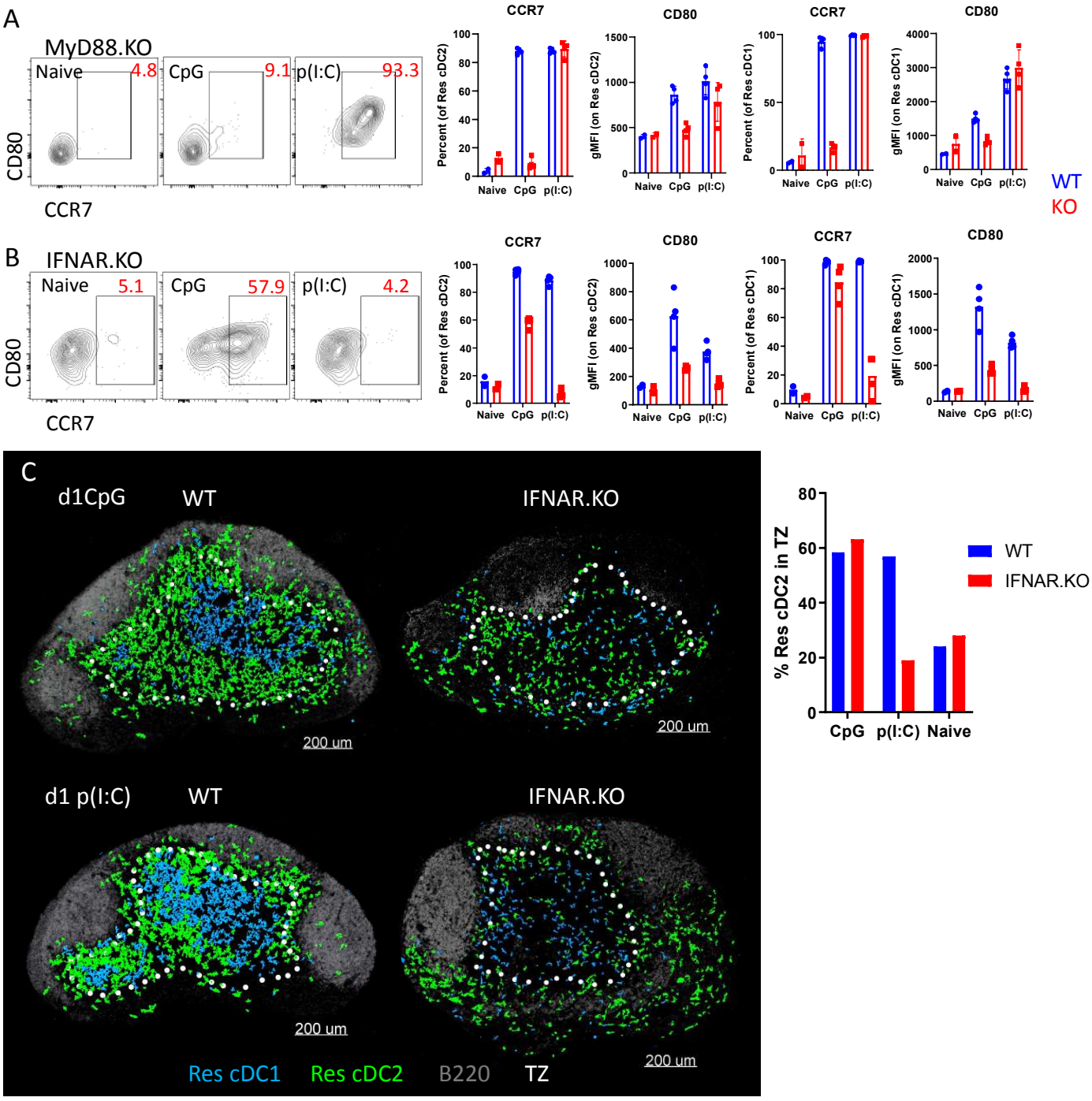

Figure 2. Res cDC maturation and relocalization during inflammation requires global MyD88 and IFNAR signaling. WT and MyD88.KO (A) or IFNAR.KO (B) mice were injected with p(I:C) or CpG and auLNs were harvested 24 hrs later for flow cytometry analysis of Res cDC maturation. (C) IFNAR.KO mice were injected with p(I:C) or CpG and auLNs were harvested 24 hrs later for confocal imaging (left) and histocytometry analysis (right) of Res cDC localization.

Res cDC maturation and relocalization during inflammation does not require cell intrinsic MyD88 or IFNAR signaling, but is required for increased cellularity of Res cDC2s

While these data suggested differential involvement of the MyD88 and IFNAR signaling modules in cDC maturation and localization, it was not clear whether cell-intrinsic direct versus indirect signaling was required in the maturation and localization of Res cDCs. Upstream direct sensing of CpG by another cell type could lead to the production of secondary inflammatory mediators other than IFN-I that can in turn activate the Res cDCs. Thus, the requirement of direct sensing of TLR agonist by Res cDC for their maturation must be determined in a model with a cell-intrinsic KO of MyD88 signaling. To that end, we created mBMCs consisting of a 50:50 mixture of MyD88.KO or IFNAR.KO and congenically marked WT BM. In this model, MyD88.KO Res cDCs would be intermixed with WT cells capable of directly sensing CpG. Thus, this mBMC models allowed us to assess the cell intrinsic roles for both MyD88 and IFNAR signaling in the maturation and localization of Res cDCs during inflammation. We immunized these chimeras with CpG or p(I:C) and assessed their activation profiles by flow cytometry 1 day post injection. Using congenic markers, we were able to clearly separate cells derived from the MyD88.KO or IFNAR.KO (CD45.2+) and WT fractions (CD45.1+) and found no major differences in the proportions of these cells at steady state (Figure 3A). We found that whether Res cDC2s lacked MyD88 or IFNAR, they were capable of upregulating CCR7 and CD86 in response to both CpG and p(I:C) (Figure 3B). The only major activation defect

observed was that IFNAR.KO Res cDC1s and cDC2s failed to fully upregulate CD86. Although we observed minor differences in CCR7 expression between IFNAR.KO and WT cDCs after p(I:C), the majority of these cells were still capable of upregulating CCR7. We next investigated the localization of MyD88.KO and IFNAR.KO Res cDCs in the LN after CpG or p(I:C) administration. Given that we observed minor defects in CCR7 upregulation in the KO cDCs, we hypothesized that there would be minor localization differences between WT and KO cDCs. Indeed, we observed no major differences in the frequencies of either cDC1 or cDC2 in the TZ by histocytometry, with KO and WT cDCs largely intermixed with one another within the TZ (Figure 3C). Of note, there was a trend towards reduced cDC relocalization in IFNAR.KO dLNs after p(I:C), indicating that although CCR7 expression was largely intact, some positional differences remain. Together, these data demonstrate that activation of cDCs after CpG can be indirect and independent of IFN-I sensing, suggesting a role for the sensing of other secondary inflammatory mediators. Activation of cDCs after p(I:C) was indirect and in part mediated by IFN-I, as previously reported, but additional inflammatory mediators likely contribute to the full maturation program. These data further suggest that while the MyD88 and IFNAR signaling axes are critical for Res cDC responses to CpG and p(I:C), respectively, this requirement is not Res cDC intrinsic, indicating profound redundancy in activation potential by additional inflammatory stimuli.

Next, we investigated whether direct MyD88 signaling regulated the shift in frequency and cellularity of Res cDC2s seen after TLR agonist immunization. Given that the Res cDC2:Res cDC1 shift occurred only in those adjuvants that signaled through MyD88, but not Alum or p(I:C), we hypothesized that MyD88 signaling would also be required to promote the enhanced Res cDC2 cellularity. To test this, we immunized MyD88.KO/WT and IFNAR.KO mBMCs with

CpG or p(I:C) and examined the frequency and number of Res cDCs by flow cytometry. We found that Res cDC2s increased in frequency and cellularity after CpG, but not p(I:C), as previously observed (Figure 3D, right). In the absence of MyD88 signaling, Res cDC2 frequency and number were comparable to steady state conditions, while the skewed Res cDC2:Res cDC1 ratio was maintained in IFNAR.KO cells after CpG (Figure 3D, left). These data indicate that skewing towards Res cDC2s was in large part dependent on cell intrinsic signaling through MyD88 and not on indirect sensing of Type I interferons.

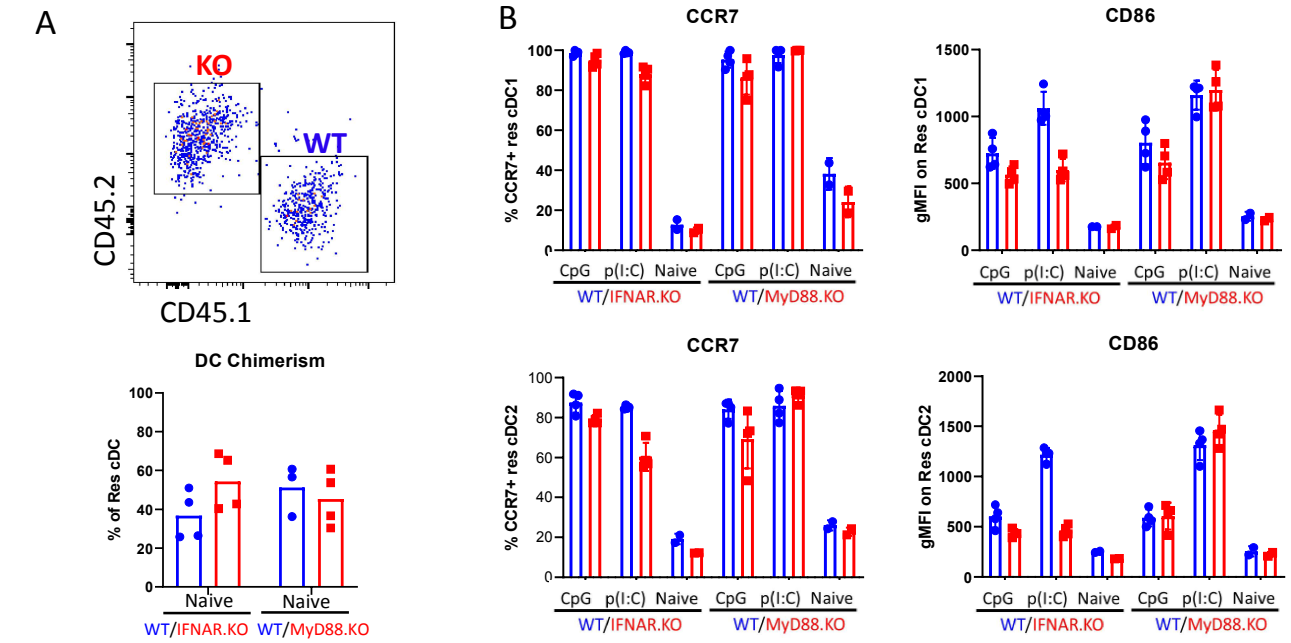
A
KO
WT
CD45.2
CD45.1
DC Chimerism
% of Res cDC
Naive
Naive
WT/IFNAR.KO
WT/MyD88.KO
B
CCR7
% CCR7+ res cDC1
CD86
gMFI on Res cDC1
CpG p(I:C) Naive CpG p(I:C) Naive
WT/IFNAR.KO
WT/MyD88.KO
CCR7
% CCR7+ res cDC2
CD86
gMFI on Res cDC2

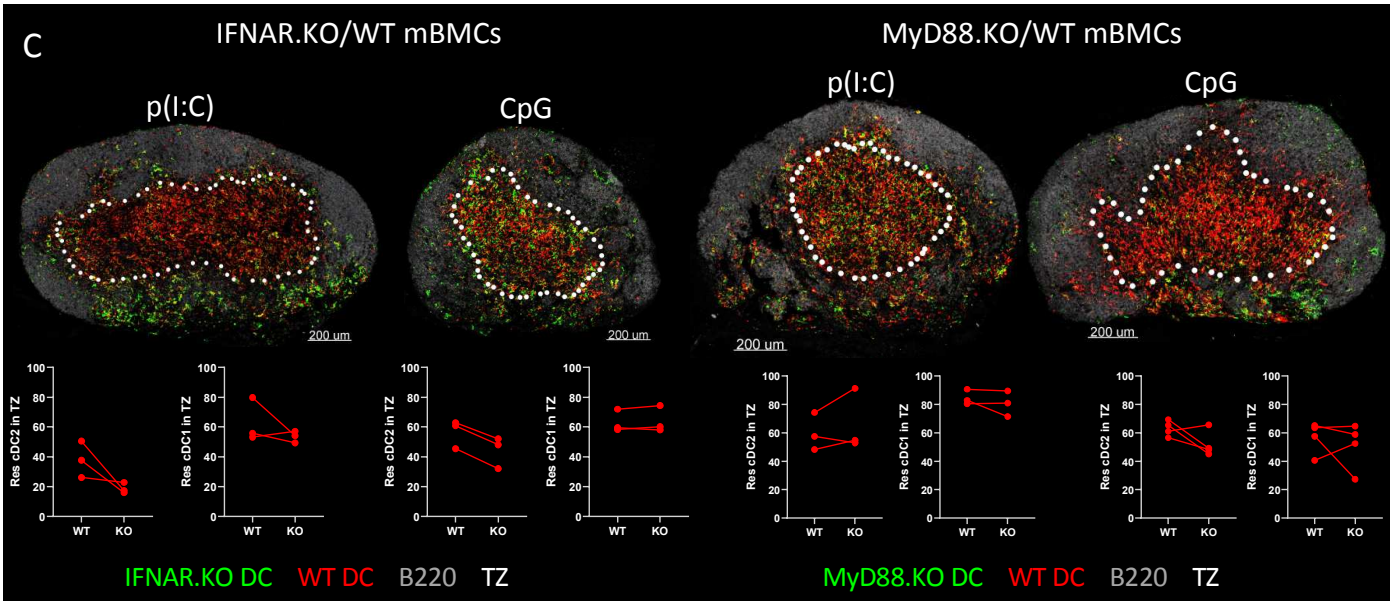
C
IFNAR.KO/WT mBMCs
MyD88.KO/WT mBMCs
p(I:C)
CpG
p(I:C)
CpG
200 um
Res cDC2 in TZ
Res cDC1 in TZ
WT
KO
IFNAR.KO DC
WT DC
B220
TZ
MyD88.KO DC
WT DC
B220
TZ

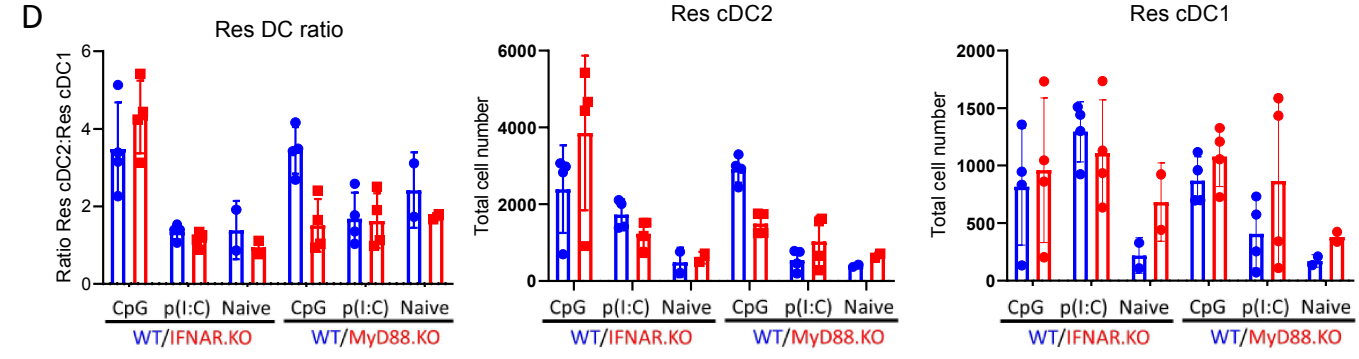
D
Res DC ratio
Ratio Res cDC2:Res cDC1
Res cDC2
Total cell number
Res cDC1
Total cell number
CpG p(I:C) Naive CpG p(I:C) Naive
WT/IFNAR.KO
WT/MyD88.KO

Figure 3. Res cDC maturation and relocalization during inflammation does not require cell intrinsic MyD88 and IFNAR signaling but is required for increased Res cDC2 cellularity. MyD88.KO/WT and IFNAR.KO/WT mixed BMCs were injected i.d in the ears with CpG or p(I:C) and auricular dLNs were harvested 24 hours later for flow cytometry and confocal imaging analysis. (A) WT and KO cells were gated based on congenic marker expression (top) and the frequency of the WT and KO cDCs was assessed at steady state (bottom). Res cDC activation (B) and localization (C) was assessed by flow and histocytometry, respectively. (D) The Res cDC ratio and cellularity showing a selective reduction in the Res cDC2 to Res cDC1 ratio (left) and Res cDC2 cellularity (right).

Increased cellularity of Res cDC2s during inflammation is associated with increased pre cDC2 recruitment to dLNs

Next, we investigated mechanisms underlying the observed increase in Res cDC2 cellularity. We hypothesized that the increase in Res cDC2s could be a result of 1) *in situ* proliferation upon direct sensing and TLR signaling, or 2) MyD88-dependent preferential recruitment of pre cDC2s, a population of bone marrow derived DC precursors fated to become cDC2s. In both cases, we hypothesized that cell intrinsic MyD88 signaling would be required. To investigate the first hypothesis, we examined Ki67 expression on Res cDC2s in WT/MyD88.KO mBMCs 24 hours after immunization with CpG or p(I:C). We found that immature Res cDC2s from naïve mice expressed significantly more Ki67 than mature Res cDC2s from immunized mice, and this expression was largely independent of the ability to signal through MyD88 (Figure 4A). These data indicate that, if anything, immature Res cDCs are in a state of self-renewal during steady state conditions and that inflammation causes activated mature Res cDC2s to stop proliferating. These preliminary findings suggest that in situ proliferation of Res cDC2s does not likely account for the observed increase in Res cDC2s during inflammation.

We next explored our second hypothesis, that recruitment of DC precursors could be responsible for boosting the frequency and numbers of Res cDC2s during inflammation. To accomplish this,

we immunized mice with either CpG or p(I:C) and used a flow cytometry panel designed for the detection of pre DCs at both 12 and 24 hr time points. Pre DCs have been described in the literature as CD11c+ MHC2- CD43+ SiglecH- SIRPa+ cells and are further divided into pre cDC2s (CD115+) or pre cDC1s (CD117+) (*18*, *127*). Using this gating strategy, we were able to detect pre cDCs in both spleen and dLNs after vaccination (Figure 4B). We found an increase in both frequency and number of pre cDC2s in dLNs and spleen after immunization with CpG, but not p(I:C) (Figure 4C). This difference was most striking at the 24 hr timepoint, although pre cDC2s began accumulating in dLNs and spleen 12 hrs post immunization compared to steady state. Together, these data indicate that pre cDC recruitment, not *in situ* proliferation, may explain observed increases in Res cDC2 cellularity during inflammation.

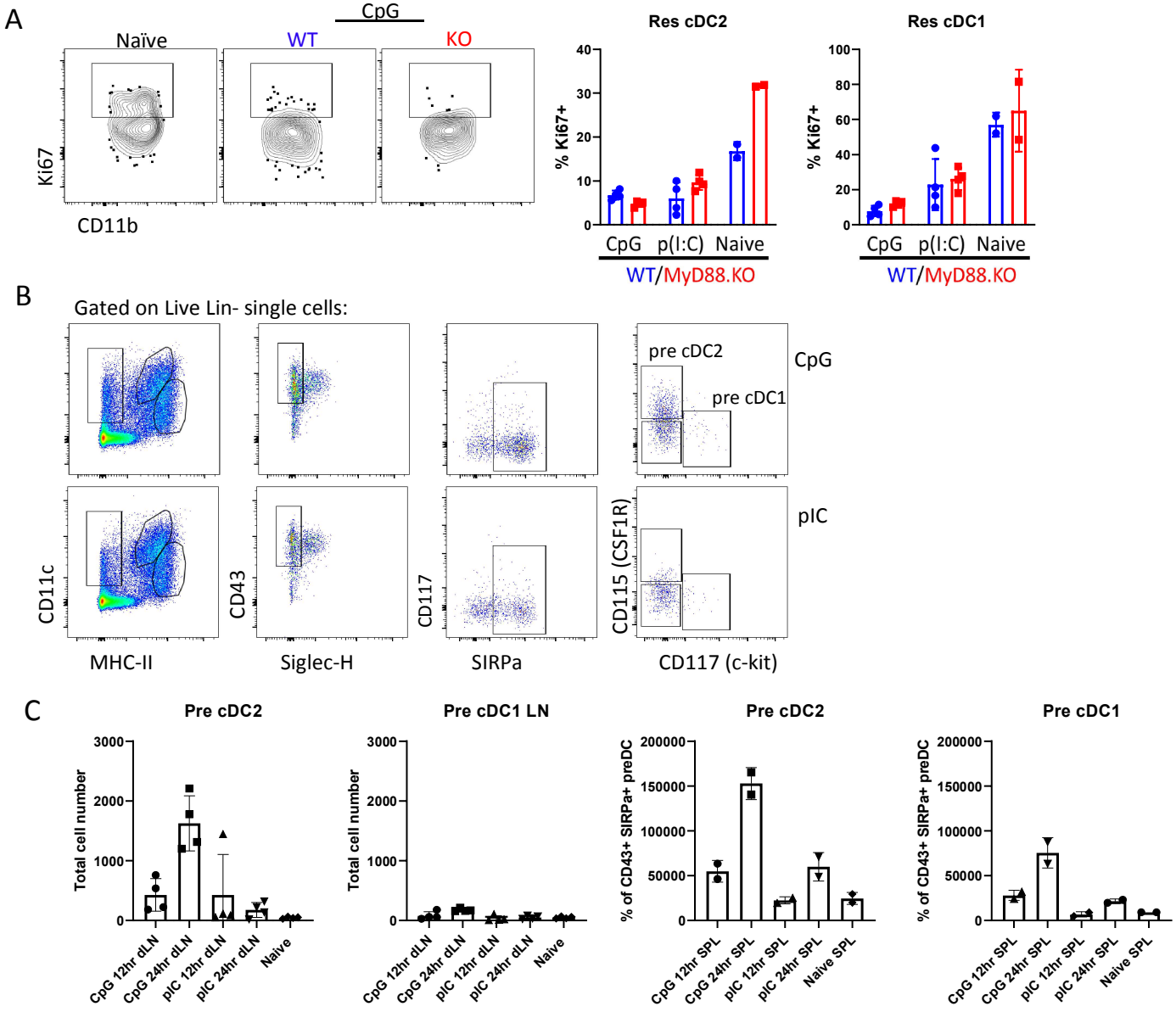

Figure 4. Increased cellularity of Res cDC2s during inflammation is likely not due to *in situ* proliferation, but rather pre cDC2 recruitment to dLNs. (A) MyD88.KO/WT mixed BMCs were injected i.d in the ears with the indicated adjuvants and auricular dLNS were harvested 24 hours later for flow cytometry and confocal imaging analysis of Res cDC expression of the proliferative marker Ki67. (B-C) WT mice were injected i.d in the ear with CpG or p(I:C) and pre cDC recruitment was assessed by flow cytometry analysis at the indicated time points. (B) Gating scheme to detect pre cDC1 and pre cDC2s. (C) Quantification of pre cDC recruitment to dLNs.

Discussion

Here, we reaffirmed the importance of the MyD88 and IFNAR signaling axes in driving cDC maturation and relocalization during inflammation. We further uncovered that Res cDC activation within LNs did not require cell intrinsic MyD88 or IFNAR signaling after CpG immunization, and IFNAR mainly affected Res cDC costimulatory molecule expression after p(I:C). The finding that Res cDC activation was largely unhindered when lacking key PAMP sensors was surprising and suggests a high degree of redundancy in the ability of DCs to become activated during inflammation. This redundancy is likely critical for cDCs to become activated in the face of pathogen-induced immune suppression or cell death. The concurrent release of multiple distinct inflammatory cytokines during the early immune response offers multiple avenues to cDC activation, pathogen elimination, and transit to and within dLNs to initiate crosstalk with naïve T cells. High redundancy likely creates a lower barrier to sense inflammation and become alerted to threats while maximizing the chances of direct immune detection. However, lowering this barrier could have consequences for overactive cDCs and the initiation of immune dysregulation and autoimmunity.

While we observed near identical Res cDC maturation in the absence of direct sensing of TLR ligands, it is still possible that although they phenocopy direct TLR sensing Res cDCs, there could remain undiscovered functional differences between Res cDCs which directly versus indirectly sense PAMPs. These differences could include, but are not limited to, differential ability to present antigen, as well as distinct capacities to secrete various cytokines. If direct versus indirect sensing by cDCs promoted different cytokine production, they could differentially instruct the T cell response. An intriguing possibility is that differences in antigen presentation and cytokine production could lead to functional cooperation between cDCs within

distinct myeloid cell microenvironments, similar to what we described in Chapter 3. In this scenario, microenvironments enriched for direct versus indirectly activated cDCs could differentially skew the T cell response. These functional differences could have a significant impact on T cell priming and differentiation, and further work is needed to elucidate these differences, including RNA sequencing to more thoroughly understand the transcriptional differences driven by direct versus indirect signaling modules.

The finding that Res cDC2 cellularity is specifically enhanced after immunization with certain TLR agonists has important implications for vaccine design and the potential for remodeling the myeloid compartment to enhance responses against a specific threat. While it remains to be investigated whether pre cDC2 recruitment is the primary mechanism behind the observed increase in mature Res cDC2s, we observed a specific recruitment of this precursor population. Previous research has shown that activated DCs often die during inflammation and are then replaced by pre DCs and MO precursors once inflammation has subsided (*128*). This replenishment is critical for the maintenance of homeostasis and enables the myeloid compartment in various tissues to recover from one threat and be prepared for the next. While this replenishment is thought to occur during the waning of the immune response, here we observed rapid recruitment of pre cDC2s during the early stages of the primary immune response. Given that specific DC populations are specialized for particular functions, it is an intriguing possibility that the emergency recruitment of pre cDC2s during the priming stage could enhance CD4+ T cell expansion and differentiation. TLR agonists such as CpG and LPS mimic bacterial infection, and given that immunity to such infections is primarily mediated by CD4+ T cells, selectively modulating the size of the cDC2 compartment could meet immunological demands during specific microbial perturbations. Such a model would allow for

the ability to tailor the immune response to a given threat in real time through specific cellular recruitment. How this specific recruitment is regulated by DC-intrinsic signaling, and how it could functionally impact the T cell response is unknown. Future work will investigate the role for the specific recruitment of pre-DC populations during inflammation in skewing T cell responses and whether this recruitment affects any semi-permanent changes in the composition of myeloid cells within the LN. If infectious "experience" in a particular draining LN could durably alter the ratio of Res cDCs, that particular LN could be better able to fight off future infections with similar pathogens. Whether these observed changes persist and lead to a prolonged state of immune readiness is unknown. Previous research on immune experienced "dirty" mice from pet stores found changes in the myeloid cell compartment compared to SPF housed laboratory mice (*129*). In addition, further work is needed to elucidate the kinetics of pre cDC2 recruitment and differentiation in the LN during inflammation. Although we saw a significant influx of pre cDC2s 24 hours after immunization, we were surprised that this increase did not occur at the 12-hour time point. Kinetically, this would have allowed for newly arrived pre cDC2s to differentiate into bona fide mature Res cDC2s and become able to participate in the generation of the adaptive immune response. That the apparent height of pre cDC2 influx is also the time point where the number and frequency of Res cDC2 increases is unexpected and will require further investigation. To that end, investigating the kinetics of *in situ* differentiation of pre cDC2s will be critical to understanding their role in the immune response. If these "emergency" pre cDC2s can differentiate rapidly, they could participate in T cell responses by providing signal 3 cytokines to enhance effector T cell differentiation, albeit it is unlikely they play a role in priming during vaccination given their relatively late arrival to the LN. However, emergency recruitment of pre cDCs may have an evolutionary purpose in the defense against

pathogens. Because many pathogens can grow exponentially before immune control, emergency pre cDC2 recruitment could provide a critical replenishment of cDCs for continued crosstalk with T cells in the face of mounting pathogen burden. Early activated cDC2s could thus perform their T cell priming functions, die, and be replaced by new cells to continue the adaptive response.

In sum, we investigated the direct versus indirect activation of Res cDCs in dLNs and found high redundancy in their ability to become activated, despite lacking the key innate signaling molecules MyD88 and IFNAR. We further demonstrated that enhanced Res cDC2 cellularity during inflammation required DC-intrinsic MyD88 signaling and was accompanied by specific recruitment of pre cDC2s into dLNs. Together, these findings suggest that while initial Res cDC activation can be indirect, pre cDC differentiation is direct. When and where this direct sensing by pre cDC2s takes place is unknown and will be a target of further investigation. Finally, this work has important implications for vaccine design, namely in the ability to target Res cDC activation and skewing of the cDC compartment to induced tailored adaptive immunity.

Chapter 5. Toll-like receptor dependent bystander B cell activation regulates T follicular helper cell responses

Introduction

B cells are a critical component of the adaptive immune system (*130*). Residing in areas of lymphoid tissue called B cell follicles, B cells are primarily responsible for making antibodies (*131*). Antibody production is a critical component of the adaptive immune response and is necessary for the immune system to target and neutralize pathogens. Once activated, B cells can dramatically improve their ability to target a particular antigen through affinity maturation, a process which occurs in specialized microenvironments within B cell follicles called germinal centers (*130*, *132*). Although the processes of B cell activation, differentiation, and antibody production have been extensively studied, much is still unknown regarding the early events regulating B cell activation and interaction with T cells. Furthermore, although much is known about antigen-specific responses by B cells (i.e those that require signaling through the BCR), much less is known about bystander activation of B cells, and whether it is important for both overall B cell and T cell responses.

B and T cell crosstalk is critical in driving the generation of Tfh cells (*39*, *42*). It has long been understood that cognate interactions between antigen specific B cells and T cells is necessary for the maintenance and final differentiation of GC T follicular helper cells (GC Tfh). Tfh cells can initially differentiate in the absence of B cells, but their continued differentiation and maintenance requires B cell interactions (*39*). These findings indicate that while cDCs are sufficient to kick start the Tfh response, B cells are critical for maintaining and amplifying that response. B cell presentation of antigen on MHC-II to pre Tfh cells, along with ICOS-ICOSL and CD40-CD40L interactions, function to reinforce the Tfh cell fate (*40*). Reciprocally, Tfh cells provide CD40L and IL-21 for activated B cells, supporting their survival and differentiation. In the germinal center, GC Tfh function to control GC B cell differentiation into

either memory B cells or high affinity plasma cells (*130*). While cognate interactions between B cells and T cells have been studied extensively, much less is known about the role bystander non-cognate B cells can play in directing the Tfh response. One study showed that ICOS-ICOSL interactions between B cells and T cells was important for pre Tfh generation and efficient migration of T cells deeper inside the B cell follicle, all in a bystander fashion (*46*). While this study demonstrated the importance of one type of non-cognate T-B cell interaction in Tfh development, additional mechanisms involving BCR-independent activation may exist. Previous work has also identified PDL-1 as an important regulator of Tfh differentiation and follicular infiltration (*48*). However, both the ICOSL and PDL1 molecules are expressed by B cells at steady state. Thus, it is unclear what the role bystander activated B cells may play in shaping the early Tfh response.

Although DCs are considered the primary antigen presenting cell and cytokine producer in the activation of T cell responses, B cells are also antigen presenting cells capable of directly initiating T cell responses. B cells express MHC-II and express numerous TLRs enabling direct sensing of PAMPs, thus possessing all the cellular machinery required for cognate interactions with naïve T cells (*133*). Meaningful participation of B cells in T cell priming has been shown in a handful of models, with one report demonstrating that virus like particles (VLPs) containing CpG were predominantly presented by B cells rather than DCs (*134*). B cells were found to be necessary and sufficient to drive the CD4+ T cell response, while DCs were dispensable. This B cell driven response was dependent on B cell intrinsic MyD88 signaling, but also required cognate interactions between B cells and T cells. Thus, although B cells were found to be important drivers of CD4+ T cell responses, it was driven by the small pool of antigen specific B cells able to bind to VLP particles via the BCR. In a model of Malaria infection, it was found

that B cells were necessary and sufficient to prime the dominant Tfh response (*135*). Thus, B cells can perform priming and other innate cell functions normally attributed to cDCs.

Here, we have used multiplexed quantitative imaging and flow cytometry to uncover a previously unappreciated role for bystander B cell activation via TLR signaling and its role in regulating the emergence and intranodal homing of Tfh cells. We found that polyclonal bystander B cells are rapidly activated in lymph nodes by certain TLR agonists, and that this activation was direct and entirely dependent on signaling through the adaptor molecule, MyD88. When B cells could no longer signal through MyD88, antigen specific T cells were greatly limited in their ability to differentiate into Tfh and home into the B cell follicle. Additionally, we found that while both adjuvants that promote bystander B cell and those that do not can both result in pre Tfh development, only B cell activating adjuvants promoted rapid follicular homing of pre Tfh cells early after priming and prior to GC establishment. Additionally, we found polarized activation of B cells in sites most proximal to TLR agonist drainage, and these areas were more dominantly infiltrated by Tfh cells. We further demonstrate that manipulating the distribution of adjuvant and antigen across the dLN using multi-site injection resulted in reduced polarization and more homogeneous infiltration of Tfh across the follicles. Together, we have shown that direct sensing of TLR ligands and bystander activation of B cells is important for pre Tfh generation and localization with dLNs. This work further demonstrates the potential to manipulate the localization of T cell responses, with implications for the rational and directed design of vaccines.

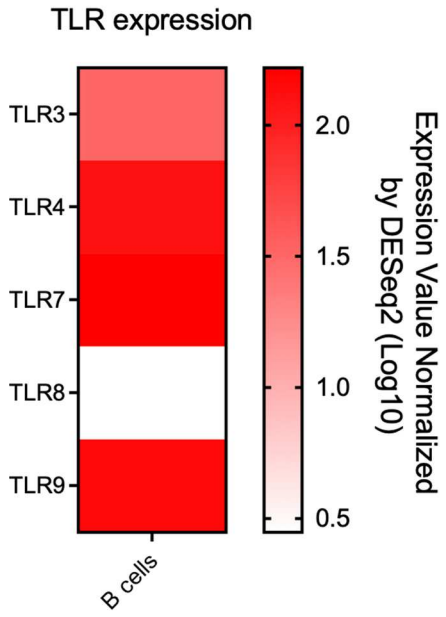

Table 1. Relative expression of toll-like receptors by splenic B cells at steady state
Source: ImmGen

RESULTS

Soluble TLR agonists are sufficient to drive large-scale naïve B cell activation

To investigate B cell responses during early vaccination, we injected mice with the TLR9 agonist CpG without additional antigen s.c. and examined B cell activation at different time points. Previous reports have suggested that bystander activation of naïve B cells by TLR ligands requires BCR dependent binding and uptake of complexed antigen (*134*). We found that most of the polyclonal naïve B cell compartment upregulated the chemokine receptor CCR7 suggesting induction of early B cell activation (Figure 1A). Furthermore, we found that B cells also dramatically upregulated the transcription factors Tbet and IRF4, which are not expressed in naïve non-activated B cells. Additionally, a subset of these activated B cells expressed Ki67, indicating cellular proliferation (Figure 1A). Memory B cells have been shown to have enhanced

expression of many TLRs, including TLR9. We observed similar activation of CD73+ CD80+ memory and CD73- CD80- naïve B cells, suggesting activation by both populations (data not shown). Next, we aimed to define the temporal kinetics of naïve B cell activation by again immunizing mice with CpG and looking at early time points post injection. We were surprised to find that B cells were activated very rapidly, upregulating CCR7 as soon as 2 hrs post injection (Figure 1B). This rapid activation is comparable to resident conventional dendritic cells (Res cDCs), which are known to respond rapidly to lymph born inflammatory agonists (Chapters 3 and 4). We next used confocal imaging to confirm our flow cytometry observation of B cell activation, again finding that B cells rapidly upregulated Tbet and Ki67 after CpG immunization (Figure 1C). We next tested the ability of other TLR agonists to activate B cells, using the TLR agonists LPS B4 (TLR4), R848 (TLR7) and p(I:C) (TLR3). We found that robust B cell activation occurred only after administration of LPS and R848 (Figure 1D), both of which the corresponding TLR has been reported to be highly expressed in B cells. p(I:C) on the other hand did not lead to large scale B cell responses, consistent with the lower expression of TLR3 on naïve B cells (*136*). Overall, these data demonstrate that large-scale B cell activation can occur after specific TLR agonist administration.

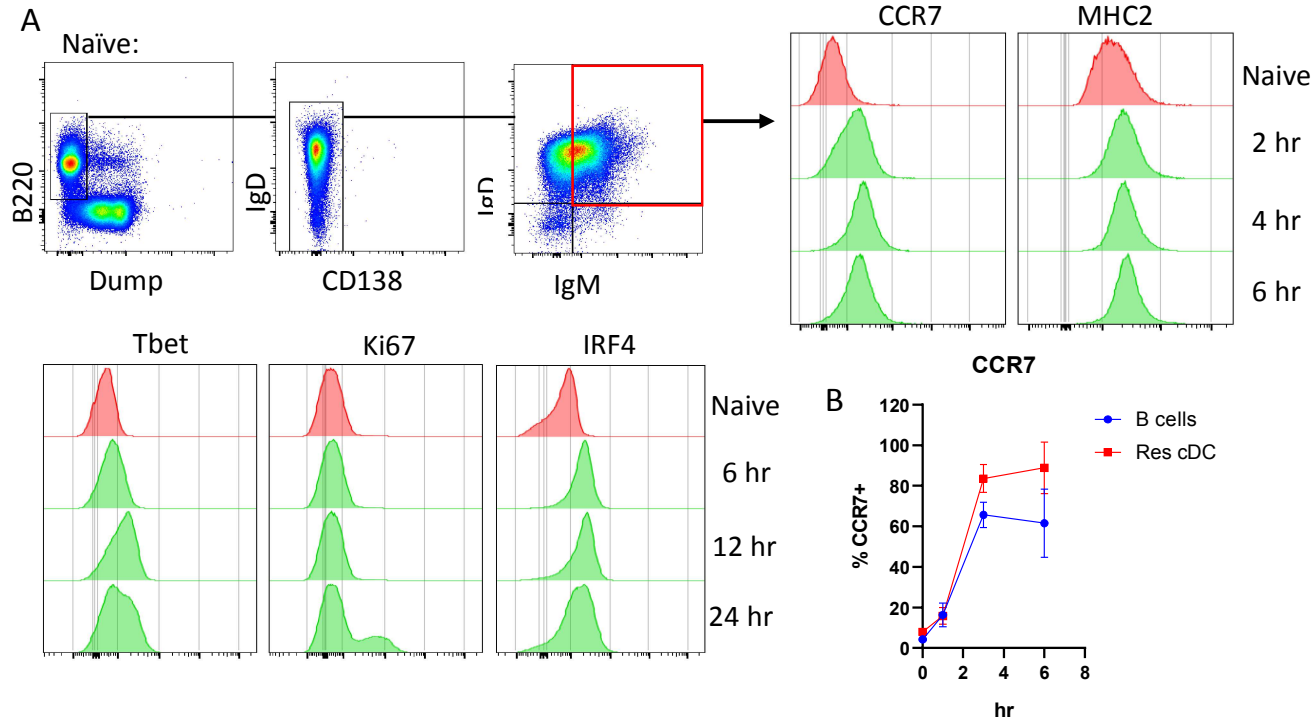
A
Naïve:
B220
Dump
IgD
CD138
IgD
IgM
CCR7
MHC2
Naive
2 hr
4 hr
6 hr
Tbet
Ki67
IRF4
Naive
6 hr
12 hr
24 hr
B
CCR7
% CCR7+
hr
B cells
Res cDC

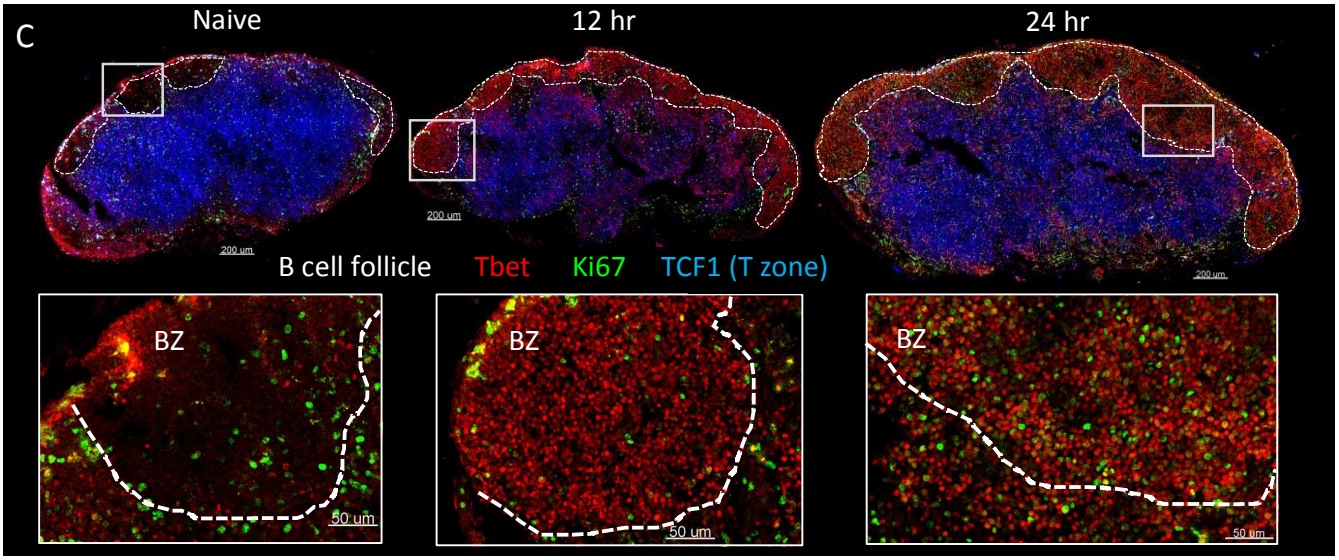
C
Naive
12 hr
24 hr
B cell follicle
Tbet
Ki67
TCF1 (T zone)
BZ
50 um

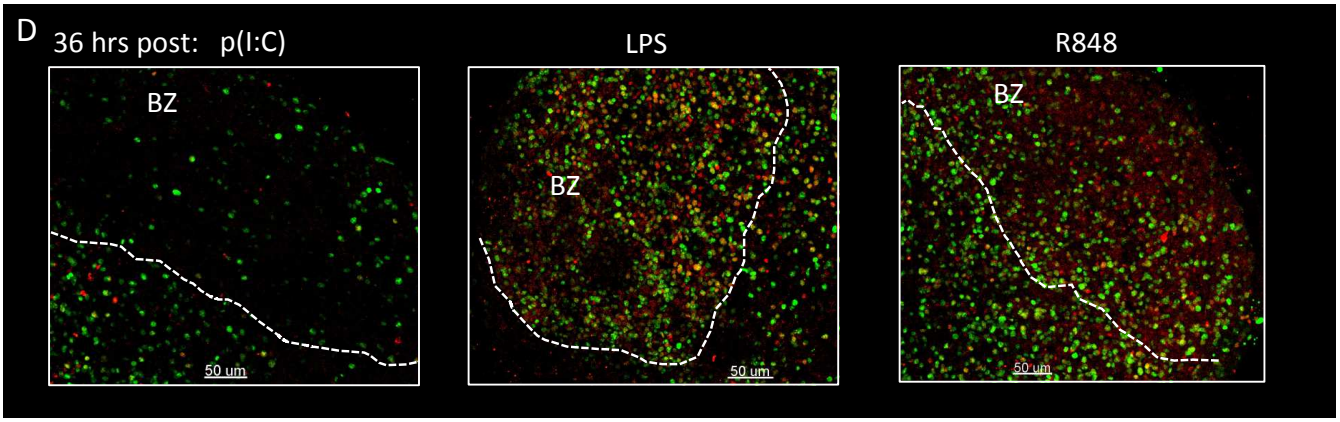
D
36 hrs post: p(I:C)
LPS
R848
BZ
50 um

Figure 1. Polyclonal bystander B cells are rapidly activated in LNs. WT B6 mice were injected i.d in the ears with the indicated adjuvants and auricular dLNs were harvested at the indicated time points for flow cytometry and confocal imaging analysis of B cell activation. (A) Gating scheme to examine large scale polyclonal activation of B cells (left) and comparison of the gMFI of CCR7 and MHC-II (right), as well as Tbet, Ki67, and IRF4 (bottom) on IgD+ IgM+ B cells at the indicated time points post injection with CpG. (B) Frequency of CCR7 positivity of the indicated cell types at early time points post injection with CpG, indicating activation of B cells on par with Res cDCs. (C-D) Representative confocal images of auricular dLNs depicting B cell activation (Tbet, Ki67) in B cell follicles (white dashed line) at various time points after CpG (C) or other TLR agonists (D). TCF1 staining represents the TZ.

TLR agonist-mediated B cell activation is MyD88-intrinsic and regulates B cell intranodal localization

The finding that immunization with TLR agonists led to B cell activation only when the specific TLR was expressed by B cells suggested direct sensing and signaling through the TLR adaptor protein MyD88. To test that hypothesis, we created mixed bone marrow chimeras (mBMCs) comprised of equal amounts of congenically marked MyD88.KO and WT bone marrow. We also tested IFNAR.KO mBMCs to test whether indirect signaling through Type I interferon was additionally involved in the activation of B cells after TLR agonist administration. After immunization with CpG, mice were harvested 24 hrs later for analysis of B cell activation and localization by flow and histocytometry, respectively. We found that MyD88.KO B cells failed to upregulate markers associated with activation, including CCR7, IRF4, Tbet, or Ki67, as compared to their WT counterparts within the same LNs (Figure 2A). No role in the sensing of Type I interferon was found in B cell activation, as IFNAR.KO B cells were similarly activated as the WT cells. Next, we examined the localization of MyD88 deficient B cells within LNs using multiplex confocal imaging. Given the failure of MyD88.KO B cells to become activated and upregulate CCR7, we hypothesized that this would alter their localization within B cell follicles. Indeed, although WT and MyD88.KO B cells were evenly dispersed throughout the B

cell follicle during steady-state conditions (Figure 2B, left), they were completely segregated 24 hr post CpG immunization (Figure 2B, right). The MyD88.KO B cells were relegated to the periphery of the follicles, proximal to the subcapsular sinus and furthest away from the TZ, while WT B cells migrated efficiently to the T/B border, consistent with increased expression of CCR7. These data suggest that B cell activation after TLR agonist administration is dependent on B cell-intrinsic signaling through the adaptor MyD88, and that increased CCR7 expression on B cells allows migration of activated B cells to the T/B border, where interactions with T cells can take place.

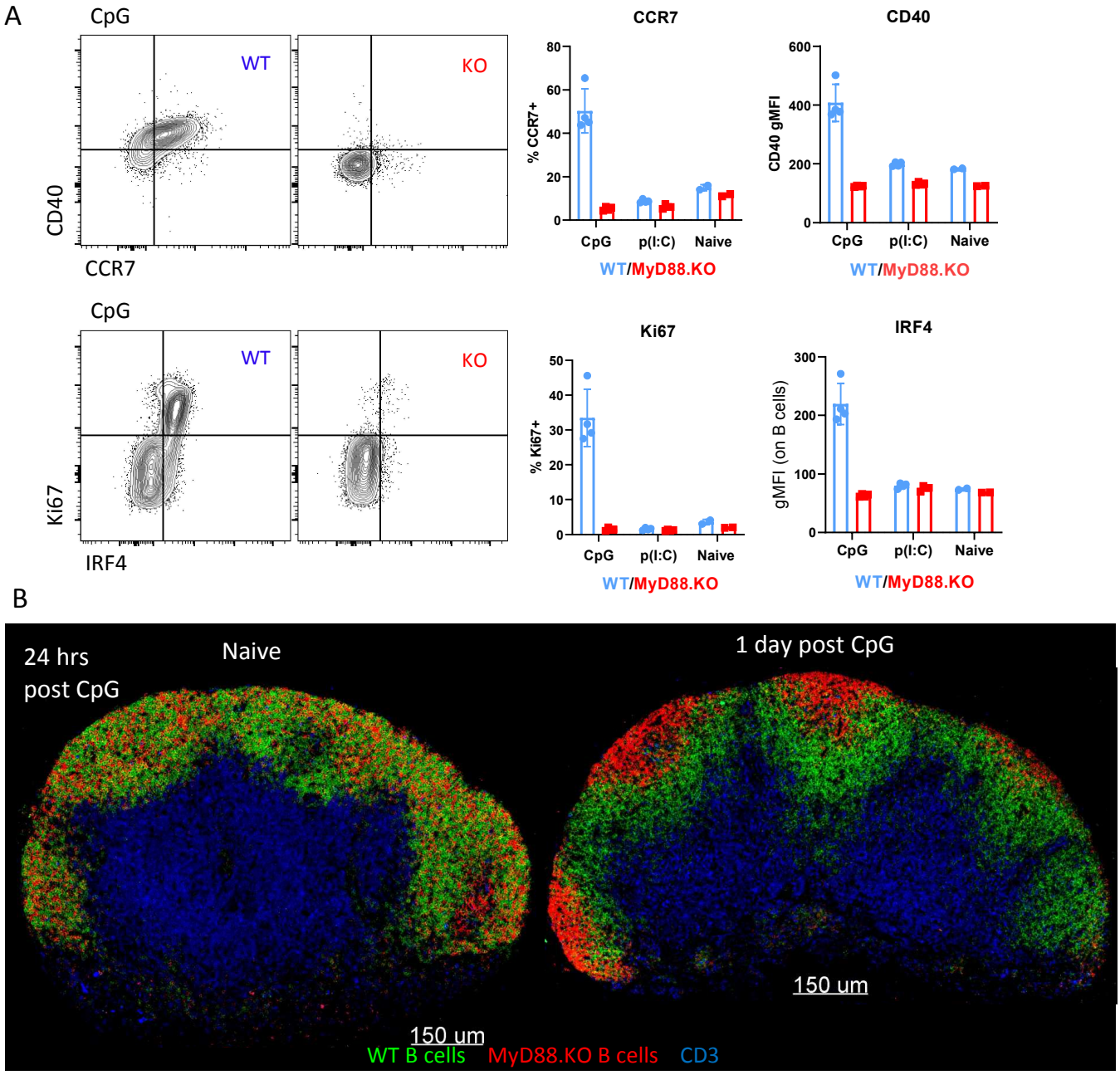

Figure 2. Large scale B cell activation after CpG is MyD88 intrinsic and regulates B cell activation and intranodal localization. MyD88.KO/WT mixed BMCs were injected i.d in the ears with the indicated adjuvants and auricular dLNs were harvested 24 hours later for flow cytometry and confocal imaging analysis of B cell activation and localization. (A) WT and MyD88.KO B cell expression of CCR7 and CD40 (top), as well as Ki67 and IRF4 (bottom), indicating MyD88 dependent activation after CpG administration. (B) Representative confocal images of auricular dLNs depicting steady state WT and KO B cell localization (left) compared 1 day post CpG (right). CD3 staining represents the TZ.

MyD88 dependent B cell activation is not required for cDC maturation or relocalization to the TZ

In Chapter 4 we investigated the role of MyD88 and IFNAR signaling in the maturation and localization of Res cDCs during TLR agonist induced inflammation and found that cell intrinsic signaling through those receptors was not required for maturation. This data suggested that a primary sensor of draining TLR ligands existed upstream of cDCs that was able to become directly activated and produce inflammatory secondary mediators. Given the requirement of MyD88 signaling in the large-scale, rapid activation of B cells, we hypothesized that B cells could promote cDC maturation, potentially through TLR dependent cytokine production. Spatially, Res cDC2s reside in the periphery of the LN proximal to B cell follicles. Thus, recently activated B cells have the potential to interact with cDCs and MOs during inflammation. Additionally, preliminary data suggested a small frequency of activated B cells could make TNFα (data not shown), a cytokine capable of robustly activating myeloid cells. To test this hypothesis, we created bone marrow chimeras wherein MyD88.KO or WT bone marrow was mixed with uMT (B cell KO) bone marrow at a 20:80 ratio. We found that neither MyD88 or CCR7 expression by B cells was necessary for Res cDC2 or cDC1 upregulation of CCR7 or CD80/86 after CpG immunization (Figure 3A). When we analyzed Res cDC relocalization by histocytometry, we found no defect in the ability of Res cDCs to relocalize to the TZ in response to CpG administration when B cells lacked MyD88 (Figure 3, B and C). These experiments in MyD88.KO/uMT and CCR7.KO/uMT mBMCs demonstrate that B cell activation does not play

a role in the maturation or relocalization of Res cDC during TLR agonist induced inflammation.

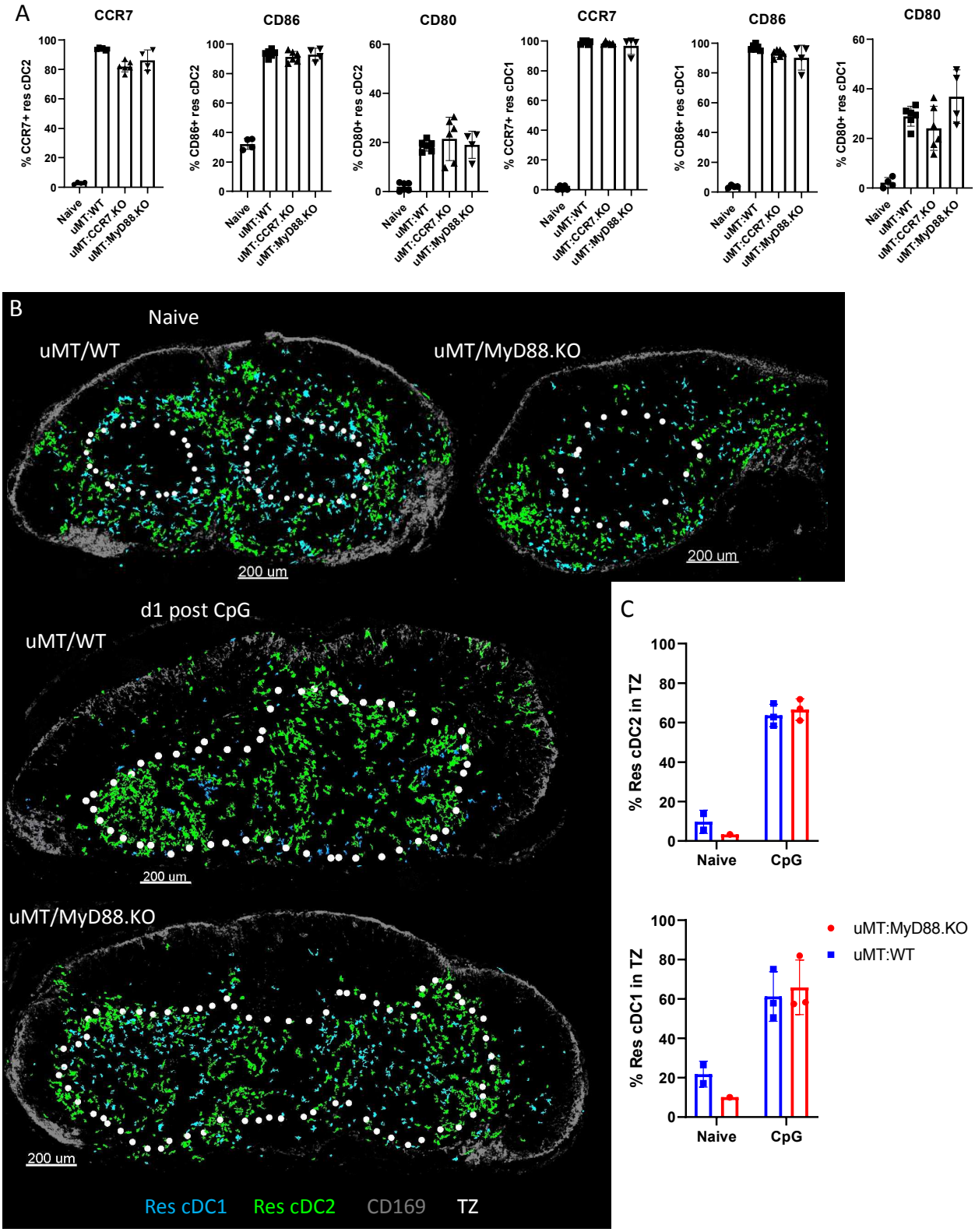

Figure 3. MyD88 dependent B cell activation is not required for Res cDC maturation or relocalization during inflammation. uMT/WT, uMT/MyD88.KO, and uMT/CCR7.KO mixed BMCs were injected i.d in the ears with CpG and auricular dLNS were harvested 1 day later for flow cytometry (A) and histocytometry analysis (B) of Res cDC maturation and TZ localization. CD169 staining represents the LN boundary.

Multi-adjuvant comparison reveals differential Tfh generation and follicular recruitment

B cell-T cell interactions are critical for the generation of adaptive immunity, namely the provision of T cell help to B cells and the effective formation of germinal center (GC) reactions. Given the observed broad and robust B cell activation and relocalization after administration of CpG, we hypothesized that MyD88-dependent B cell responses may play an additional role in the generation of Tfh. To test this hypothesis, we wanted to understand the relationship between B cell activation and Tfh generation across a range of adjuvants, including those that activate B cells directly and those that do not. To do so, we transferred OT-II transgenic T cells into WT mice and immunized them with OVA plus adjuvant, including CpG (TLR9), LPS (TLR4), R848 (TLR7/8), p(I:C) (TLR3), and the protease Papain, which induces a Type 2 immune response. As we observed in Figure 1, B cells were activated after LPS and R848, expressing elevated levels of both Ki67 and IRF4 (Figure 4A). Of note, although B cells express TLR7/8 and respond robustly to R848 *in vitro*, their response was markedly lower here compared to other TLR agonists, potentially due to R848 being a small molecule that is rapidly cleared into the circulation. When we examined the OT-II T cell response, we found that both B cell activating adjuvants (LPS and CpG) and those that do not activate B cells (p(I:C)) were able to stimulate the robust differentiation of Tfh cells (Figure 4B), defined as those early differentiated cells that express the B cell homing chemokine receptor CXCR5 and PD-1. Indeed, we observed that 30-50% of all activated antigen-specific T cells had a Tfh phenotype by flow cytometry (Figure 4B). Furthermore, multiple adjuvants stimulated B cells to upregulate ICOSL (Figure 4C), a molecule

critical for Tfh generation and follicular infiltration, albeit CpG stimulated the strongest upregulation. Given these findings, we next examined whether direct B cell sensing of TLR ligands could influence the localization of Tfh cells within the LN and early infiltration of the B cell follicles. The localization of Tfh cells is critically important to their function, as germinal center reactions within B cell follicles requires the presence of Tfh cells to proceed. Additionally, past studies have identified B cells as cellular gate keepers that can regulate the entry of T cells in the follicle, but it is not certain whether MyD88 dependent activation can regulate that entry. Using confocal imaging, we found that a significant portion of OT-II T cells were found within B cell follicles after CpG and LPS, but not other adjuvants (Figure 4D), suggesting a correlation between localization of early activated Tfh cells and B cell activation. Interestingly, although p(I:C), CpG, and LPS all induced dominant Tfh responses, only the latter two TLR agonists appeared to drive Tfh into the B cell follicles. To quantitate these observations, we used histocytometry and a previously published follicular homing coefficient, calculated by dividing the density of T cells within the B cell follicle by the density in the proximal T-B border region. We found that OT-II T cells homed far less to B cell follicles after p(I:C) compared to LPS (Figure 4E), suggesting there may be a role for large scale B cell activation in driving early follicular recruitment of T cells. Together, this data shows that while multiple TLR agonists can drive a dominant Tfh response, only those adjuvants that induce large scale B cell activation also induce rapid B cell follicle entry by Tfh.

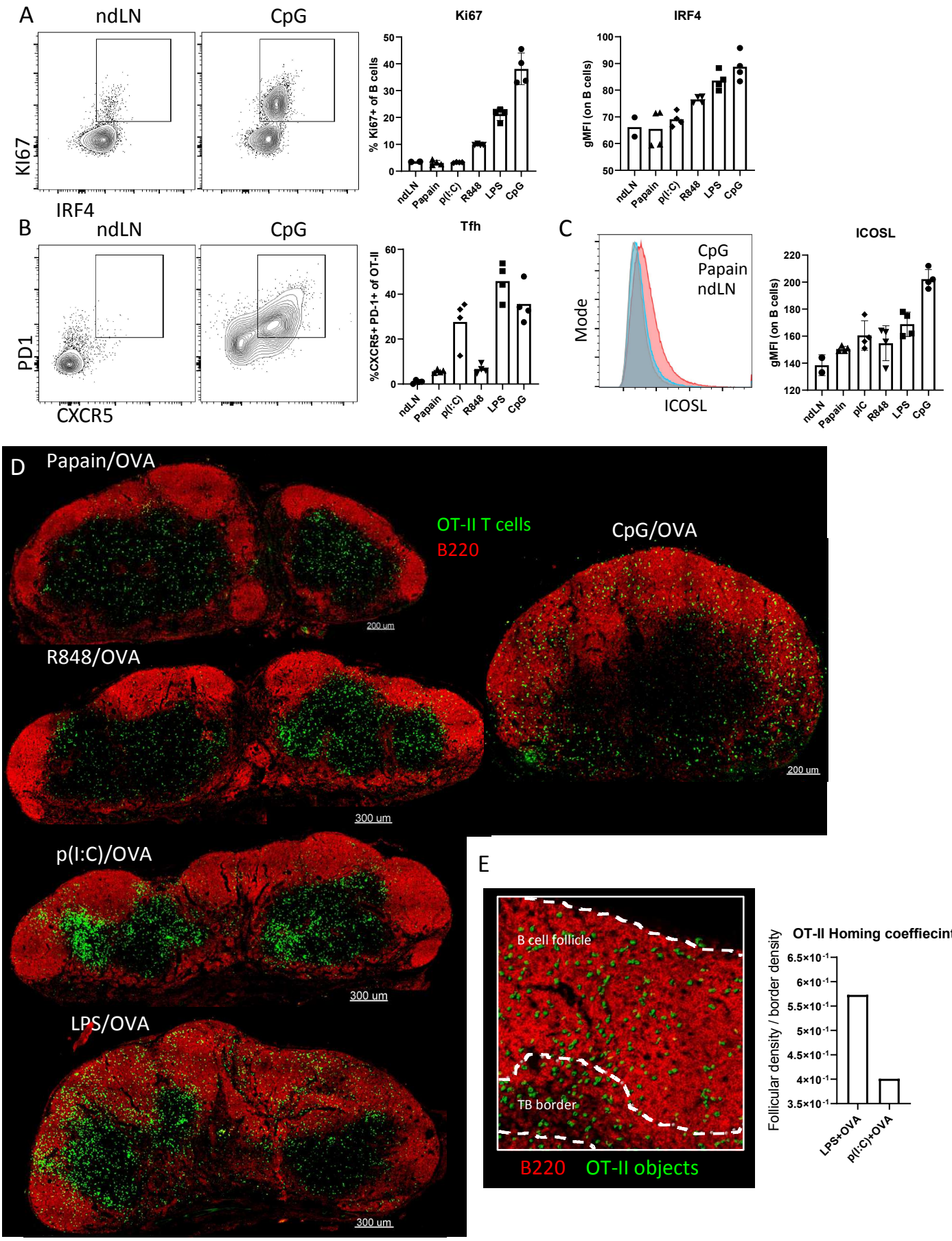
A
ndLN
CpG
KI67
IRF4
Ki67
% Ki67+ of B cells
IRF4
gMFI (on B cells)
ndLN
Papain
p(I:C)
R848
LPS
CpG
B
ndLN
CpG
PD1
CXCR5
Tfh
%CXCR5+ PD-1+ of OT-II
C
CpG
Papain
ndLN
Mode
ICOSL
ICOSL
gMFI (on B cells)
ndLN
Papain
pIC
R848
LPS
CpG
D
Papain/OVA
OT-II T cells
B220
CpG/OVA
200 um
R848/OVA
300 um
200 um
p(I:C)/OVA
300 um
LPS/OVA
300 um
E
B cell follicle
TB border
B220
OT-II objects
OT-II Homing coeffiecint
Follicular density / border density
LPS+OVA
p(I:C)+OVA

Figure 4. Multi-adjuvant comparison reveals differential Tfh generation and follicular recruitment. WT mice were injected i.d in the ears with the indicated adjuvants and auricular dLNs were harvested 3 days later for flow cytometry analysis of B cell (A) and OT-II T cell (B) activation and differentiation. (C) B cell expression of the ICOSL receptor, as gMFI. (D) Representative confocal images of auricular dLNs (left) and popliteal LN (CpG, right) depicting differential intranodal OT-II T cell localization. The CpG dLN is from a separate experiment. (E) OT-II infiltration of the B cell follicles was analyzed using histocytometry by dividing the density of OT-IIs in the follicle by the density of those in the TB border region.

MyD88-dependent B cell activation is required for optimal Tfh generation and follicular localization of T cells

We next hypothesized that the MyD88-dependent activation of B cells was critical for the early generation of pre Tfh cells after vaccination. To investigate this, we transferred congenically marked transgenic OT-II T cells into MyD88.KO/uMT or CCR7.KO/uMT mBMCs, immunized with CpG+OVA, and examined Tfh responses 3 days later by flow cytometry. A critical function of B cells is the provision of B cell help to activated T cells, and this is known to be dependent on direct B cell-T cell interactions at the TB border. To provide this help, B cells must relocalize to the TB border by upregulating the receptor CCR7 (which draws cells to CCL19/21 produced in the TZ by T zone reticular cells, or TRC), and downregulating the B cell follicle homing receptor CXCR5 (*39*). Thus, by investigating both MyD88.KO/uMT and CCR7.KO/uMT mBMCs we examined both the necessity of MyD88 dependent B cell activation as well as the need for B cells to interact locally with T cells at the TB border. We found by flow cytometry that while there were no differences in OT-II expansion (Figure 5A), there were significantly fewer Tfh cells in the dLNs of mice lacking MyD88 signaling in B cells, as well as a significant reduction in T cell BCL6 expression, the master transcription factor controlling Tfh differentiation (Figure 5B). Together, these data demonstrate that immunization with CpG/OVA

was associated with robust pre Tfh generation, and this process was heavily dependent on the ability of B cells to directly sense CpG and signal through MyD88. Furthermore, as expected, the B cells from the MyD88.KO/uMT chimeras did not upregulate Ki67 or Tbet after immunization with CpG, indicating a successful abrogation of MyD88 signaling in B cells.

It has been previously reported that expression of the receptor ICOSL on B cells was critical for the homing of activated Tfh cells into the B cells through ICOS-ICOSL interactions (*46*). Although ICOSL is constitutively expressed on B cells at steady state, we sought to investigate whether its expression could be regulated by immunization with CpG. We found that mean fluorescent intensity of ICOSL was significantly increased on B cells after CpG immunization and that this upregulation was dependent on B cell intrinsic MyD88 signaling (Figure 5C). Thus, enhanced ICOS-ICOSL interactions driven by MyD88 dependent signaling in B cells could be one mechanism by which B cells promote Tfh responses following CpG+OVA immunization.

Next, we analyzed the localization of OT-II T cells within dLNs of MyD88.KO/uMT or CCR7.KO/uMT mBMCs 3 days after immunization with CpG+OVA. We observed that OT-II infiltration of the follicle appeared to be reduced in MyD88.KO/uMT dLNs (Figure 5D). Using the follicular homing coefficient, we quantified this observation and found that T cells homed to B cell follicles far less in both MyD88.KO/uMT and CCR7.KO/uMT chimeras compared to WT/uMT chimeras (Figure 5E). Together, these data demonstrate that both direct sensing of draining TLR ligand by B cells and CCR7-dependent relocalization to the TB border are important for the generation of Tfh cells and their ability to home to B cell follicles.

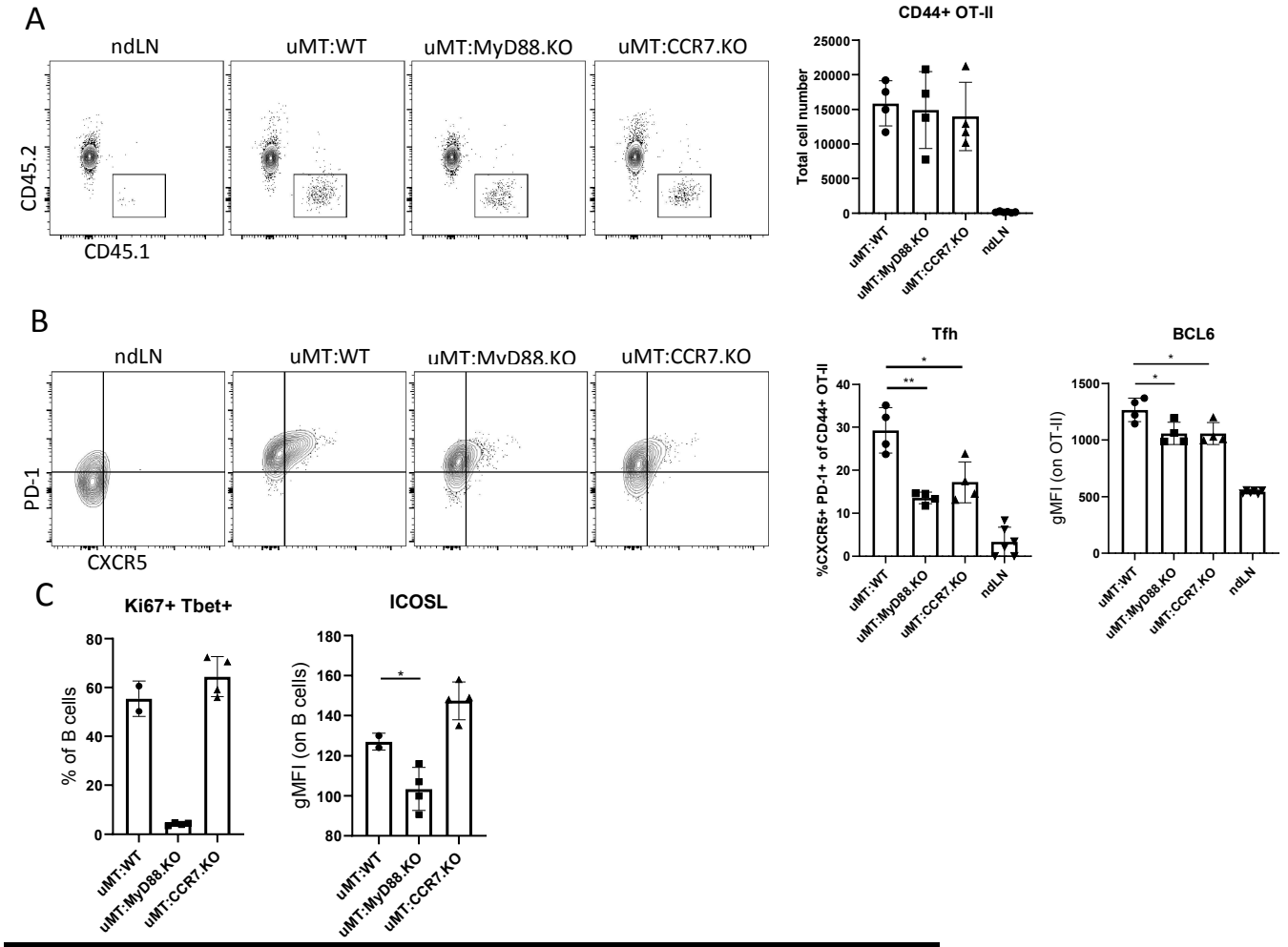
A
ndLN
uMT:WT
uMT:MyD88.KO
uMT:CCR7.KO
CD45.2
CD45.1
CD44+ OT-II
Total cell number
B
PD-1
CXCR5
Tfh
%CXCR5+ PD-1+ of CD44+ OT-II
BCL6
gMFI (on OT-II)
C
Ki67+ Tbet+
% of B cells
ICOSL
gMFI (on B cells)

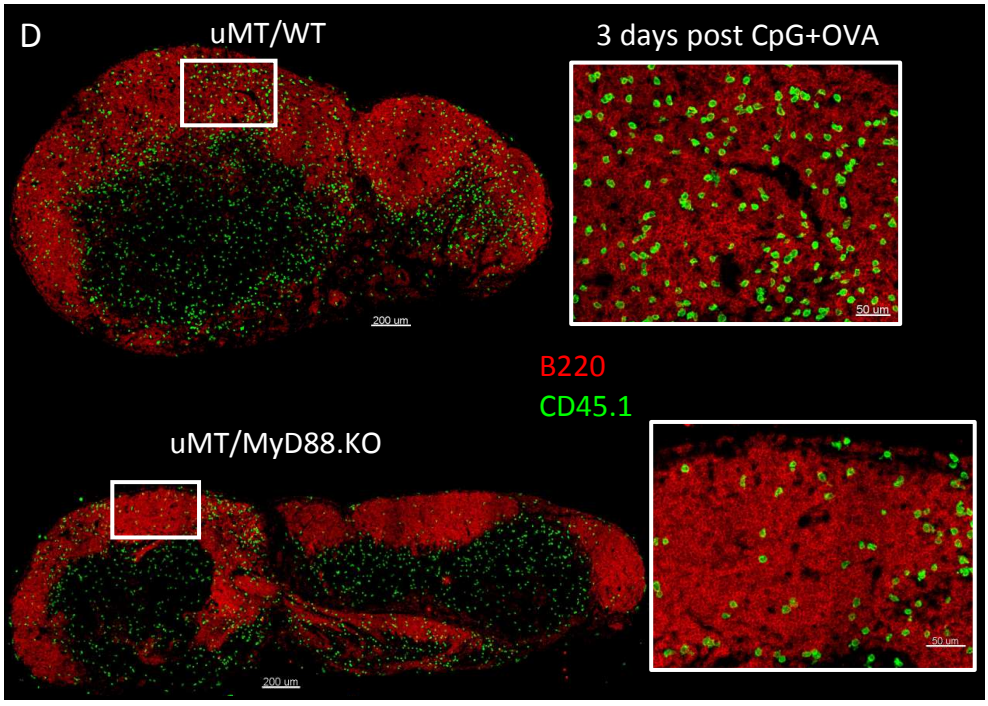
D
uMT/WT
3 days post CpG+OVA
200 um
50 um
B220
CD45.1
uMT/MyD88.KO

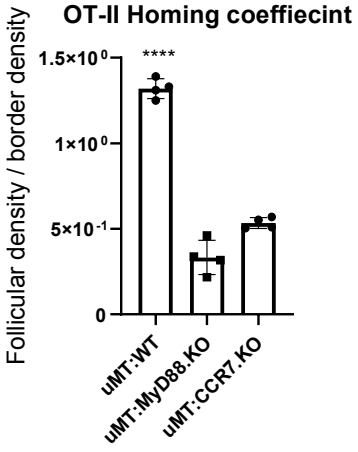
E
OT-II Homing coeffiecint
Follicular density / border density
uMT:WT
uMT:MyD88.KO
uMT:CCR7.KO

Figure 5. MyD88 dependent B cell activation is required for pre Tfh differentiation and follicular infiltration after CpG. (A) uMT/WT and uMT/MyD88.KO BMCs were given $5x10^6$ OT-II cells and 1 day later were injected i.d in the ears with CpG. Auricular dLNs were then harvested 3 days later for flow cytometry and histocytometry analysis of OT-II cellularity, differentiation, and follicular infiltration. (A) Detection and quantification of OT-II expansion. (B) Analysis of Tfh differentiation, assessed by expression of CXCR5, PD-1 And BCL6. (C) Analysis of B cell activation, indicating MyD88 dependence for both proliferation, Tbet expression, and ICOSL upregulation. (D) Representative confocal images of auricular dLNs depicting OT-II infiltration into B cell follicles (left) with accompanying zoom ins (right). (E) The homing coefficient of OT-II T cells was calculated using the density of OT-II objects in the B cell follicles divided the density of those in the TB border region. Densities encompass all B cell follicles and TB border regions in each dLN. Each point represents an independent dLN.

B cell activation is polarized to LN regions proximal to ligand drainage and generates heterogeneous microenvironments promoting pre Tfh generation

We previously reported the formation of spatially polarized inflammatory microenvironments within dLNs that are most likely caused by asymmetric drainage of TLR ligands via the afferent lymph (Chapter 3). Therefore, we next investigated whether similar asymmetric drainage could also lead to polarized activation of B cells. Also, given that B cell sensing of draining TLR ligand and signaling through MyD88 was necessary for optimal Tfh generation and migration of T cells into the B cell follicle, we wanted to examine whether T cell infiltration of the follicle could also be polarized to zones of the LN with enhanced B cell activation. To that end, we transferred congenic OT-II T cells into WT recipient mice and then immunized them with CpG/OVA 1 day later. Importantly, we targeted different lobes of the LN by taking advantage of the distinct drainage properties conferred by different immunization sites. Namely, different lobes of the inguinal LN can be targeted by s.c immunization of either the dorsal or ventral skin of the mouse (Figure S1A). This immunization scheme leads to either symmetric (dorsal and ventral immunized) or asymmetric (dorsal only) drainage of antigen and adjuvant to dLNs. When dLNs from these mice were analyzed by confocal imaging, we observed that there was indeed

polarized activation of B cells after single sided injection of CpG/OVA, but not dual sided (Figure 6A). When we investigated the localization of transferred T cells, we found that they appeared polarized to regions proximal to activated IRF4+ B cells (Figure 6A). Additionally, many of these follicle-localized OT-II T cells expressed BCL6, indicating bona fide Tfh status (Figure 6A, bottom right). These data demonstrate that Tfh generation and follicular recruitment can be polarized in dLNs, corresponding to sites of asymmetric antigen and adjuvant drainage, and indicates that rationally designed immunization schemes may allow for regulation of LN polarity and the downstream Tfh and GC B cell responses.

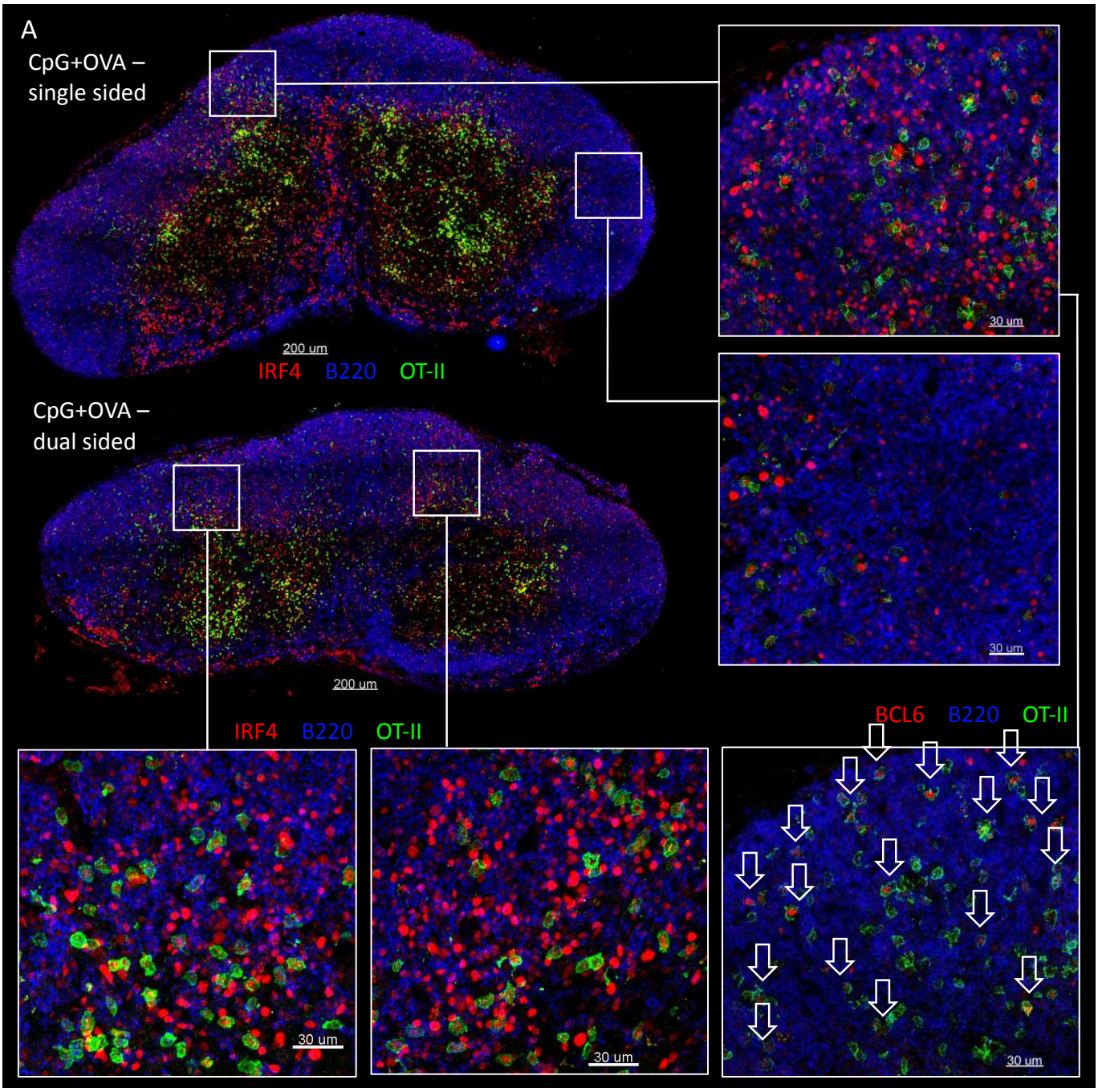

Figure 6. Asymmetric TLR ligand drainage generates LN microenvironments composed of activated B cells and infiltrating T cells. (A) WT mice were given $1x10^7$ OT-II cells and 1 day later were injected either s.c in the stomach (single sided) or stomach and back (dual sided) with CpG/OVA. For dual sided injections, the antigen and adjuvant dose was split between injection sites, thus keeping the same dose as the single sided injection. Inguinal dLNs were then harvested 3 days later for confocal imaging analysis of B cell activation and OT-II follicular infiltration. Zoom ins demonstrating differential spatial activation of B cells and corresponding OT-II infiltration from single sided (top left) and dual sided (bottom left) immunizations. Bottom

right panel shows that many of the OT-II T cells in the follicle express the Tfh master transcription factor BCL6, depicting bona fide Tfh.

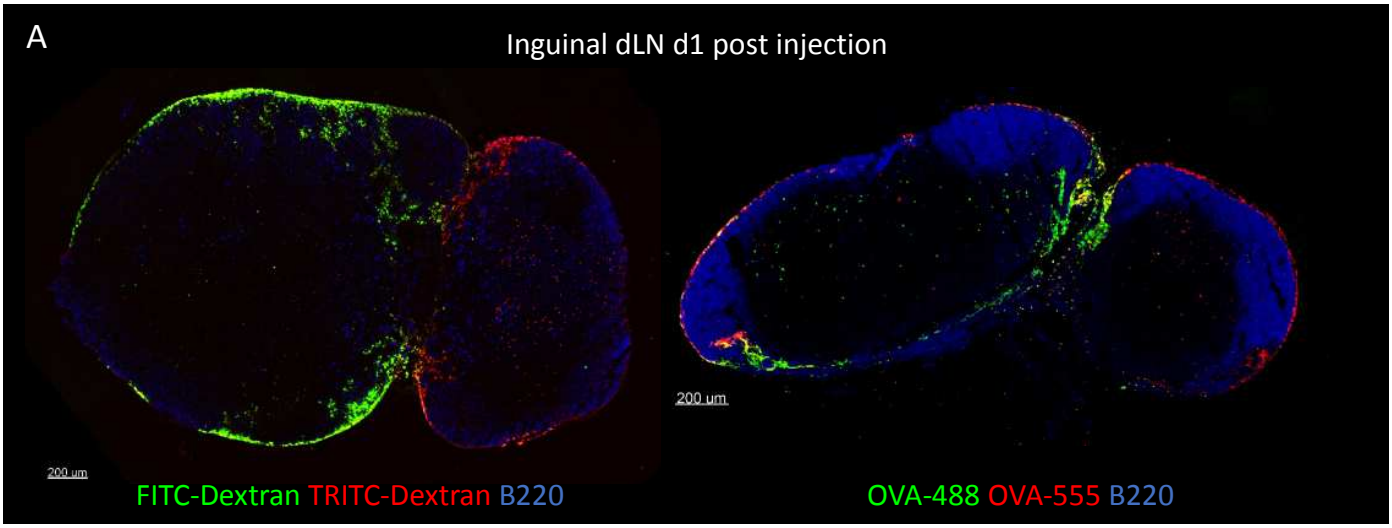

Supplemental Figure 1. Asymmetric drainage with dorsal and ventral s.c injection of fluorescent antigen. WT mice were immunized s.c with FITC-Dextran in the back skin and TRITC-Dextran in the stomach skin (left), or OVA-488 in the back skin and OVA-555 in the stomach skin (right). Inguinal dLNs were harvested 1 day later for analysis of intranodal antigen localization using multiplex confocal imaging, demonstrating targeting of different LN lobes.

Discussion

Here, we found large scale B cell activation after administration of TLR ligands alone *in* vivo, and that this activation was dependent on cell intrinsic expression of the adaptor of TLR signaling, MyD88. This activation was limited to immunization with MyD88 dependent TLR ligands, as administration of p(I:C) did not lead to large scale B cell activation *in vivo.* We further found that in order for optimal Tfh generation to occur in response to immunization with CpG and LPS adjuvants, B cells had to express MyD88. In the absence of B cell MyD88 signaling, we found not only deficient Tfh responses, but an accompanied absence of T cell

infiltration of the B cell follicles. Strikingly, we found that while immunization with CpG, LPS and p(I:C) all induced robust early Tfh responses, only the former induced rapid infiltration of the follicles by Tfh, coinciding with widespread B cell activation. Finally, we found that B cell activation could be highly polarized and correlated to asymmetric lymphatic drainage of TLR ligands. This polarized B cell activation further correlated with T cell follicular infiltration.

The finding that soluble TLR agonists were sufficient to drive broad bystander B cell activation in vivo is contrary to prevailing model of BCR-dependent mechanism for B cell activation via protein-bound TLRs (*137*). This observed activation was characterized by expression of molecules previously thought to be dependent on BCR activation, such as CCR7, IRF4, and Tbet. The upregulation of CCR7 across a majority of LN B cells resulted in a remarkable migration of B cells to the TB border, where they could interact with T cells.

The finding that MyD88 dependent B cell activation occurred within 2 hours of immunization and was spatially proximal to Res cDC2s and MO entry sites encouraged the hypothesis that they could play some role in myeloid cell recruitment or activation. However, we found that B cell activation played no detectable role in myeloid cell recruitment and maturation in dLNs, suggesting the presence of additional cell types capable of directly sensing draining TLR ligands and producing secondary inflammatory cytokines like TNF or IFN-I. The cellular and molecular mediators responsible for promoting indirect activation of myeloid cells in dLNs require further elucidation.

We can speculate that the broad activation of bystander B cells could be beneficial to the host by potentially driving the recruitment and differentiation of antigen specific Tfh cells into the follicle, thereby increasing the degree and potency of subsequent GC reactions. We speculate that this could be particularly involved during sensing of specific TLR agonists, as not all

adjuvants elicited B cell activation. Such divergent engagement of B cell responses could influence the speed at which GCs are formed and this additional work is necessary to dissect this further. Although we find that CpG enhanced ICOSL expression in B cells was MyD88-dependent, it is unknown whether ICOSL upregulation on B cells is the mechanism by which B cells can recruit pre Tfh into the follicle. Previous work demonstrating a role for B cell expression of ICOSL in driving follicular Tfh recruitment did not rigorously examine the activation status of those B cells, albeit their immunization included LPS, which we demonstrated directly activates B cells. In addition, we and others find that most B cells in the LN express ICOSL at steady state conditions. Thus, more investigation is needed to determine the mechanisms by which bystander activated B cells can drive pre Tfh development and follicular infiltration. It is tempting to implicate IL-6, a cytokine known to induce Tfh differentiation. Recent work has suggested that viral infection with copious amounts of early IFN-I production can induce IL-6 production by DCs, and this DC-derived IL-6 can drive Tfh development independent of B cells (*47*). However, given that B cell-derived IL-6 has also been implicated in Tfh development (*138*), one can envision a model wherein the cellular source of IL-6 is stimulus dependent (i.e. DC or B cell derived) and can in turn determine the early cellular mediators of early pre Tfh cell development during inflammation. In such a model, B cell-activating adjuvants could potentiate bystander B cell-derived IL-6 production and early infiltration of B cell follicles, whereas adjuvants that drive high quantities of early IFN-I could drive DC-derived IL-6 production within the deep TZ, where activated DCs are found. Thus, we hypothesize that multiple distinct LN microenvironments could lead to the development of Tfh cells depending on the specific TLR agonist and the downstream cellular source of IL-6.

Importantly, this information could be used to improve vaccine design by rationally targeting specific cellular sources of IL-6 and driving early follicular trafficking of Tfh.

Additionally, our finding that bystander B cell activation can be polarized to sites of asymmetric antigen drainage further demonstrates that microenvironments can form across LNs and influence T cell differentiation. Whether the polarized early infiltration of B cell follicles is accompanied by polarized generation of GCs is unknown and requires further investigation. Furthermore, these findings of spatial heterogeneity in dLNs could help to shed further light on the heterogeneous nature of T cell responses.

Together, this work defines a key role for TLR-dependent bystander activation of B cells in the generation and localization of Tfh cells.

Summary and impact

In Chapter 3, we found that after TLR agonist vaccination, innate cell microenvironments form in dLNs that support the divergent differentiation of T cells. These divergent microenvironments had varying compositions of MO and Res cDCs, and both cell types cooperated to efficiently drive the activation and differentiation of naïve T cells. The identification of microenvironments during Type 1 inflammation provides new insight into the heterogeneity of T cell differentiation, with implications for designing vaccines that harness these microenvironments to achieve effective immunity. In Chapter 4, we explored the signals regulating Res cDC activation and cellularity after administration of vaccines targeting specific innate signaling pathways. We found that Res cDCs do not need to directly sense draining TLR ligands to become activated. However, direct sensing was important for increasing the cellularity of Res cDC2s, potentially through the enhanced recruitment of pre cDC2s from the BM. These insights into the activation and remodeling of the Res cDC compartment during inflammation has implications for vaccine design, as skewing the Res cDC compartment towards a Res cDC1 or Res cDC2 dominated composition could have profound effects on the initiation of T cell responses. In Chapter 5, we found that B cells rapidly sense draining TLR ligand and become activated, a process that was critical for the generation of Tfh cells. Furthermore, we were able to spatially direct B cell activation and Tfh generation within LNs. The ability to modulate B cell activation and Tfh generation may be favorable for the design of future vaccines.

Overall, this work has emphasized the presence and importance of lymphoid tissue microenvironments in steady state and inflammation. Future research should consider these spatial relationships when designing the next generation of vaccines and therapeutics.

References

1. T. J. Moyer, A. C. Zmolek, D. J. Irvine, Beyond antigens and adjuvants: formulating future vaccines. *J. Clin. Invest.* **126**, 799–808 (2016).

2. A. J. Pollard, E. M. Bijker, A guide to vaccinology: from basic principles to new developments. *Nat. Rev. Immunol.* **21**, 83–100 (2021).

3. G. Forni, A. Mantovani, COVID-19 vaccines: where we stand and challenges ahead. *Cell Death Differ.* **28**, 626–639 (2021).

4. S. C. Eisenbarth, Dendritic cell subsets in T cell programming: location dictates function. *Nat. Rev. Immunol.* **19**, 89–103 (2019).

5. M. Merad, P. Sathe, J. Helft, J. Miller, A. Mortha, The dendritic cell lineage: ontogeny and function of dendritic cells and their subsets in the steady state and the inflamed setting. *Annu. Rev. Immunol.* **31**, 563–604 (2013).

6. M. Cabeza-Cabrerizo, A. Cardoso, C. M. Minutti, M. Pereira da Costa, C. Reis e Sousa, *Annu. Rev. Immunol.*, in press, doi:10.1146/annurev-immunol-061020-053707.

7. M. Y. Gerner, K. A. Casey, W. Kastenmuller, R. N. Germain, Dendritic cell and antigen dispersal landscapes regulate T cell immunity. *J. Exp. Med.* **214**, 3105–3122 (2017).

8. M. Y. Gerner, W. Kastenmuller, I. Ifrim, J. Kabat, R. N. Germain, Histo-Cytometry: A Method for Highly Multiplex Quantitative Tissue Imaging Analysis Applied to Dendritic Cell Subset Microanatomy in Lymph Nodes. *Immunity*. **37**, 364–376 (2012).

9. M. Y. Gerner, P. Torabi-Parizi, R. N. Germain, Strategically Localized Dendritic Cells Promote Rapid T Cell Responses to Lymph-Borne Particulate Antigens. *Immunity*. **42**, 172–185 (2015).

10. S. Plotkin, History of vaccination. *Proc. Natl. Acad. Sci. U. S. A.* **111**, 12283–12287 (2014).

11. T. Kawasaki, T. Kawai, Toll-Like Receptor Signaling Pathways. *Front. Immunol.* **5** (2014), doi:10.3389/fimmu.2014.00461.

12. T. Worbs, S. I. Hammerschmidt, R. Förster, Dendritic cell migration in health and disease. *Nat. Rev. Immunol.* **17**, 30–48 (2017).

13. L. Ohl, M. Mohaupt, N. Czeloth, G. Hintzen, Z. Kiafard, J. Zwirner, T. Blankenstein, G. Henning, R. Förster, CCR7 Governs Skin Dendritic Cell Migration under Inflammatory and Steady-State Conditions. *Immunity*. **21**, 279–288 (2004).

14. M. C. Woodruff, B. A. Heesters, C. N. Herndon, J. R. Groom, P. G. Thomas, A. D. Luster, S. J. Turley, M. C. Carroll, Trans-nodal migration of resident dendritic cells into medullary

interfollicular regions initiates immunity to influenza vaccine. *J. Exp. Med.* **211**, 1611–1621 (2014).

15. H. K. Lee, M. Zamora, M. M. Linehan, N. Iijima, D. Gonzalez, A. Haberman, A. Iwasaki, Differential roles of migratory and resident DCs in T cell priming after mucosal or skin HSV-1 infection. *J. Exp. Med.* **206**, 359–370 (2009).

16. R. S. Allan, J. Waithman, S. Bedoui, C. M. Jones, J. A. Villadangos, Y. Zhan, A. M. Lew, K. Shortman, W. R. Heath, F. R. Carbone, Migratory dendritic cells transfer antigen to a lymph node-resident dendritic cell population for efficient CTL priming. *Immunity*. **25**, 153–162 (2006).

17. G. Iezzi, A. Fröhlich, B. Ernst, F. Ampenberger, S. Saeland, N. Glaichenhaus, M. Kopf, Lymph node resident rather than skin-derived dendritic cells initiate specific T cell responses after Leishmania major infection. *J. Immunol. Baltim. Md 1950*. **177**, 1250–1256 (2006).

18. A. Schlitzer, V. Sivakamasundari, J. Chen, H. R. B. Sumatoh, J. Schreuder, J. Lum, B. Malleret, S. Zhang, A. Larbi, F. Zolezzi, L. Renia, M. Poidinger, S. Naik, E. W. Newell, P. Robson, F. Ginhoux, Identification of cDC1- and cDC2-committed DC progenitors reveals early lineage priming at the common DC progenitor stage in the bone marrow. *Nat. Immunol.* **16**, 718–728 (2015).

19. C. C. Brown, H. Gudjonson, Y. Pritykin, D. Deep, V.-P. Lavallée, A. Mendoza, R. Fromme, L. Mazutis, C. Ariyan, C. Leslie, D. Pe'er, A. Y. Rudensky, Transcriptional Basis of Mouse and Human Dendritic Cell Heterogeneity. *Cell*. **179**, 846-863.e24 (2019).

20. D. A. Anderson, C.-A. Dutertre, F. Ginhoux, K. M. Murphy, Genetic models of human and mouse dendritic cell development and function. *Nat. Rev. Immunol.* **21**, 101–115 (2021).

21. C. V. Jakubzick, G. J. Randolph, P. M. Henson, Monocyte differentiation and antigen-presenting functions. *Nat. Rev. Immunol.* **17**, 349–362 (2017).

22. C. Shi, E. G. Pamer, Monocyte recruitment during infection and inflammation. *Nat. Rev. Immunol.* **11**, 762–774 (2011).

23. L. B. Rodda, E. Lu, M. L. Bennett, C. L. Sokol, X. Wang, S. A. Luther, B. A. Barres, A. D. Luster, C. J. Ye, J. G. Cyster, Single-Cell RNA Sequencing of Lymph Node Stromal Cells Reveals Niche-Associated Heterogeneity. *Immunity*. **48**, 1014-1028.e6 (2018).

24. M. Sixt, N. Kanazawa, M. Selg, T. Samson, G. Roos, D. P. Reinhardt, R. Pabst, M. B. Lutz, L. Sorokin, The Conduit System Transports Soluble Antigens from the Afferent Lymph to Resident Dendritic Cells in the T Cell Area of the Lymph Node. *Immunity*. **22**, 19–29 (2005).

25. A. P. Baptista, A. Gola, Y. Huang, P. Milanez-Almeida, P. Torabi-Parizi, J. F. Urban, V. S. Shapiro, M. Y. Gerner, R. N. Germain, The Chemoattractant Receptor Ebi2 Drives

Intranodal Naive CD4+ T Cell Peripheralization to Promote Effective Adaptive Immunity. *Immunity*. **50**, 1188-1201.e6 (2019).

26. J. A. Villadangos, P. Schnorrer, Intrinsic and cooperative antigen-presenting functions of dendritic-cell subsets in vivo. *Nat. Rev. Immunol.* **7**, 543–555 (2007).

27. D. A. P. Louie, S. Liao, Lymph Node Subcapsular Sinus Macrophages as the Frontline of Lymphatic Immune Defense. *Front. Immunol.* **10** (2019), doi:10.3389/fimmu.2019.00347.

28. G. V. Reynoso, A. S. Weisberg, J. P. Shannon, D. T. McManus, L. Shores, J. L. Americo, R. V. Stan, J. W. Yewdell, H. D. Hickman, Lymph node conduits transport virions for rapid T cell activation. *Nat. Immunol.* **20**, 602 (2019).

29. K. Hoshino, T. Kaisho, Nucleic acid sensing Toll-like receptors in dendritic cells. *Curr. Opin. Immunol.* **20**, 408–413 (2008).

30. S. Pandey, T. Kawai, S. Akira, Microbial Sensing by Toll-Like Receptors and Intracellular Nucleic Acid Sensors. *Cold Spring Harb. Perspect. Biol.* **7** (2015), doi:10.1101/cshperspect.a016246.

31. C. D. Trez, B. Pajak, M. Brait, N. Glaichenhaus, J. Urbain, M. Moser, G. Lauvau, E. Muraille, TLR4 and Toll-IL-1 Receptor Domain-Containing Adapter-Inducing IFN-β, but Not MyD88, Regulate Escherichia coli-Induced Dendritic Cell Maturation and Apoptosis In Vivo. *J. Immunol.* **175**, 839–846 (2005).

32. A. Pantel, A. Teixeira, E. Haddad, E. G. Wood, R. M. Steinman, M. P. Longhi, Direct type I IFN but not MDA5/TLR3 activation of dendritic cells is required for maturation and metabolic shift to glycolysis after poly IC stimulation. *PLoS Biol.* **12**, e1001759 (2014).

33. M. P. Longhi, C. Trumpfheller, J. Idoyaga, M. Caskey, I. Matos, C. Kluger, A. M. Salazar, M. Colonna, R. M. Steinman, Dendritic cells require a systemic type I interferon response to mature and induce CD4+ Th1 immunity with poly IC as adjuvant. *J. Exp. Med.* **206**, 1589–1602 (2009).

34. L. S. deLuca, J. L. Gommerman, Fine-tuning of dendritic cell biology by the TNF superfamily. *Nat. Rev. Immunol.* **12**, 339–351 (2012).

35. L. B. Ivashkiv, L. T. Donlin, Regulation of type I interferon responses. *Nat. Rev. Immunol.* **14**, 36–49 (2014).

36. S. D. Koker, L. V. Hoecke, A. D. Beuckelaer, K. Roose, K. Deswarte, M. A. Willart, P. Bogaert, T. Naessens, B. G. D. Geest, X. Saelens, B. N. Lambrecht, J. Grooten, Inflammatory monocytes regulate Th1 oriented immunity to CpG adjuvanted protein vaccines through production of IL-12. *Sci. Rep.* **7**, 5986 (2017).

37. H. Nakano, K. L. Lin, M. Yanagita, C. Charbonneau, D. N. Cook, T. Kakiuchi, M. D. Gunn, Blood-derived inflammatory dendritic cells in lymph nodes stimulate acute T helper type 1 immune responses. *Nat. Immunol.* **10**, 394–402 (2009).

38. B. Spellberg, J. E. Edwards, Type 1/Type 2 Immunity in Infectious Diseases. *Clin. Infect. Dis.* **32**, 76–102 (2001).

39. S. Crotty, Follicular Helper CD4 T Cells (TFH). *Annu. Rev. Immunol.* **29**, 621–663 (2011).

40. Z. Wan, Y. Lin, Y. Zhao, H. Qi, TFH cells in bystander and cognate interactions with B cells. *Immunol. Rev.* **288**, 28–36 (2019).

41. C. G. Vinuesa, M. A. Linterman, D. Yu, I. C. M. MacLennan, Follicular Helper T Cells. *Annu. Rev. Immunol.* **34**, 335–368 (2016).

42. S. Crotty, T Follicular Helper Cell Biology: A Decade of Discovery and Diseases. *Immunity*. **50**, 1132–1148 (2019).

43. J. Li, E. Lu, T. Yi, J. G. Cyster, EBI2 augments Tfh cell fate by promoting interaction with IL-2-quenching dendritic cells. *Nature*. **533**, 110–114 (2016).

44. Y. S. Choi, R. Kageyama, D. Eto, T. C. Escobar, R. J. Johnston, L. Monticelli, C. Lao, S. Crotty, ICOS receptor instructs T follicular helper cell versus effector cell differentiation via induction of the transcriptional repressor Bcl6. *Immunity*. **34**, 932–946 (2011).

45. E. L. Stone, M. Pepper, C. D. Katayama, Y. M. Kerdiles, C.-Y. Lai, E. Emslie, Y. C. Lin, E. Yang, A. W. Goldrath, M. O. Li, D. A. Cantrell, S. M. Hedrick, ICOS Coreceptor Signaling Inactivates the Transcription Factor FOXO1 to Promote Tfh Cell Differentiation. *Immunity*. **42**, 239–251 (2015).

46. H. Xu, X. Li, D. Liu, J. Li, X. Zhang, X. Chen, S. Hou, L. Peng, C. Xu, W. Liu, L. Zhang, H. Qi, Follicular T-helper cell recruitment governed by bystander B cells and ICOS-driven motility. *Nature*. **496**, 523–527 (2013).

47. M. De Giovanni, V. Cutillo, A. Giladi, E. Sala, C. G. Maganuco, C. Medaglia, P. Di Lucia, E. Bono, C. Cristofani, E. Consolo, L. Giustini, A. Fiore, S. Eickhoff, W. Kastenmüller, I. Amit, M. Kuka, M. Iannacone, Spatiotemporal regulation of type I interferon expression determines the antiviral polarization of CD4 + T cells. *Nat. Immunol.* **21**, 321–330 (2020).

48. J. Shi, S. Hou, Q. Fang, X. Liu, X. Liu, H. Qi, PD-1 Controls Follicular T Helper Cell Positioning and Function. *Immunity*. **49**, 264-274.e4 (2018).

49. K. Reif, E. H. Ekland, L. Ohl, H. Nakano, M. Lipp, R. Förster, J. G. Cyster, Balanced responsiveness to chemoattractants from adjacent zones determines B-cell position. *Nature*. **416**, 94–99 (2002).

50. J. Lian, A. D. Luster, Chemokine-guided cell positioning in the lymph node orchestrates the generation of adaptive immune responses. *Curr. Opin. Cell Biol.* **36**, 1–6 (2015).

51. R. Förster, A. Schubel, D. Breitfeld, E. Kremmer, I. Renner-Müller, E. Wolf, M. Lipp, CCR7 coordinates the primary immune response by establishing functional microenvironments in secondary lymphoid organs. *Cell*. **99**, 23–33 (1999).

52. J. R. Groom, J. Richmond, T. T. Murooka, E. W. Sorensen, J. H. Sung, K. Bankert, U. H. von Andrian, J. J. Moon, T. R. Mempel, A. D. Luster, CXCR3 Chemokine Receptor-Ligand Interactions in the Lymph Node Optimize CD4+ T Helper 1 Cell Differentiation. *Immunity*. **37**, 1091–1103 (2012).

53. B. C. Duckworth, F. Lafouresse, V. C. Wimmer, B. J. Broomfield, L. Dalit, Y. O. Alexandre, A. A. Sheikh, R. Z. Qin, C. Alvarado, L. A. Mielke, M. Pellegrini, S. N. Mueller, T. Boudier, K. L. Rogers, J. R. Groom, Effector and stem-like memory cell fates are imprinted in distinct lymph node niches directed by CXCR3 ligands. *Nat. Immunol.*, 1–15 (2021).

54. A. Brewitz, S. Eickhoff, S. Dähling, T. Quast, S. Bedoui, R. A. Kroczek, C. Kurts, N. Garbi, W. Barchet, M. Iannacone, F. Klauschen, W. Kolanus, T. Kaisho, M. Colonna, R. N. Germain, W. Kastenmüller, CD8+ T Cells Orchestrate pDC-XCR1+ Dendritic Cell Spatial and Functional Cooperativity to Optimize Priming. *Immunity*. **46**, 205–219 (2017).

55. B. León, A. Ballesteros-Tato, J. L. Browning, R. Dunn, T. D. Randall, F. E. Lund, Regulation of TH2 development by CXCR5+ dendritic cells and lymphotoxin-expressing B cells. *Nat. Immunol.* **13**, 681–690 (2012).

56. T. Yi, J. G. Cyster, EBI2-mediated bridging channel positioning supports splenic dendritic cell homeostasis and particulate antigen capture. *eLife*. **2**, e00757 (2013).

57. H. Qi, W. Kastenmüller, R. N. Germain, Spatiotemporal Basis of Innate and Adaptive Immunity in Secondary Lymphoid Tissue. *Annu. Rev. Cell Dev. Biol.* **30**, 141–167 (2014).

58. W. R. Heath, F. R. Carbone, Dendritic cell subsets in primary and secondary T cell responses at body surfaces. *Nat. Immunol.* **10**, 1237–1244 (2009).

59. S. F. Gonzalez, V. Lukacs-Kornek, M. P. Kuligowski, L. A. Pitcher, S. E. Degn, Y.-A. Kim, M. J. Cloninger, L. Martinez-Pomares, S. Gordon, S. J. Turley, M. C. Carroll, Capture of influenza by medullary dendritic cells via SIGN-R1 is essential for humoral immunity in draining lymph nodes. *Nat. Immunol.* **11**, 427–434 (2010).

60. R. Roozendaal, T. R. Mempel, L. A. Pitcher, S. F. Gonzalez, A. Verschoor, R. E. Mebius, U. H. von Andrian, M. C. Carroll, Conduits Mediate Transport of Low-Molecular-Weight Antigen to Lymph Node Follicles. *Immunity*. **30**, 264–276 (2009).

61. M. Kitano, C. Yamazaki, A. Takumi, T. Ikeno, H. Hemmi, N. Takahashi, K. Shimizu, S. E. Fraser, K. Hoshino, T. Kaisho, T. Okada, Imaging of the cross-presenting dendritic cell subsets in the skin-draining lymph node. *Proc. Natl. Acad. Sci.* **113**, 1044–1049 (2016).

62. S. Eickhoff, A. Brewitz, M. Y. Gerner, F. Klauschen, K. Komander, H. Hemmi, N. Garbi, T. Kaisho, R. N. Germain, W. Kastenmüller, Robust Anti-viral Immunity Requires Multiple Distinct T Cell-Dendritic Cell Interactions. *Cell*. **162**, 1322–1337 (2015).

63. J. L. Hor, P. G. Whitney, A. Zaid, A. G. Brooks, W. R. Heath, S. N. Mueller, Spatiotemporally Distinct Interactions with Dendritic Cell Subsets Facilitates CD4+ and CD8+ T Cell Activation to Localized Viral Infection. *Immunity*. **43**, 554–565 (2015).

64. M. K. Ruhland, E. W. Roberts, E. Cai, A. M. Mujal, K. Marchuk, C. Beppler, D. Nam, N. K. Serwas, M. Binnewies, M. F. Krummel, Visualizing Synaptic Transfer of Tumor Antigens among Dendritic Cells. *Cancer Cell*. **37**, 786-799.e5 (2020).

65. S. Celli, Z. Garcia, P. Bousso, CD4 T cells integrate signals delivered during successive DC encounters in vivo. *J. Exp. Med.* **202**, 1271–1278 (2005).

66. C. Jakubzick, E. L. Gautier, S. L. Gibbings, D. K. Sojka, A. Schlitzer, T. E. Johnson, S. Ivanov, Q. Duan, S. Bala, T. Condon, N. van Rooijen, J. R. Grainger, Y. Belkaid, A. Ma'ayan, D. W. H. Riches, W. M. Yokoyama, F. Ginhoux, P. M. Henson, G. J. Randolph, Minimal Differentiation of Classical Monocytes as They Survey Steady-State Tissues and Transport Antigen to Lymph Nodes. *Immunity*. **39**, 599–610 (2013).

67. P. Leirião, C. del Fresno, C. Ardavín, Monocytes as effector cells: Activated Ly-6Chigh mouse monocytes migrate to the lymph nodes through the lymph and cross-present antigens to CD8+ T cells. *Eur. J. Immunol.* **42**, 2042–2051 (2012).

68. R. T. Palframan, S. Jung, G. Cheng, W. Weninger, Y. Luo, M. Dorf, D. R. Littman, B. J. Rollins, H. Zweerink, A. Rot, U. H. von Andrian, Inflammatory chemokine transport and presentation in HEV: a remote control mechanism for monocyte recruitment to lymph nodes in inflamed tissues. *J. Exp. Med.* **194**, 1361–1373 (2001).

69. C. R. Stoltzfus, J. Filipek, B. H. Gern, B. E. Olin, J. M. Leal, Y. Wu, M. R. Lyons-Cohen, J. Y. Huang, C. L. Paz-Stoltzfus, C. R. Plumlee, T. Pöschinger, K. B. Urdahl, M. Perro, M. Y. Gerner, CytoMAP: A Spatial Analysis Toolbox Reveals Features of Myeloid Cell Organization in Lymphoid Tissues. *Cell Rep.* **31**, 107523 (2020).

70. J. R. Groom, Regulators of T-cell fate: Integration of cell migration, differentiation and function. *Immunol. Rev.* **289**, 101–114 (2019).

71. S. Grassmann, L. Mihatsch, J. Mir, A. Kazeroonian, R. Rahimi, S. Flommersfeld, K. Schober, I. Hensel, J. Leube, L. O. Pachmayr, L. Kretschmer, Q. Zhang, A. Jolly, M. Z. Chaudhry, M. Schiemann, L. Cicin-Sain, T. Höfer, D. H. Busch, M. Flossdorf, V. R. Buchholz, Early emergence of T central memory precursors programs clonal dominance during chronic viral infection. *Nat. Immunol.* **21**, 1563–1573 (2020).

72. V. R. Buchholz, M. Flossdorf, I. Hensel, L. Kretschmer, B. Weissbrich, P. Gräf, A. Verschoor, M. Schiemann, T. Höfer, D. H. Busch, Disparate Individual Fates Compose Robust CD8+ T Cell Immunity. *Science*. **340**, 630–635 (2013).

73. C. Gerlach, J. C. Rohr, L. Perié, N. van Rooij, J. W. J. van Heijst, A. Velds, J. Urbanus, S. H. Naik, H. Jacobs, J. B. Beltman, R. J. de Boer, T. N. M. Schumacher, Heterogeneous Differentiation Patterns of Individual CD8+ T Cells. *Science*. **340**, 635–639 (2013).

74. C. R. Plumlee, B. S. Sheridan, B. B. Cicek, L. Lefrançois, Environmental cues dictate the fate of individual CD8+ T cells responding to infection. *Immunity*. **39**, 347–356 (2013).

75. F. Annunziato, C. Romagnani, S. Romagnani, The 3 major types of innate and adaptive cell-mediated effector immunity. *J. Allergy Clin. Immunol.* **135**, 626–635 (2015).

76. W. C. Gause, T. A. Wynn, J. E. Allen, Type 2 immunity and wound healing: evolutionary refinement of adaptive immunity by helminths. *Nat. Rev. Immunol.* **13**, 607–614 (2013).

77. H. C. Yip, A. Y. Karulin, M. Tary-Lehmann, M. D. Hesse, H. Radeke, P. S. Heeger, R. P. Trezza, F. P. Heinzel, T. Forsthuber, P. V. Lehmann, Adjuvant-Guided Type-1 and Type-2 Immunity: Infectious/Noninfectious Dichotomy Defines the Class of Response. *J. Immunol.* **162**, 3942–3949 (1999).

78. E. Lu, E. V. Dang, J. G. McDonald, J. G. Cyster, Distinct oxysterol requirements for positioning naïve and activated dendritic cells in the spleen. *Sci. Immunol.* **2** (2017), doi:10.1126/sciimmunol.aal5237.

79. H. Liu, K. D. Moynihan, Y. Zheng, G. L. Szeto, A. V. Li, B. Huang, D. S. Van Egeren, C. Park, D. J. Irvine, Structure-based programming of lymph-node targeting in molecular vaccines. *Nature*. **507**, 519–522 (2014).

80. C. Langlet, S. Tamoutounour, S. Henri, H. Luche, L. Ardouin, C. Grégoire, B. Malissen, M. Guilliams, CD64 Expression Distinguishes Monocyte-Derived and Conventional Dendritic Cells and Reveals Their Distinct Role during Intramuscular Immunization. *J. Immunol.*, 1102744 (2012).

81. M. Plantinga, M. Guilliams, M. Vanheerswynghels, K. Deswarte, F. Branco-Madeira, W. Toussaint, L. Vanhoutte, K. Neyt, N. Killeen, B. Malissen, H. Hammad, B. N. Lambrecht, Conventional and Monocyte-Derived CD11b+ Dendritic Cells Initiate and Maintain T Helper 2 Cell-Mediated Immunity to House Dust Mite Allergen. *Immunity*. **38**, 322–335 (2013).

82. T. Lämmermann, W. Kastenmüller, Concepts of GPCR-controlled navigation in the immune system. *Immunol. Rev.* **289**, 205–231 (2019).

83. S. Calabro, D. Liu, A. Gallman, M. S. L. Nascimento, Z. Yu, T. Zhang, P. Chen, B. Zhang, L. Xu, U. Gowthaman, J. K. Krishnaswamy, A. M. Haberman, A. Williams, S. C. Eisenbarth, Differential Intrasplenic Migration of Dendritic Cell Subsets Tailors Adaptive Immunity. *Cell Rep.* **16**, 2472–2485 (2016).

84. G. De Becker, V. Moulin, B. Pajak, C. Bruck, M. Francotte, C. Thiriart, J. Urbain, M. Moser, The adjuvant monophosphoryl lipid A increases the function of antigen-presenting cells. *Int. Immunol.* **12**, 807–815 (2000).

85. M. M. Meredith, K. Liu, G. Darrasse-Jeze, A. O. Kamphorst, H. A. Schreiber, P. Guermonprez, J. Idoyaga, C. Cheong, K.-H. Yao, R. E. Niec, M. C. Nussenzweig,

Expression of the zinc finger transcription factor zDC (Zbtb46, Btbd4) defines the classical dendritic cell lineage. *J. Exp. Med.* **209**, 1153–1165 (2012).

86. A. A. Itano, S. J. McSorley, R. L. Reinhardt, B. D. Ehst, E. Ingulli, A. Y. Rudensky, M. K. Jenkins, Distinct Dendritic Cell Populations Sequentially Present Antigen to CD4 T Cells and Stimulate Different Aspects of Cell-Mediated Immunity. *Immunity*. **19**, 47–57 (2003).

87. C. Shi, T. Jia, S. Mendez-Ferrer, T. M. Hohl, N. V. Serbina, L. Lipuma, I. Leiner, M. O. Li, P. S. Frenette, E. G. Pamer, Bone marrow mesenchymal stem and progenitor cells induce monocyte emigration in response to circulating Toll-like receptor ligands. *Immunity*. **34**, 590–601 (2011).

88. S. Nourshargh, R. Alon, Leukocyte migration into inflamed tissues. *Immunity*. **41**, 694–707 (2014).

89. J.-P. Girard, C. Moussion, R. Förster, HEVs, lymphatics and homeostatic immune cell trafficking in lymph nodes. *Nat. Rev. Immunol.* **12**, 762–773 (2012).

90. A. Woodfin, M.-B. Voisin, M. Beyrau, B. Colom, D. Caille, F.-M. Diapouli, G. B. Nash, T. Chavakis, S. M. Albelda, G. E. Rainger, P. Meda, B. A. Imhof, S. Nourshargh, The junctional adhesion molecule JAM-C regulates polarized transendothelial migration of neutrophils in vivo. *Nat. Immunol.* **12**, 761–769 (2011).

91. H. H. Zhang, K. Song, R. L. Rabin, B. J. Hill, S. P. Perfetto, M. Roederer, D. C. Douek, R. M. Siegel, J. M. Farber, CCR2 identifies a stable population of human effector memory CD4+ T cells equipped for rapid recall response. *J. Immunol. Baltim. Md 1950*. **185**, 6646–6663 (2010).

92. E. Zigmond, C. Varol, J. Farache, E. Elmaliah, A. T. Satpathy, G. Friedlander, M. Mack, N. Shpigel, I. G. Boneca, K. M. Murphy, G. Shakhar, Z. Halpern, S. Jung, Ly6C hi monocytes in the inflamed colon give rise to proinflammatory effector cells and migratory antigen-presenting cells. *Immunity*. **37**, 1076–1090 (2012).

93. C. Bosteels, K. Neyt, M. Vanheerswynghels, M. J. van Helden, D. Sichien, N. Debeuf, S. D. Prijck, V. Bosteels, N. Vandamme, L. Martens, Y. Saeys, E. Louagie, M. Lesage, D. L. Williams, S.-C. Tang, J. U. Mayer, F. Ronchese, C. L. Scott, H. Hammad, M. Guilliams, B. N. Lambrecht, Inflammatory Type 2 cDCs Acquire Features of cDC1s and Macrophages to Orchestrate Immunity to Respiratory Virus Infection. *Immunity*. **52**, 1039-1056.e9 (2020).

94. V. Krishnamoorthy, S. Kannanganat, M. Maienschein-Cline, S. P. face Cook, J. Chen, N. Bahroos, E. Sievert, E. Corse, A. Chong, R. Sciammas, The IRF4 Gene Regulatory Module Functions as a Read-Write Integrator to Dynamically Coordinate T Helper Cell Fate. *Immunity*. **47**, 481-497.e7 (2017).

95. K. Man, M. Miasari, W. Shi, A. Xin, D. C. Henstridge, S. Preston, M. Pellegrini, G. T. Belz, G. K. Smyth, M. A. Febbraio, S. L. Nutt, A. Kallies, The transcription factor IRF4 is essential for TCR affinity-mediated metabolic programming and clonal expansion of T cells. *Nat. Immunol.* **14**, 1155–1165 (2013).

96. H. A. Schreiber, J. Loschko, R. A. Karssemeijer, A. Escolano, M. M. Meredith, D. Mucida, P. Guermonprez, M. C. Nussenzweig, Intestinal monocytes and macrophages are required for T cell polarization in response to Citrobacter rodentium. *J. Exp. Med.* **210**, 2025–2039 (2013).

97. M. Martínez□López, S. Iborra, R. Conde□Garrosa, D. Sancho, Batf3-dependent CD103+ dendritic cells are major producers of IL-12 that drive local Th1 immunity against Leishmania major infection in mice. *Eur. J. Immunol.* **45**, 119–129 (2015).

98. M. Mashayekhi, M. M. Sandau, I. R. Dunay, E. M. Frickel, A. Khan, R. S. Goldszmid, A. Sher, H. L. Ploegh, T. L. Murphy, L. D. Sibley, K. M. Murphy, CD8α+ Dendritic Cells Are the Critical Source of Interleukin-12 that Controls Acute Infection by Toxoplasma gondii Tachyzoites. *Immunity*. **35**, 249–259 (2011).

99. R. L. Reinhardt, S. Hong, S.-J. Kang, Z. Wang, R. M. Locksley, Visualization of IL-12/23p40 In Vivo Reveals Immunostimulatory Dendritic Cell Migrants that Promote Th1 Differentiation. *J. Immunol.* **177**, 1618–1627 (2006).

100. L. Conejero, S. C. Khouili, S. Martínez-Cano, H. M. Izquierdo, P. Brandi, D. Sancho, Lung CD103+ dendritic cells restrain allergic airway inflammation through IL-12 production. *JCI Insight*. **2**, doi:10.1172/jci.insight.90420.

101. B. Everts, R. Tussiwand, L. Dreesen, K. C. Fairfax, S. C.-C. Huang, A. M. Smith, C. M. O'Neill, W. Y. Lam, B. T. Edelson, J. F. Urban, K. M. Murphy, E. J. Pearce, Migratory CD103+ dendritic cells suppress helminth-driven type 2 immunity through constitutive expression of IL-12. *J. Exp. Med.* **213**, 35–51 (2016).

102. H. Borges da Silva, H. Wang, L. J. Qian, K. A. Hogquist, S. C. Jameson, ARTC2.2/P2RX7 Signaling during Cell Isolation Distorts Function and Quantification of Tissue-Resident CD8+ T Cell and Invariant NKT Subsets. *J. Immunol. Baltim. Md 1950*. **202**, 2153–2163 (2019).

103. E. M. Steinert, J. M. Schenkel, K. A. Fraser, L. K. Beura, L. S. Manlove, B. Z. Igyártó, P. J. Southern, D. Masopust, Quantifying Memory CD8 T Cells Reveals Regionalization of Immunosurveillance. *Cell*. **161**, 737–749 (2015).

104. J. M. Curtsinger, M. F. Mescher, Inflammatory cytokines as a third signal for T cell activation. *Curr. Opin. Immunol.* **22**, 333–340 (2010).

105. J. Zhu, H. Yamane, W. E. Paul, Differentiation of Effector CD4 T Cell Populations. *Annu. Rev. Immunol.* **28**, 445–489 (2010).

106. T. R. Mempel, S. E. Henrickson, U. H. von Andrian, T-cell priming by dendriticcells in lymph nodes occurs in three distinct phases. *Nature*. **427**, 154–159 (2004).

107. S. Bajaña, K. Roach, S. Turner, J. Paul, S. Kovats, IRF4 Promotes Cutaneous Dendritic Cell Migration to Lymph Nodes during Homeostasis and Inflammation. *J. Immunol.*, 1102613 (2012).

108. J. K. Krishnaswamy, U. Gowthaman, B. Zhang, J. Mattsson, L. Szeponik, D. Liu, R. Wu, T. White, S. Calabro, L. Xu, M. A. Collet, M. Yurieva, S. Alsén, P. Fogelstrand, A. Walter, W. R. Heath, S. N. Mueller, U. Yrlid, A. Williams, S. C. Eisenbarth, Migratory CD11b+ conventional dendritic cells induce T follicular helper cell–dependent antibody responses. *Sci. Immunol.* **2**, eaam9169 (2017).

109. B. Vander Lugt, A. A. Khan, J. A. Hackney, S. Agrawal, J. Lesch, M. Zhou, W. P. Lee, S. Park, M. Xu, J. DeVoss, C. J. Spooner, C. Chalouni, L. Delamarre, I. Mellman, H. Singh, Transcriptional programming of dendritic cells for enhanced MHC class II antigen presentation. *Nat. Immunol.* **15**, 161–167 (2014).

110. B. Z. Igyártó, K. Haley, D. Ortner, A. Bobr, M. Gerami-Nejad, B. T. Edelson, S. M. Zurawski, B. Malissen, G. Zurawski, J. Berman, D. H. Kaplan, Skin-resident murine dendritic cell subsets promote distinct and opposing antigen-specific T helper cell responses. *Immunity*. **35**, 260–272 (2011).

111. Y. Kumamoto, M. Linehan, J. S. Weinstein, B. J. Laidlaw, J. E. Craft, A. Iwasaki, CD301b+ dermal dendritic cells drive T helper-2 cell mediated immunity. *Immunity*. **39** (2013), doi:10.1016/j.immuni.2013.08.029.

112. C. Levin, O. Bonduelle, C. Nuttens, C. Primard, B. Verrier, A. Boissonnas, B. Combadière, Critical Role for Skin-Derived Migratory DCs and Langerhans Cells in TFH and GC Responses after Intradermal Immunization. *J. Invest. Dermatol.* **137**, 1905–1913 (2017).

113. K. Kohli, A. Janssen, R. Förster, Plasmacytoid dendritic cells induce tolerance predominantly by cargoing antigen to lymph nodes. *Eur. J. Immunol.* **46**, 2659–2668 (2016).

114. S. Srivastava, J. D. Ernst, Cell-to-cell transfer of M. tuberculosis antigens optimizes CD4 T cell priming. *Cell Host Microbe*. **15**, 741–752 (2014).

115. S. Hutchison, R. A. Benson, V. B. Gibson, A. H. Pollock, P. Garside, J. M. Brewer, Antigen depot is not required for alum adjuvanticity. *FASEB J.* **26**, 1272–1279 (2011).

116. A. Schudel, D. M. Francis, S. N. Thomas, Material design for lymph node drug delivery. *Nat. Rev. Mater.* **4**, 415–428 (2019).

117. E. L. Gautier, T. Shay, J. Miller, M. Greter, C. Jakubzick, S. Ivanov, J. Helft, A. Chow, K. G. Elpek, S. Gordonov, A. R. Mazloom, A. Ma'ayan, W.-J. Chua, T. H. Hansen, S. J. Turley, M. Merad, G. J. Randolph, Immunological Genome Consortium, Gene-expression profiles and transcriptional regulatory pathways that underlie the identity and diversity of mouse tissue macrophages. *Nat. Immunol.* **13**, 1118–1128 (2012).

118. J. C. Miller, B. D. Brown, T. Shay, E. L. Gautier, V. Jojic, A. Cohain, G. Pandey, M. Leboeuf, K. G. Elpek, J. Helft, D. Hashimoto, A. Chow, J. Price, M. Greter, M. Bogunovic, A. Bellemare-Pelletier, P. S. Frenette, G. J. Randolph, S. J. Turley, M. Merad, Immunological Genome Consortium, Deciphering the transcriptional network of the dendritic cell lineage. *Nat. Immunol.* **13**, 888–899 (2012).

119. A.-C. Villani, R. Satija, G. Reynolds, S. Sarkizova, K. Shekhar, J. Fletcher, M. Griesbeck, A. Butler, S. Zheng, S. Lazo, L. Jardine, D. Dixon, E. Stephenson, E. Nilsson, I. Grundberg, D. McDonald, A. Filby, W. Li, P. L. De Jager, O. Rozenblatt-Rosen, A. A. Lane, M. Haniffa, A. Regev, N. Hacohen, Single-cell RNA-seq reveals new types of human blood dendritic cells, monocytes, and progenitors. *Science*. **356** (2017), doi:10.1126/science.aah4573.

120. R. Blecher-Gonen, P. Bost, K. L. Hilligan, E. David, T. M. Salame, E. Roussel, L. M. Connor, J. U. Mayer, K. Bahar Halpern, B. Tóth, S. Itzkovitz, B. Schwikowski, F. Ronchese, I. Amit, Single-Cell Analysis of Diverse Pathogen Responses Defines a Molecular Roadmap for Generating Antigen-Specific Immunity. *Cell Syst.* **8**, 109-121.e6 (2019).

121. R. Spörri, C. Reis e Sousa, Inflammatory mediators are insufficient for full dendritic cell activation and promote expansion of CD4+ T cell populations lacking helper function. *Nat. Immunol.* **6**, 163–170 (2005).

122. H. Hochrein, K. Shortman, D. Vremec, B. Scott, P. Hertzog, M. O'Keeffe, Differential Production of IL-12, IFN-α, and IFN-γ by Mouse Dendritic Cell Subsets. *J. Immunol.* **166**, 5448–5455 (2001).

123. C. R. e Sousa, S. Hieny, T. Scharton-Kersten, D. Jankovic, H. Charest, R. N. Germain, A. Sher, In Vivo Microbial Stimulation Induces Rapid CD40 Ligand–independent Production of Interleukin 12 by Dendritic Cells and their Redistribution to T Cell Areas. *J. Exp. Med.* **186**, 1819–1829 (1997).

124. C. H. K. Lehmann, L. Heger, G. F. Heidkamp, A. Baranska, J. J. Lühr, A. Hoffmann, D. Dudziak, Direct Delivery of Antigens to Dendritic Cells via Antibodies Specific for Endocytic Receptors as a Promising Strategy for Future Therapies. *Vaccines*. **4**, 8 (2016).

125. M. Guilliams, L. van de Laar, A Hitchhiker's Guide to Myeloid Cell Subsets: Practical Implementation of a Novel Mononuclear Phagocyte Classification System. *Front. Immunol.* **6** (2015), doi:10.3389/fimmu.2015.00406.

126. C. A. Janeway, R. Medzhitov, Innate immune recognition. *Annu. Rev. Immunol.* **20**, 197–216 (2002).

127. M. Cabeza-Cabrerizo, J. van Blijswijk, S. Wienert, D. Heim, R. P. Jenkins, P. Chakravarty, N. Rogers, B. Frederico, S. Acton, E. Beerling, J. van Rheenen, H. Clevers, B. U. Schraml, M. Bajénoff, M. Gerner, R. N. Germain, E. Sahai, F. Klauschen, C. R. e Sousa, Tissue clonality of dendritic cell subsets and emergency DCpoiesis revealed by multicolor fate mapping of DC progenitors. *Sci. Immunol.* **4** (2019), doi:10.1126/sciimmunol.aaw1941.

128. M. Merad, M. G. Manz, Dendritic cell homeostasis. *Blood*. **113**, 3418–3427 (2009).

129. D. Masopust, C. P. Sivula, S. C. Jameson, Of Mice, Dirty Mice, and Men: Using Mice to Understand Human Immunology. *J. Immunol. Baltim. Md 1950*. **199**, 383–388 (2017).

130. J. G. Cyster, C. D. C. Allen, B Cell Responses: Cell Interaction Dynamics and Decisions. *Cell*. **177**, 524–540 (2019).

131. M. Akkaya, K. Kwak, S. K. Pierce, B cell memory: building two walls of protection against pathogens. *Nat. Rev. Immunol.* **20**, 229–238 (2020).

132. J. G. Cyster, B cell follicles and antigen encounters of the third kind. *Nat. Immunol.* **11**, 989–996 (2010).

133. C. M. Buchta, G. A. Bishop, Toll-like receptors and B cells: functions and mechanisms. *Immunol. Res.* **59**, 12–22 (2014).

134. S. Hong, Z. Zhang, H. Liu, M. Tian, X. Zhu, Z. Zhang, W. Wang, X. Zhou, F. Zhang, Q. Ge, B. Zhu, H. Tang, Z. Hua, B. Hou, B Cells Are the Dominant Antigen-Presenting Cells that Activate Naive CD4+ T Cells upon Immunization with a Virus-Derived Nanoparticle Antigen. *Immunity*. **49**, 695-708.e4 (2018).

135. E. N. Arroyo, M. Pepper, B cells are sufficient to prime the dominant CD4+ Tfh response to Plasmodium infection. *J. Exp. Med.* **217** (2020), doi:10.1084/jem.20190849.

136. E. P. Browne, Regulation of B-cell responses by Toll-like receptors. *Immunology*. **136**, 370–379 (2012).

137. Z. Hua, B. Hou, The role of B cell antigen presentation in the initiation of CD4+ T cell response. *Immunol. Rev.* **296**, 24–35 (2020).

138. T. Arkatkar, S. W. Du, H. M. Jacobs, E. M. Dam, B. Hou, J. H. Buckner, D. J. Rawlings, S. W. Jackson, B cell–derived IL-6 initiates spontaneous germinal center formation during systemic autoimmunity. *J. Exp. Med.* **214**, 3207–3217 (2017).